STUDIA

UNIVERSITATIS BABEŞ-BOLYAI

CHEMIA

1

1990

CLUJ-NAPOCA

Anul XXXV 1990

STUDIA

UNIVERSITATIS BABEŞ BOLYAI

CHEMIA

1

Redacţia: 3400 CLUJ-NAPOCA, str. M. Kogălniceanu, 1 ● Telefon 11 61 01

SUMAR — CONTENTS — INHALT

In memoriam

Recenzii — Book Reviews — Buchbesprechungen

SEMICONDUCTOR GAS SENSORS
II[1]. Sensor and Device for the Determination of Ethyl Alcohol Vapours in Air

MIRCEA ANTON*, FERENC PUSKÁS*, CECILIA ROMAN*, NICOLAE PRODAN*, I. CĂTĂLIN POPESCU** and EMIL CORDOŞ**

Received: March 21, 1989

The results concerning the realization and characterization of a SnO_2 based semiconductor sensor for ethyl alcohol vapours in air are presented. The sensor equips an alcoholtest device for breathed alcohol determination. The calibration method of the device as well as the first experimental results obtained are also presented.

Since their appearance [1], semiconductor metallic oxides based gas sensors have been studied to a large extent. Under certain circumstances, on the surface of a n type semiconductor oxide the reversible adsorbtion of some reducing gases occurs, which determines the increase of the electric conductance of the material. Making use of this property, semiconductor sensors for the respective gases have been built. Tin dioxide is one of the most often employed material to which other oxides or noble metals are added in small amounts, with a catalytic role (Table 1).

Using SnO_2 doped with certain additives semiconductor sensors for ethyl alcohol were obtained and were incorporated in device for detecting and measuring the concentration of ethyl alcohol vapours in the air [19, 20, 21].

This paper presents the results concerning the design and the caracterization of a SnO_2 based semiconductor sensor for ethanol as well as the construction and testing of a device for breathed alcohol determination (Alcoholtest).

Results and Discussion. A. *Semiconductor sensor for ethyl vapours.*

The sensor is of Taguchi type [19]. On an alumina tube ($Ø_{inner} = 0.9$mm; $Ø_{outer} = 1.2$ mm) of 5 mm length, two gold film electrodes have been painted, at 1 mm distance each other, and at both ends of the tube platinum terminals ($Ø = 0.1$ mm) have been mounted. The SnO_2 based semiconductor material has been coated on the electrodes as a paste (Fig. 1a). The sintering process has been performed in air, between 400°C and 800°C, in 6 — 9 hours. A heating filament has been inserted into the inner part of the alumina cylinder. The sensor thus obtained has been mounted on a 7 pins socket (Fig. 1b).

The electric circuit the sensor has been included in is shown in Fig. 2.

The installation for obtaining standard gaseous mixtures in air, necesary for the study of the sensor, has been described in a previous paper [22].

---

[1] Part I, *Stud. Univ. Babeş-Bolyai, Chem.*, 33(2), 91 (1988).

* *I.A.U.C. Cluj-Napoca, Arany Janos 11, 3400 Cluj-Napoca, Romania.*
** *University of Cluj-Napoca, Faculty of Chemical Technology, Arany Janos 11, 3400 Cluj-Napoca, Romania*

Table 1

SnO_2 based sensors

Composition	Sintering temperature (K)	Detected gases	Constructive variant	References
SnO_2 (60%) + ZrO_2 (22%), SiO_2 (17,3%), PdO (0,5%)	970—1270	fuel gases	thick layer	[2]
SnO_2 (87,6—92,5%) + Al_2O_3 (8,6—10,7%), WO_3 (1,6—2,1%), P_2O (0,4—0,6%), Na_2O (0,2—0,25%), PdO	820—970	reducing gases	disk	[3]
SnO_2 + MgO (0,1—20 mol%), Nb_2O_5	870	O_2	disk	[4]
SnO_2 + $PdCl_2$ (1%), MgO (1%), Nb max. 20%	870—1070	propane	thick layer	[5]
SnO_2 + (Sb, Bi), Pt		NO_2	thin film RF sputtering	[6]
SnO_2	620—720	NO	thin film	[7]
SnO_2 + $PdCl_2$ (1%), MgO (1%), ThO_2 (5%)	670	CO	thick layer	[8,9]
SnO_2 + (Sb, Bi), Pt, Au		CO	thin layer	[10]
SnO_2 + MgO, Pd, (ThO_2, SiO_2)		CO	thick layer	[11]
SnO_2		NO	thin film	[12]
SnO_2	620 oxidizing	EtOH	thick layer	[13]
SnO_2		H_2, H_2S	thin film RF sputtering	[14]
SnO_2	720	CO, propane ethanol	film deposited by spray-pyrolysis	[15]
SnO_2 + Cr, Ru		$C(CH_3)_4$ n-propane		[16]
SnC_2 + Ag	870	H_2	disk	[17]
SnO_2 + Al silicate (36%), $PdCl_2$ (1,5%)	1070	CH_4		[18]
SnO_2 + Bi_2O_3 (15%), $PdCl_2$ (1,5%)	870	CO		[18]

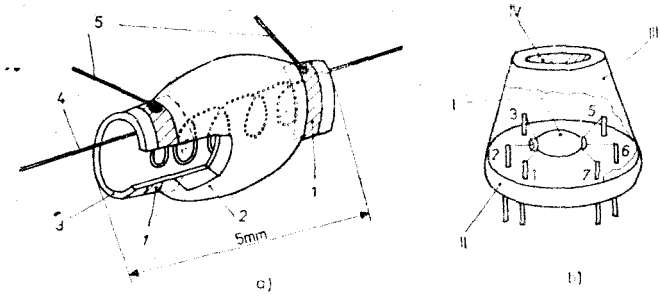

Fig. 1. The costruction of the sensor. a) the sensitive element: 1 — electrodes; 2 — sintered SnO_2 layer; 3 — alumina tube; 4 — filament; 5 — terminals. b) the sensor-socket assembly: I — sensor; II — socket; III — protection lid; IV — stainless steel gauze.

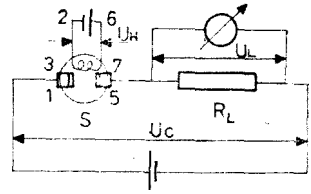

Fig. 2. The electric circuit diagram. S — sensor; R_{L} — standard resistance (10 kΩ); U_C — measuring circuit supply voltage (5 $V_{D.C.}$); U_H — heating circuit supply voltage (4.75 $V_{D.C.}$); U_{L} — analytical signal; T — 20 °C; R.H. — 65%

The operating temperature — For a given gas concentration in air, the analytical signal depends on the temperature of the sensor, as it results from Fig. 3, for ethanol, acetone and acetic acid, respectively.

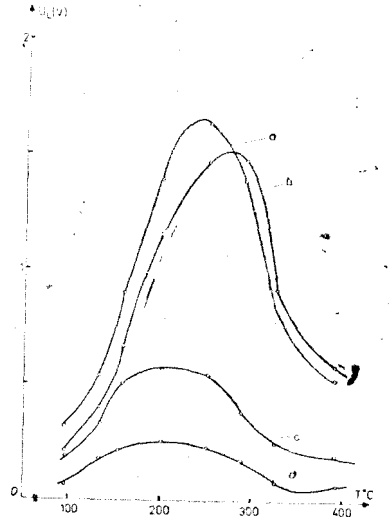

Fig. 3. The dependence of U_{L} upon the temperature. a) 100 ppm ethanol in air; b) 100 ppm acetone in air; c) 100 ppm acetic acid in air; d) air; U_C — 5 $V_{D.C.}$; R_{L} — 10 KΩ; T — 20 °C; R.H. — 65%.

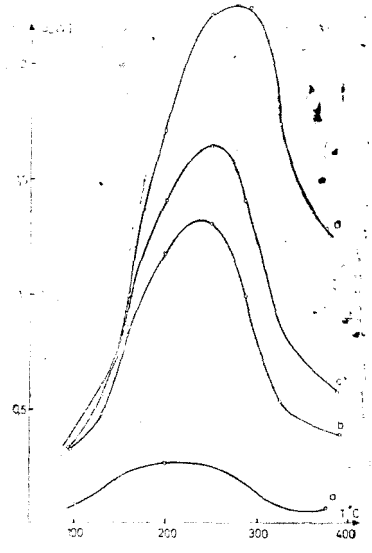

Fig. 4. The dependence of U_{L} upon the temperature for different concentrations of ethanol vapours in air. a) air; b) 42 ppm; c) 100 ppm; d) 400 ppm (experimental conditions: see Fig. 3).

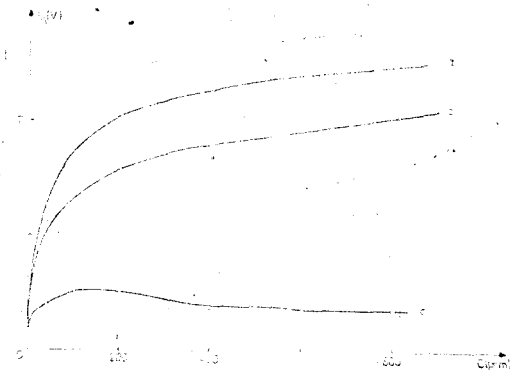

Fig 5. The calibration of the sensor. a) ethyl alcohol; b) acetone; c) acetic acid (experimental conditions: see. Fig. 3).

The temperature characteristic of the sensor signal is similar to the data existing in literature [23].

The optimum operating temperature has been chosen so that to a signal amplitude as large as possible, little energy consumption and a great speed of response should correspond. Hence, the best working temperature for the ethanol detection has been found to be at 250°C. This value does not vary with the gas concentration (Fig. 4).

The calibration — In Fig. 5 are shown the calibration curves for ethyl alcohol, acetic acid and acetone. For this purpose, the sensor signal for different concentrations of C_2H_5OH, CH_3COOH and CH_3COCH_3 obtained with the equipment used to prepare standard gas mixtures in the air, have been measured [22]. The saturation phenomena occurs at concentrations higher than 600 ppm for ethyl alcohol and acetone and at values higher than 200 ppm for acetic acid respectively.

The response time — The response time of the sensor, defined as the time the sensor reaches 90% of the utmost signal, decreases with the increase of the ethanol concentration (Fig. 6a). At a concentration of 100 ppm ethanol (Fig. 6a, curve 3), the response time does not exceed 30 s. The response time is also reduced with the rise of the sensor temperature (Fig. 6b).

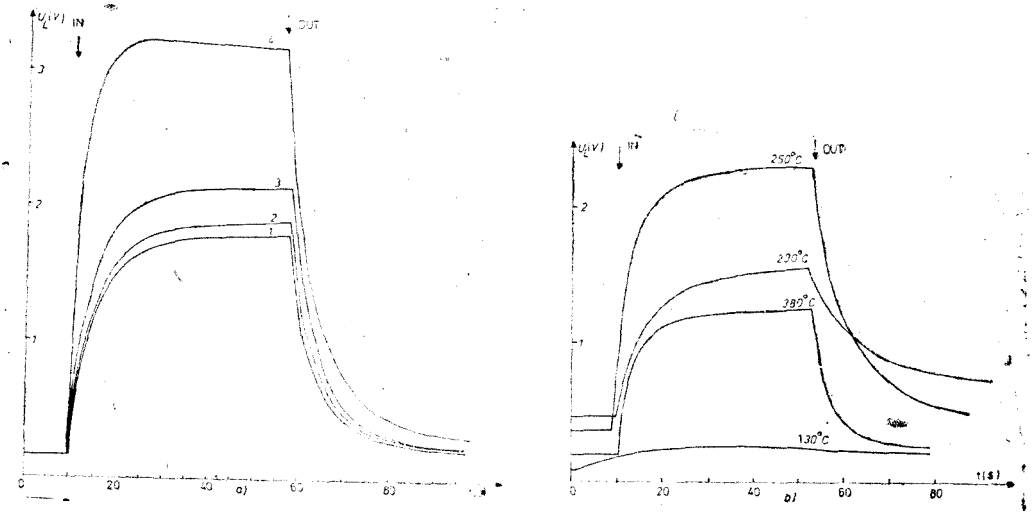

Fig. 6. The dependence of U_L upon time. a) at different concentrations of ethanol: 1 — 42ppm; 2 — 84 ppm; 3 — 100 ppm; 4 — 400 ppm. b) at different temperatures of the sensor.

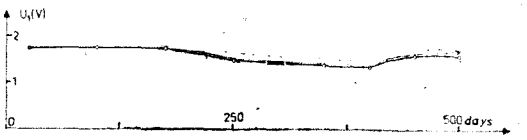

Fig. 7. The stability of the sensor operating in discontinuous working conditions (experimental conditions: see Fig. 2).

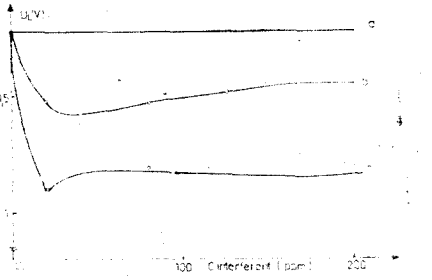

Fig. 8. The U_L dependence upon the interferent concentration. a) 100 ppm ethanol; b) 100 ppm ethanol + x acetone; c) 100 ppm ethanol + x acetic acid (experimental conditions: see Fig. 3).

The stability — In conditions of a discontinuous operation which is characteristic to Alcoholtest device, the sensor is stable in time, as it results form Fig. 7. A monthly calibration is enough.

The selectivity — The sensor response in the case of the simultaneous presence of alcohol and acetone vapours, or alcohol and acetic acid vapours, respectively, is shown in Fig. 8. It has been observed that the interference is not additive, the signal correspondig to the simultaneous presence of alcohol vapours and that which interferent being inferior to that corresponding only to ethyl alcohol. The strongest interferent from the studied ones is the acetic acid. In the presence of only one component in the air, the corresponding signal at 400 ppm acetone is equal to that one given by 100 ppm ethyl alcohol (see Fig. 5).

The influence of the moisture — Generally, the atmospheric moisture has a great influence on the response of such a type sensors [19]. However, a relatively reduced influence of the moisture content on the value of the signal in the reference conditions (100 ppm ethyl alcohol, R.H. = 65%, T = 20°C, T_{sensor} = 520 K) is observable in Fig. 9.

B. *Alcoholtest device with semiconductor sensor*

Semiconductor sensors of this type are used for the construction of some devices for determination of the concentration of alcohol in air or of the alcoholemia at human subjects [20, 21].

The construction — The conductance of the sensor depends on the concentration of the alcohol vapours in the air according to

$$G = kc^n \tag{1}$$

where k is a constant characteristic to the type of sensor and $n \simeq 0{,}5$ [23]. The analytic signal (U_L) depends on the sensor conductance following the relation:

$$U_L = U_c \frac{G}{G_L + G} \tag{2}$$

where $G_L = \frac{1}{R_L}$ (see Fig. 2)

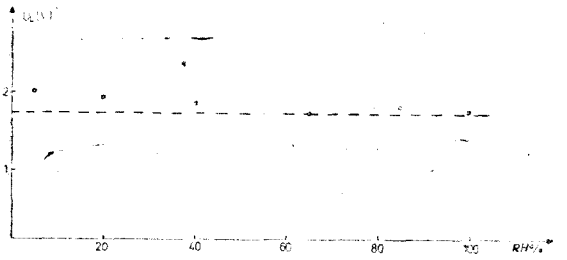

Fig. 9. The influence of the moisture content upon the sensor signal. — — — the reference level: 100 ppm ethanol, R.H. — 65%.

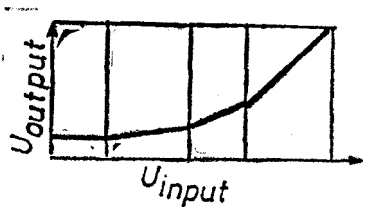

Fig. 10. The linearization of the sensor response.

In order to the Alcoholtest device should reflect directly the vapour concentration in the air, the sensor has been incorporated in an electronic circuit with an input — output characteristic presented in Fig. 10.

Reprezenting graphically the indications of the device versus the concentration of ethyl alcohol vapours (in static condition) the straight line from Fig. 11 has been obtained with the equation $\bar{C}_{device} = -6.95 + 1.07C$; COR = = 0.999.

The functional characteristics — In order to permit the measuring of the alcohol vapours concentration in the breath the device is provided with a mouthpiece. This has the role of maintaining relatively constant the quantity of air breathed over the sensor (Fig. 12), no matter of the tested guman subject. On the other hand, the mouthpiece maintains for a while the has to be analysed in the neighborhood of the sensor. To avoid the contamination from one sample to another the mouthpiece is changed each measurement.

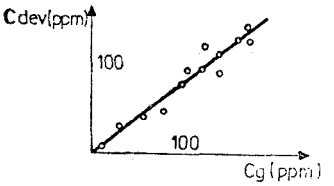

Fig. 11. The linear characteristic of the device.

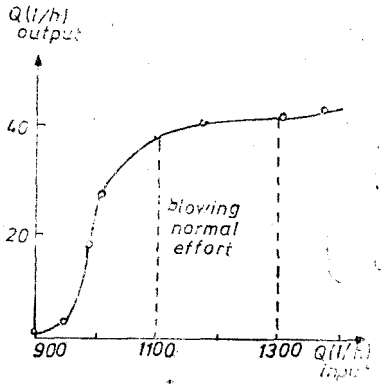

Fig. 12. The dependence between the air input and the air output through the mouthpiece.

The testing of the Alcoholtest device in real dynamic functioning conditions — To verify the correctness of the Alcoholtest device functioning in real conditions (when the air runs over the sensor with a flow rate of 1100—1300 l/min, see Fig. 12), the instructions given by the device were compared to the results of the chromatographic analysis [22]. Thus, the concentration of the alcohol vapours from the air breathed by a human subject who has previously ingested a quantity of alcohol — was determinated both through chromatographic way and by means of the Alcoholtest device. The results obtained are presented in Table 2.

Table 2

Concentrations of ethanol vapours in air determinated by the chromatograph and Alcoholtest device

No.	Peak area (mm²)	C_{cr} (ppm) (ppm)	C_{device} (ppm)	$\bar{C}_{device}$ (ppm)	$\Delta C = C_{cr} - \bar{C}_{device}$ (ppm)
1.	136.5	178.8	150; 150; 150	153.3	+25.5
2.	128.7	168.6	160; 150; 190	166.6	+2
3.	123.2	161.4	160; 130; 180	156.6	+4.8
4.	147	192.6	170; 160; 180	170	+22
5.	106.6	139.7	160; 160; 150	156.6	−26
6.	106.6	139.7	130; 150; 140	140	−0,3
7.	106.6	139.7	130; 130; 130	130	+9.7
8.	100.8	132	130; 130; 120	126.6	+5.4
9.	89.6	117.4	120; 110; 100	110	+7.4
10.	82.6	108	140; 130; 100	123.3	−15
11.	82.6	108	70; 100; 100	90	+18
12.	63.7	83.4	70; 80; 80	76.6	+6.8
13.	48	62.9	40; 60; 50	50	+12.9
14.	39.6	51	40; 60; 50	50	+1
15.	26.2	34.4	30; 20; 20	26.6	+7.8
16.	14.4	18.9	20; 20; 20	20	−1.2

The equation of the line calculated by the least squares method corresponding to the correlation of the concentration indicated by the Alcoholtest device with that one given by the chromatograph is: $C_{device} = 0.426 + 0.947\ C_{cr}$, with the correlation coefficient COR = 0.976.

A M-9 ITIM model chromatograph was used, under the following working conditions: detector FID, Cromosorb 102 column, length = 2 m, Ø = 2.2 mm, $T_{evaporator} = 200°C$, $T_{detector} = 200°C$, $T_{chamber} = 190°C$. The chromatographic device was calibrated with a mixture of ethyl alcohol vapours in the air with a concentration of 84 ppm, moisture 100% at 34°C [22]. The data are to be found in Table 3.

Table 3

The calibration of the chromatograph

No.	Peak area A (mm²)	$\bar{A}$ (mm²)
1.	66.3	
2.	71.4	64.1
3.	54.6	

Finally, the possibility of calibrating the device in alcoholemia has been examinated. For this purpose, we have started from the fact that 2100 ml alveolar air contain a quantity of alcohol equal to that found in 1 ml blood [25]. By a simultaneous determination of the alcoholemia employing the official method at the Legal Medicine Institute and the concentration of the alcohol

vapours from the breathed air by the Alcoholtest device, for three human subjects, we have obtained the results presented in Table 4.

Table 4

The corespondence of the alcoholemia determined with the Alcoholtest device and the legal method

Subject no.	Time from ingestion (h)	Blood alcoholemia legal method (g‰)	Alcoholtest alcoholemia (g‰)
1.	0,5	0,43	0,31
	2	0,29	0,23
2.	0,5	0,2	0,31
	2	0,33	0,46
3.	0,5	0,62	0,50
	2	0,62	0,47

Through the least squares method, the equation of the regression line has been calculated: $A_{blood} = -0.01 + 1.125\ A_{device}$, with COR = 0.701. The poor correlation coefficient could be explained by the small number of the experimental points as well as by the peculiarities of each individual's metabolism.

Conclusions. A SnO_2 based semiconductor sensor, of Taguchi type, for ethyl alcohol vapours has been obtained. The performance of the sensor recommend it to be incorporated into an Alcoholtest device. This device measures the concentration of the ethanol from the breathed air with the possibility of calibration in alcoholemia. It is small sized, portable, capable of operating in severe environmental conditions. The possibility of false indications owing to acetone and acetic acid is minimum. The correctness of the chromatographic method for calibration is attested by the concordance of the alcoholemia analyses determinated through the official method with the device indication, with an error of max. 0.15 g‰. The device solves the specific problems with minimum means and its performances are comparable with more sophisticated similar devices [20, 21].

REFERENCES

1. T. Seiyama, A. Kato, K. Fujiishi, M. Nagatani, *Analyt. Chem.*, *34*, 1502 (1962).
2. Y. Ogata, N. Ogyu, *Japan Kokai*, 76—126897 (1976).
3. M. Hiiata, *Japan Kokai*, 77—70892 (1977).
4. D. Baresel, P. Scharner, G. Huth, Ger. Offen., 2 648 373 (1978).
5. M. Nitta, S. Kanefusa, H. Haradome, *J. Electrochem. Soc.*, **125**, (10), 1676 (1978).
6. T. Takahama, T. Kazama, *Ger. Offen.*, 2 831 394 (1979).
7. T. Takahama, T. Kazama, *Ger. Offen.*, 2 831 400 (1979).
8. S. C. Chang, *IEEE Trans. El. Dev.*, E.D.-**26** (12), 1875 (1979).
9. M. Nitta, M. Haradome, *IEEE Trans. El. Dev.*, E.D.-**36** (3), 247 (1979).
10. M. Nitta, M. Haradome, *J. El. Mat.*, **8** (5), 571 (1979).
11. M. Nitta, M. Haradome, *Oyo Butsuri*, **49**, 132 (1980).
12. S. Chiang, (Electr. Dep., Gen. Motors Res. Lab.) SAE Tech. Pap. Ser. 800537, 107 (1980).

13. Matsushita Electric Industrial Co., Ltd., *Japan Kokai*, 80—158549, (1980).
14. G. N. Advani, A.G. Jordan, *J. El. Mat.*, *9* (1), 29 (1980).
15. H. Pink, L. Freitinger, L. Vitć, *Jap. J. Appl. Phys.*, *19* (3), 513 (1980).
16. Asahi Glass Co., Ltd., Nihon Seiki Co., Ltd., *Jpn. Kokai Tokyo Koho*, 81—51655 (1981).
17. N. Yamazoe, Y. Kurokawa, T. Seiyama, *Chem. Lett.*, 1899 (1982).
18. G. S. V. Coles, K. J. Gallagher, *Sens. Act.*, **7**, 89 (1985).
19. Figaro Gas Sensors, Prospectus (1987).
20. „Atemalkohol-M geräte", Dräger, Austria, 1987.
21. „Alert", Alcohol Contrameasure Systems Co., Canada, 1988.
22. M. Anton, I. Leoca, D. Gheţe, F. Puskas, C. Roman, N. Prodan, I. C. Popescu, E. Cordoş, *Stud. Univ. Babeş-Bolyai, Chem.* **33**, (2), 92 (1988).
23. H. Windischmann, P. Mark, *J. Electrochem. Soc.*, **126** (4), 627 (1979).
24. S. Duţu, I. Teodorescu Exarcu, „Fiziologia şi fiziopatologia respiraţiei", Ed. Medicală, Bucureşti, 1979.
25. I. Quai, M. Terbancea, V. Mărgineanu, L. Popa, „Introducere în teoria şi practica medico-legală", vol. II, Ed. Dacia, Cluj-Napoca, 1979.

STUDIA UNIV. BABEŞ BOLYAI, CHEMIA, XXXV, 1, 1990

SEMICONDUCTOR GAS SENSORS

III[1]. The Operating Mechanism of a SnO_2 Based Sensor for Ethanol

MIRCEA ANTON*, FERENC PUSKÁS*, CARMEN DĂNCESCU**, I. CĂTĂLIN POPESCU*, and EMIL CORDOŞ*.

Received May 9, 1989

The experimental results obtained with a semiconductor SnO_2 based sensor made in our laboratory are discussed referring to the theoretical operating model proposed by Windischmann and Mark.

Introduction. The great interest in creating new semiconductor gas sensors is justified by a number of functional characteristics as: small size, rapidly in response, high sensitivity and the posibility of them being included into a high integrated structure. These qualities confer them a certain competitivity among different methods of gas analysis [1]. Nowadays, the efforts are made in the direction of improving the main deficiency of this type of sensor, the reduced selectivity [2—5]. On the other hand, although these sensors are utilized in practice on a large scale, their operating mechanism is not yet entirely cleared up [6, 7].

The present paper presents a number of experimental results obtained with a semiconductor SnO_2 based sensor of a proper construction [8], Taguchi model [9]. The results are examined on the basis of the operating model proposed by Windischmann and Mark [10].

Experimental results. The electric circuit in which the sensors are included for measurement performance, the sensor construction as well as the installation for gas mixture preparation have been previously described [11, 12].

1. *The temperature window.* An important characteristic of the sensors is the temperature window, i.e. the temperature range in which they can function. The dependence of the sensor signal, upon the working temperature, at different concentrations of ethanol vapours in the air, is shown in fig. 1. The measurings have been fulfilled in the dynamic way. The temperature variation rate has been chosen in a manner the sensor should work at equilibrium.

2. *The determination of the order of reaction.* Measuring the evolution of the signal vs time at different concentrations of ethanol and acetaldehyde, at constant temperature, the order of reaction corresponding to the reaction lying at the basis of the response of the sensor can be determined. Hence, the conductance variation of the sensor $\Delta G_{3s} = G_g - G_a$ has been measured, where G_g is the conductance after 3 s from the moment of introducing the sensor into the gas and G_a is the conductance in the air. The experimental data are presented in Table 1.

3. *The estimation of the activation energy.* The study on the evolution of the signal depending on the temperature (in the „a" zone of the temperature window) at a constant gas concentration enables the calculation of the activation energy of the detection reaction for various substances of interest. The sensor signal value after 3 s since its appearance, at different temperatures, has been measured. The experimental data are shown in Table 2.

* *University of Cluj, Faculty of Chemical Technology*
** *Territorial Computing Center, Cluj, Romania*

Discussions. Windischmann and Mark [10] have proposed an operating model for a thin film SnO_2 CO sensor. The model takes into consideration the following experimental data: [i] the existence of an optimum temperature range in the function of the sensor, [ii] the dependence of the sensor conductance upon the square root of the CO concentration in the air, [iii] the Arrhenius type temperature dependence of the sensor signal.

The experimental results obtained with a thick sintered film SnO_2 sensor functioning in ethanol vapours correspond to a large extent to the model mentioned above.

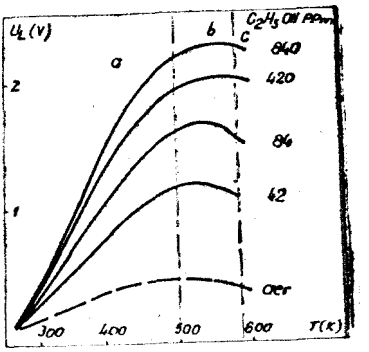

Fig. 1. The temperature window; the increasing temperature rate 15 K/min.

Table 1

The dependence of the conductance variation upon the concentration of the volatile substance

Substance	Concentration (ppm)	$\Delta G_{as} \times 10^{-5}$ ($\Omega^{-1}s^{-1}$)
C_2H_5OH	42	1.87
	84	3.01
	420	8.38
	840	11.8
	1260	15.0
C_3H_6O	43	0,57
	87	1,72
	435	2,48
	870	5,03
	1305	5,14

1. *The temperature window.* As fig. 1 shows, one can notice the existence of a temperature range for the best performance of the sensor. At a too low temperature, the reaction products of the ethanol on the surface of the sensor are not desorbed, thus blocking the surface. At a too high temperature, the oxygen from the atmosphere as well as the ethanol are not adsorbed on the surface so that the detection reaction can not occur.

Using the data (table 3) corresponding to a temperature of 530 K from the „b" zone of the temperature window, it has been calculated the equation $\lg \Delta G/G_a = f(\lg c)$: $\lg \Delta G/G_a = -0.81 + 0.545 \lg c$. The slope of the line calculated through the least squares method is in good agree to the theoretical value 0.500 and the correlation coefficient is 0.974.

2. *The order of reaction.* It can be determined taking into consideration the chemical kinetics. The variation rate of the sensor conductance provides informations about the surface reaction rate. Hence, in the first approximation,

Table 2

The dependence of the conductance variation upon the temperature

Substance	T(K)	$\Delta G_{gs} \times 10^{-5}$ ($\Omega^{-1}s^{-1}$
C_2H_5OH (420 ppm)	398	0,66
	425	6,96
	453	6,83
	485	10.5
CH_3OH (606 ppm)	440	0.27
	469	0,72
	502	2.72
	537	9.12
	576	10.7
C_2H_4O (434 ppm)	401	0.63
	428	1.36
	457	2.74
	488	5.25
	522	9.22
$C_2H_4O_2$ (428 ppm)	488	0.28
	522	0.46
	558	2.16
	598	7.18
	617	8.31

Table 3

Experimental data for sensor calibration (in C_2H_5OH)

Ethanol concentration (ppm)	lg c	U_{Lgas} (V)	U_{Lair} (V)	lg $\frac{\Delta G}{Ga}$
16.8	1.22	1.24		−0.23
42	1.62	1.56		0.07
84	1.92	2.10	0.86	0.39
252	2.40	2.30		0.49
420	2.62	2.56		0.61
840	2.92	2.84		0.73

the rate equation of the detection reaction is considered to be: $-\Delta G_{gs}/\Delta t = kc$. Representing the data from Table 1 in coordinates of $\lg \Delta G_{gs} = f(\lg c)$, we obtain the lines the parameters of which are shown in Table 4.

The order of reaction vs the substance to be detected is numerically equal to the slope of the line (B). The obtained experimental values are smaller than the theoretical value, equal to 1, which derives from the reaction mechanism [10]. This discrepancy results, probably, from the fact that in the process of detecting ethanol and acetaldehyde much more stages appear than in that one corresponding to CO oxidation considered for the theoretical model proposed

and verified by Windischimann and Mark. It is also necessary to take into account the possible difference in the sensor construction.

3. *The activation energy*. The activation energy used in the process of detection has been determined employing the data from table 2 in a representation $\lg G_{gs} = f(1/T)$. From the slope of the obtained line, E_a is determined.

Table 4

The parameters of the lines $\lg G_{gs} = f(\lg c)$

Substance	Line parameters		Correlation coefficient
C_2H_5OH	−5.702	0.610	0.999
C_2H_4O	−5.820	0.545	0.900

Table 5

The activation energies

Substance	Activation energy (K cal/mol)	Correlation coefifcient
Ethanol	2.30	0.953
Methanol	2.30	0.983
Acetaldehyde	1.60	0.999
Acetic acid	2.45	0.985

The values of the activation energies for the studied substances as well as the correlation coefficient are presented in table 5. The activation energy has minimum values for acetaldehyde in conformity with the established fact that acetaldehyde appears as the main agent in the reaction of ethanol on SnO_2 [13]:

$$C_2H_5OH \longrightarrow H + C_2H_5O$$
$$H + C_2H_5O \longrightarrow C_2H_5OH$$
$$C_2H_5O \longrightarrow H + H(CH_3)CO$$
$$H + H + O \longrightarrow H_2O$$
$$C_2H_5OH \longrightarrow H_2O + C_2H_4$$
$$H(CH_3)CO \longrightarrow V_0 + CH_3COOH$$
$$CH_3COOH \longrightarrow CH_2 = CO + H_2O$$

Taking into account that the values of the activation energies are relatively small and they have been measured in the „a" zone from Fig. 1, we consider that they correspond rather to the physisorption of the detected vapours than to a chemisorption.

Conclusions. The experimental results obtained with a thick sintered film SnO_2 sensor in the presence of ethanol are, to a great extent, in conformity with the theoretical model proposed for CO detection with a thin film SnO_2 sensor. Thus: [i] a temperature range in which the sensor functions has been found, [ii] the sensor conductance depends on the concentration of ethanol in the air as in the equation $\Delta G = kc^n$, where $n \approx 0.5$, [iii] the sensor signal has an Arrhenius type temperature. This operating model is, probably, common regarding the basic characteristics to the semiconductors employed in gas sensor construction, indifferently the constructive variant and the nature of the gas.

REFERENCES

1. G. S. V. Coles, K. J. Gallagher, J. Watson, *Sensors and Actuators*, **7**, 89 (1985).
2. A. Hooper, B. C. Tofield, P. T. Moseley, D. E. Williams, *Solid State Gas Sensors*, The State of the Art, AERE Harwell, Oxfordshire, March 1984.
3. N. Yamazoe, Y. Kurokawa, T. Seiyama, *Chem. Lett.*, 1899 (1982).
4. T. E. Edmonds, *Trends in Analytical Chem.*, **4**, (9), 220 (1985).
5. D. K. Burns, P. N. Kember, S. Taylor, E. W. Williams, *Environmental Technol. Lett.*, **1**, 259 (1980).
6. H. Ogawa, A. Abe, M. Nishikawa, S. Hayakawa, *J. Electrochem. Soc.*, **128** (9), 2020 (1981).
7. N. Yamazoe, Y. Kurokawa, T. Seiyama, *Sensors and Actuators*, **4**, 283 (1983).
8. M. Anton, F. Puskas, C. Roman, N. Prodan, I. C. Popescu, E. Cordoş, Procedeu de obţinere a unui senzor semiconductor pe bază de SnO_2 pentru vapori de alcool etilic în aer, Patent RSR (in patenting).
9. Figaro Gas Sensors, Prospectus (1987).
10. H. Wiedischmann, P. Mark, *J. Electrochem. Soc.*, **126** (4), 627 (1979).
11. M. Anton, I. Leoca, D. Ghete, F. Puskas, C. Roman, N. Prodan, I. C. Popescu, E. Cordoş, *Stud. Univ. Babeş-Bolyai, Chem.*, **33** (2), 92 (1988).
12. M. Anton, F. Puskas, C. Roman, N. Prodan, I. C. Popescu, E. Cordoş, *Stud. Univ. Babeş-Bolyai, Chem.*, **33** (1) (1939).
13. G. Heilard, D. Kohl, International Meeting on Chemical Sensors, Fukuoka, Japan (198)

STUDIA UNIV. BABEŞ BOLYAI, CHEMIA, XXXV, 1, 1990

MOLECULAR TOPOLOGY. 5. [1]. RECURSIVE RELATIONSHIPS FOR COMPUTING Y-INDICES IN SOME PARTICULAR GRAPHS

MIRCEA V. DIUDEA* and LUCINIA BAL**

Received: December 13, 1989

The matrix representation of graphs, including the newly proposed layer matrices [1] meant to characterize molecular branching, is presented. On this ground, recursive relationships that compute the Y-topological index in some particular graphs were derived. The above mentioned Y-topological indices have been tested for their correlating ability on a heterogeneous set of straight-chain chemical compounds.

1. **Introduction.** In mathematical chemistry, molecular structures are represented by unoriented planar graphs in which vertices stand for atoms and edges for covalent bonds. Thus, a graph G is defined as an ordered pair consisting of two sets V and E, $G = (V, E)$, where V is the finite (and nonempty) set of vertices and E represents the set of ordered pairs (u, v) of adjacent vertices, or in other words, the set of edges. A molecular graph will always be a connected graph. A multigraph denotes molecules with multiple covalent bonds. The covalent bonds will be represented by weights showing their conventional bond order: 1 for single, 2 for double, 3 for triple and 1.5 for aromatic bond, respectively. The graph theoretical distance d(u, v), is the number of edges in the shortest path joining the vertices $u \in V$ and $v \in V$.

Some graph constructions (nonnumerical characteristics) in G can be expressed as follows [2]:

— vertex eccentricity

$$e(u) = \max_{v \in V} d(u, v) \tag{1}$$

— graph radius

$$r(G) = \min_{u \in V} e(u) = \min \max_{v \in V} d(u, v) \tag{2}$$

— graph diameter

$$d(G) = \max_{u \in V} e(u) = \max \max_{v \in V} d(u, v) \tag{3}$$

The last two constructions are 'max-min' concepts [3]. The degree of a vertex u, denoted k (or δ or deg u) equals the number of edges incident in u.

Two graphs are said isomorphic ($G_1 \simeq G_2$) if there is an one-to-one application $V_1 \rightarrow V_2$ that preserves node adjacency. An automorphism is an isomorphism of G onto itself.

The set V can include all atoms of an empirical formula or only the 'nonhydrogen' atoms. If the hydrogen atoms are not involved in important steric or electronic interactions, one prefers the 'hydrogen suppressed graphs'.

* University of Cluj, Faculty of Chemical Technology, 3400 Cluj-Napoca, Romania
** Territorial Computing Center, 3400 Cluj-Napoca, Romania

2. **Matrix Reprezentation of Molecular Graphs.** Since 1874 Sylvester [4] has prompted that an organic molecule can be represented by an adjacency matrix, A(G), defined as in (4):

$$A(G) = \begin{cases} a_{ii} = 0 \\ a_{ij} = 0\,;\ (i,\ j) \notin E(G) \\ a_{ij} = 1\,;\ (i,\ j) \in E(G) \end{cases} \qquad (4)$$

For the graph G_1, $A(G_1)$ will be:

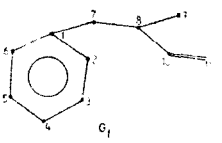

$$A(G_1) = \begin{Vmatrix} 0 & 1 & 0 & 0 & 0 & 1 & 1 & 0 & 0 & 0 & 0 \\ 1 & 0 & 1 & 0 & 0 & 0 & 0 & 0 & 0 & 0 & 0 \\ 0 & 1 & 0 & 1 & 0 & 0 & 0 & 0 & 0 & 0 & 0 \\ 0 & 0 & 1 & 0 & 1 & 0 & 0 & 0 & 0 & 0 & 0 \\ 0 & 0 & 0 & 1 & 0 & 1 & 0 & 0 & 0 & 0 & 0 \\ 1 & 0 & 0 & 0 & 1 & 0 & 0 & 0 & 0 & 0 & 0 \\ 1 & 0 & 0 & 0 & 0 & 0 & 0 & 1 & 0 & 0 & 0 \\ 0 & 0 & 0 & 0 & 0 & 0 & 1 & 0 & 1 & 1 & 0 \\ 0 & 0 & 0 & 0 & 0 & 0 & 0 & 1 & 0 & 0 & 0 \\ 0 & 0 & 0 & 0 & 0 & 0 & 0 & 1 & 0 & 0 & 1 \\ 0 & 0 & 0 & 0 & 0 & 0 & 0 & 0 & 0 & 1 & 0 \end{Vmatrix}$$

Fig. 1.

To indicate the weight of bonds, one uses the connectivity matrix, A'(G') where nonzero entries equal the conventional bond order. Figure 2 shows $A'(G_1)$:

$$A'(G_1) = \begin{Vmatrix} 0 & 1.5 & 0 & 0 & 0 & 1.5 & 1 & 0 & 0 & 0 & 0 \\ 1.5 & 0 & 1.5 & 0 & 0 & 0 & 0 & 0 & 0 & 0 & 0 \\ 0 & 1.5 & 0 & 1.5 & 0 & 0 & 0 & 0 & 0 & 0 & 0 \\ 0 & 0 & 1.5 & 0 & 1.5 & 0 & 0 & 0 & 0 & 0 & 0 \\ 0 & 0 & 0 & 1.5 & 0 & 1.5 & 0 & 0 & 0 & 0 & 0 \\ 1.5 & 0 & 0 & 0 & 1.5 & 0 & 0 & 0 & 0 & 0 & 0 \\ 1 & 0 & 0 & 0 & 0 & 0 & 0 & 1 & 0 & 0 & 0 \\ 0 & 0 & 0 & 0 & 0 & 0 & 1 & 0 & 1 & 1 & 0 \\ 0 & 0 & 0 & 0 & 0 & 0 & 0 & 1 & 0 & 0 & 0 \\ 0 & 0 & 0 & 0 & 0 & 0 & 0 & 1 & 0 & 0 & 2 \\ 0 & 0 & 0 & 0 & 0 & 0 & 0 & 0 & 0 & 2 & 0 \end{Vmatrix}$$

Fig 2.

Another useful matrix is the distance matrix, D(G). It does not specify bond weights but only collects the topological distances for each vertex $i \in G$. This matrix can be obtained by calculating the power matrices $\mathfrak{A}^p (p \leqslant d(G))$; $\mathfrak{A} = U.A$, (with U — the unity matrix), by using the boolean operators. For G_2, the power matrices are depicted in Fig. 3 (with the newly introduced entries enclosed in rings):

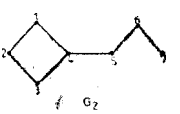

$$\mathfrak{A}(G_2) = \begin{Vmatrix} \textcircled{1} & 1 & 0 & 1 & 0 & 0 & 0 \\ 1 & \textcircled{1} & 1 & 0 & 0 & 0 & 0 \\ 0 & 1 & \textcircled{1} & 1 & 0 & 0 & 0 \\ 1 & 0 & 1 & \textcircled{1} & 1 & 0 & 0 \\ 0 & 0 & 0 & 1 & \textcircled{1} & 1 & 0 \\ 0 & 0 & 0 & 0 & 1 & \textcircled{1} & 1 \\ 0 & 0 & 0 & 0 & 0 & 1 & \textcircled{1} \end{Vmatrix}$$

Fig 3.

$$\mathfrak{A}^2(G_2)x = \left\| \begin{matrix} 1 & 1 & \textcircled{1} & 1 & \textcircled{1} & 0 & 0 \\ 1 & 1 & 1 & \textcircled{1} & 0 & 0 & 0 \\ \textcircled{1} & 1 & 1 & 1 & \textcircled{1} & 0 & 0 \\ 1 & \textcircled{1} & 1 & 1 & 1 & \textcircled{1} & 0 \\ \textcircled{1} & 0 & \textcircled{1} & 1 & 1 & 1 & \textcircled{1} \\ 0 & 0 & 0 & \textcircled{1} & 1 & 1 & 1 \\ 0 & 0 & 0 & 0 & \textcircled{1} & 1 & 1 \end{matrix} \right\| \qquad \mathfrak{A}^3(G_2) = \left\| \begin{matrix} 1 & 1 & 1 & 1 & 1 & \textcircled{1} & 0 \\ 1 & 1 & 1 & 1 & \textcircled{1} & 0 & 0 \\ 1 & 1 & 1 & 1 & 1 & \textcircled{1} & 0 \\ 1 & 1 & 1 & 1 & 1 & 1 & \textcircled{1} \\ 1 & \textcircled{1} & 1 & 1 & 1 & 1 & 1 \\ \textcircled{1} & 0 & \textcircled{1} & 1 & 1 & 1 & 1 \\ 0 & 0 & 0 & \textcircled{1} & 1 & 1 & 1 \end{matrix} \right\|$$

$$\mathfrak{A}^4(G_2) = \left\| \begin{matrix} 1 & 1 & 1 & 1 & 1 & 1 & \textcircled{1} \\ 1 & 1 & 1 & 1 & 1 & \textcircled{1} & 0 \\ 1 & 1 & 1 & 1 & 1 & 1 & \textcircled{1} \\ 1 & 1 & 1 & 1 & 1 & 1 & 1 \\ 1 & 1 & 1 & 1 & 1 & 1 & 1 \\ 1 & \textcircled{1} & 1 & 1 & 1 & 1 & 1 \\ \textcircled{1} & 0 & \textcircled{1} & 1 & 1 & 1 & 1 \end{matrix} \right\| \qquad \mathfrak{A}^5(G_2) = \left\| \begin{matrix} 1 & 1 & 1 & 1 & 1 & 1 & 1 \\ 1 & 1 & 1 & 1 & 1 & 1 & \textcircled{1} \\ 1 & 1 & 1 & 1 & 1 & 1 & 1 \\ 1 & 1 & 1 & 1 & 1 & 1 & 1 \\ 1 & 1 & 1 & 1 & 1 & 1 & 1 \\ 1 & 1 & 1 & 1 & 1 & 1 & 1 \\ 1 & \textcircled{1} & 1 & 1 & 1 & 1 & 1 \end{matrix} \right\|$$

Fig. 3. (continued)

Thus, the D matrix is constructed by introducing the distance p instead of the marker rings, for each power matrix:

$$D(G_2) = \left\| \begin{matrix} 0 & 1 & 2 & 1 & 2 & 3 & 4 \\ 1 & 0 & 1 & 2 & 3 & 4 & 5 \\ 2 & 1 & 0 & 1 & 2 & 3 & 4 \\ 1 & 2 & 1 & 0 & 1 & 2 & 3 \\ 2 & 3 & 2 & 1 & 0 & 1 & 2 \\ 3 & 4 & 3 & 2 & 1 & 0 & 1 \\ 4 & 5 & 4 & 3 & 2 & 1 & 0 \end{matrix} \right\|$$

Fig. 4.

Layer matrices. The layer matrices $\{2\}$ are arrays which collect the ordered partitions of all vertices $v_i \in G$. Fig. 5 shows such relative partitions in G_2:

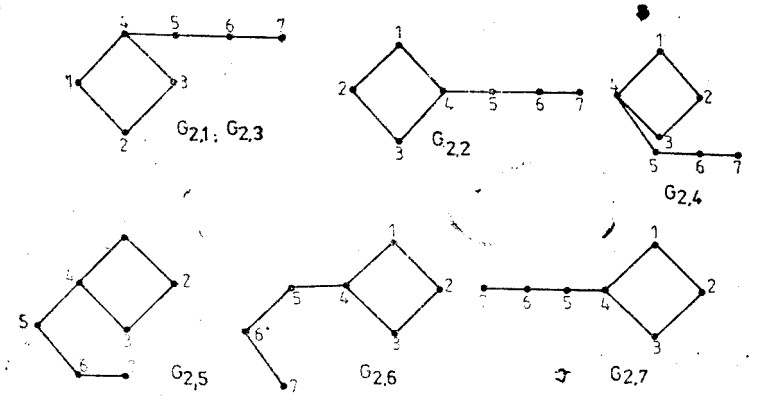

Fig. 5.

F matrix. Distance frequency matrix, F, counts the number of chains of lenght j in the relative partition of vertex i (row i in D matrix). Its entries, f_{ij} also

mean the number of vertices in a layer at distance j from the relative partition i, in G. Skorobogatov [2], called this array the λ matrix.

$$F(G_2) = \begin{Vmatrix} 2 & 2 & 1 & 1 & 0 \\ 2 & 1 & 1 & 1 & 1 \\ 2 & 2 & 1 & 1 & 0 \\ 3 & 2 & 1 & 0 & 0 \\ 2 & 3 & 1 & 0 & 0 \\ 2 & 1 & 2 & 1 & 0 \end{Vmatrix} \qquad X(G_2) = \begin{Vmatrix} 2 & 3 & 1 & 1 & 0 \\ 2 & 2 & 1 & 1 & 1 \\ 2 & 3 & 1 & 1 & 0 \\ 3 & 3 & 1 & 0 & 0 \\ 2 & 3 & 2 & 0 & 0 \\ 2 & 1 & 2 & 2 & 0 \end{Vmatrix}$$

Fig. 6.

X matrix. Analog to matrix F, one can construct a layer matrix X(G)(also called λx in ref. [2]), that counts the ares connecting layers j and j−1 in the relative partition i. Figure 6 shows the matrices F and X for G_2.

B matrix (branch). The entries b_{ij} of the branch matrix B (see ref. [1]) represent the sum of the vertex degrees in the layer j of the relative partition i in G. B can be built starting from the DDG matrix (see Fig. 7), defined as:

$$DDG(G) = D(G) + DG(G) \tag{5}$$

where D(G) is the distance matrix and DG(G) stands for the diagonal matrix of the vertex degrees (see ref. [5]). In B, the diagonal entries of DDG will become the column j = 1. The next j layers result by summing the diagonal entries of DDG corresponding to distance j−1 on the i-th row in DDG.

$$\begin{Vmatrix} 2 & 1 & 2 & 1 & 2 & 3 & 4 \\ 1 & 2 & 1 & 2 & 3 & 4 & 5 \\ 2 & 1 & 2 & 1 & 2 & 3 & 4 \\ 1 & 2 & 1 & 3 & 1 & 2 & 3 \\ 2 & 3 & 2 & 1 & 2 & 1 & 2 \\ 3 & 4 & 3 & 2 & 1 & 2 & 1 \\ 4 & 5 & 4 & 3 & 2 & 1 & 1 \end{Vmatrix} \quad \begin{Vmatrix} 2 & 5 & 4 & 2 & 1 & 0 \\ 2 & 4 & 3 & 2 & 2 & 1 \\ 2 & 5 & 4 & 2 & 1 & 0 \\ 3 & 6 & 4 & 1 & 0 & 0 \\ 2 & 5 & 5 & 2 & 0 & 0 \\ 2 & 3 & 3 & 4 & 2 & 0 \\ 1 & 2 & 2 & 3 & 4 & 2 \end{Vmatrix} \quad \begin{Vmatrix} 2 & 3 & 1 & 1 & 0 \\ 2 & 2 & 1 & 1 & 1 \\ 2 & 3 & 1 & 1 & 0 \\ 3 & 3 & 1 & 0 & 0 \\ 2 & 3 & 2 & 0 & 0 \\ 2 & 1 & 2 & 2 & 0 \\ 1 & 1 & 1 & 2 & 2 \end{Vmatrix} \quad \begin{Vmatrix} 2 & 4 & 2.5 & 1.5 & 0.5 & 0 \\ 2 & 3 & 2 & 1.5 & 1.5 & 0.5 \\ 2 & 4 & 2.5 & 1.5 & 0.5 & 0 \\ 3 & 4.5 & 2.5 & 1.5 & 0 & 0 \\ 2 & 4 & 3.5 & 1 & 0 & 0 \\ 2 & 2 & 2.5 & 3 & 1 & 0 \\ 1 & 1.5 & 1.5 & 2.5 & 3 & 1 \end{Vmatrix}$$

DDG (G_2) B(G_2) Fig. 7. E(G_2) S(G_2)

The matrix B is a n*(d + 1) array; n equals the number of vertices in G and d is the graph diameter. In B, $\sum_i b_{i1} = 2q$ and $\sum_j b_{ij} = 2q$, where q stands for the number of edges in G. This matrix was introduced [1] with the aim to characterise the molecular branching.

E matrix (edges). This matrix collects the number of edges emerging from the vertices in layer j of the relative partition i in G (fig. 7). In E, $\sum_i e_{i1} = 2q$ and $\sum_j e_{ij} = q$, the last relation being general for E but not for X matrices (see ref. [1]). Thus, in the case of an elementary cycle, e.g. cyclopentane (fig. 8), the two matrices X and E are different. One is to observe that for X stands $\sum_j x_{ij} \neq q$.

S matrix (sigma). This matrix corresponds to the complete FX(G) matrix (see ref. [2]). Its entries are $s_{ij} = 1/2\ (b_{ij} + e_{ij})$. This matrix has been constructed (see fig. 7 and ref. [1]) with the aim to discriminate pairs of graphs showing the same B (but different E). However, Skorobogatov's nonisomorphic pair shows the same S (fig. 9).

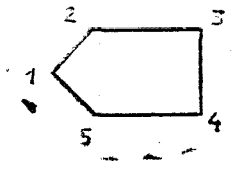

$$X = \begin{Vmatrix} 2 & 2 \\ 2 & 2 \\ 2 & 2 \\ 2 & 2 \\ 2 & 2 \end{Vmatrix} \qquad E = \begin{Vmatrix} 2 & 2 & 1 \\ 2 & 2 & 1 \\ 2 & 2 & 1 \\ 2 & 2 & 1 \\ 2 & 2 & 1 \end{Vmatrix}$$

Fig. 8.

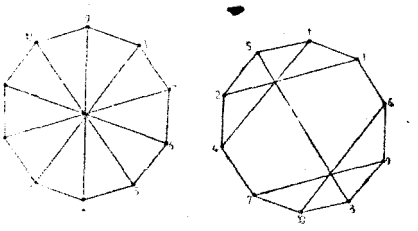

Fig. 9.

Although the sigma matrix does not solve the isomorphism problem, its degeneracy is extremely low and provides a good tool in ordering the structures [1].

The layer — matrices can be represented in a linear from as:

$$B(G_2) \;||\, 1,3(2,5,4,2,1,0)\,;\; 2(2,4,3,2,2,1)\,;\; 4(3,6,4,1,0,0)\,; \\ 5(2,5,5,2,0,0)\,;\; 6(2,3,3,4,2,0)\,;\; 7(1,2,2,3,4,2)\;|| \qquad (6)$$

When the vertex numbers are not necessary, the canonical linear form (including a multiplicity of a similar rows) will be:

$$B(G_2) = ||\, (2,4,3,2,2,1)\,;\; (1,2,2,3,4,2)\,;\; 2(2,5,4,2,1,0)\,; \\ (2,3,3,4,2,0)\,;\; (3,6,4,1,0,0)\,;\; (2,5,5,2,0,0)\;|| \qquad (7)$$

The regressive degrees index. Y. In the above work we stated that th-regressive degree of a vertex i in G_i represents its degree weighted by the entries b_{ij} in the relative partition i, in a distance decreasing manner. This manner can differ from operator to operator. The present work deals only with the two operators proposed in ref. [1], some others being detailed in the next paper [6].

Thus, the regressive degrees $YR_i^{(t)}$ and the corresponding local contributions for multigraph (if needed) are as follows:

$$YR_i^{(1)} = \sum_j (y_{ij}) j^{-3}\,; \qquad YL_i^{(1)} = f_i * \sum_{j=i}^{2} (y_{ij})(j+1)^{-3} \qquad (8)$$

$$YR_i^{(2)} = \sum_j (y_{ij})\, 10^{1-j}\,; \qquad YL_i^{(2)} = f_i * \sum_{j=1}^{2} (y_{ij})\, 10^{-j} \qquad (9)$$

where: y_{ij} — denotes the entries in one of the matrices B, E or S, respectively

f_i — the multigraph factor, $f_i = \sum_j (c_{ij} - 1)$, with

c_{ij} — the conventional bond order.

The Y indices, constructed with these operators show the general form

$$MY^{(t')} = k'\left[\sum_i (YR_i^{(t)} + YI_i^{(t)})\, w_i\right]^p \qquad (10$$

where t', t represent labels for global (operational stage) and local (assignment stage) operators, respectively

M — stands for the matrix type (E, B or S)

k' — is a normalizing multiplicator (for $t = t' = 1$; $k' = 2nq$; $M = B$ $k' = nq$, $M = E$; $k' = 3nq$, $M = S$)

w_i — is a weighting factor, characterizing the vertices by group electronegativities or fragmental van der Waals volumes (see [1]); $w_i =$ for nonweighted graphs

p — is the exponent (if $t' = 1$ then $p = -1$; $t' = 2$ then $p = 1$).

3. **Recursive relationships for computing Y — indices.** In the above work [1] we presented some recursive relationships for computing the Y — indices. We also introduced the linear forms for the matrices of some graphs: straight chain alkanes, cycloalkanes, stars and complete graphs (the last two of interest in the graph theory). In the present work we complete the list with some other recurrences.

Recurrences for straight-chain alkanes. For a straight-chain (i.e. n-alkanes) the rows of the B-matrix do not have a very simple form. Considering the symmetry of the straight-chaing, the relationships can be written as follows

$$B(P_n\text{-even}) = \| \underbrace{2(1,2\ldots2,1)}_{2k-2};\ \underbrace{2(2,4\ldots4,3,2\ldots2,1,0\ldots0)}_{i-2\quad 2(k-i)\quad i-1};\ i \in \{2, k-1\}$$

$$\underbrace{2(2,4\ldots4,3,1,0\ldots0)}_{i-2\quad i-1} \| \qquad (11)$$

$$i = k;\quad i > 1$$

$$\text{with } n = 2k$$

$$B(P_n\text{-odd}) = \| \underbrace{2(1,2\ldots2,1)}_{2k-1};\ \underbrace{2(2,4\ldots4,3,2\ldots2,1,0\ldots0)}_{i-2\quad 2(k-i)+1\quad i-1};\ i \in \{2, k\}$$

$$\underbrace{(2,4\ldots4,2,0\ldots0)}_{i-2\quad i-1} \| \qquad (12)$$

$$i = k + 1$$

$$\text{with } n = 2k + 1$$

$$BY^{(1)}(P_n\text{-even}) = 4k(2k-1)\left\{\sum_{p=1}^{2}\left[1+2\sum_{j=2}^{2k-1}j^{-3}+(2k)^{-3}\right]w_{1p}+\right.$$

$$+\sum_{p=1}^{2}\sum_{i=2}^{k-1}\left[2+4\sum_{j=2}^{i-1}j^{-3}+3i^{-3}+2\sum_{j=i+1}^{2k-i}j^{-3}+(2k-i+1)^{-3}\right]w_{ip}+$$

$$\left.+\sum_{p=1}^{2}\left[2,+4\sum_{j=2}^{k-1}j^{-3}+3k^{-3}+(k+1)^{-3}\right]w_{kp}\right\}^{-1} \qquad (13)$$

$$BY^{(1)}(P_n\text{-odd}) = 4k(2k+1)\left\{\sum_{p=1}^{2}\left[1+2\sum_{j=2}^{2k}j^{-3}+(2k+1)^{-3}\right]w_{1p}+\right.$$

$$+\sum_{p=1}^{2}\sum_{i=2}^{k}\left[2+4\sum_{j=2}^{i-1}j^{-3}+3i^{-3}+2\sum_{j=i+1}^{2k+1-i}j^{-3}+(2k-i+2)^{-3}\right]w_{ip}+$$

$$\left.+\left[2+4\sum_{j=2}^{k}j^{-3}+2(k+1)^{-3}\right]w_{k+1}\right\}^{-1} \qquad (14)$$

$$EY^{(2)}(P_n\text{-even}) = \sum_{p=1}^{2}(1+2\sum_{j=2}^{2k-1}10^{1-j}+10^{1-2k})w_{1p}+\sum_{p=1}^{2}\sum_{i=2}^{k-1}(2+4\sum_{j=2}^{i-1}10^{1-j}+$$

$$+3*10^{1-i}+2\sum_{j=i+1}^{2k+1-i}10^{1-j}+10^{i-2k})w_{ip}+\sum_{p=1}^{2}(2+4\sum_{j=2}^{k-1}10^{1-j}+$$

$$+3*10^{1-k}+10^{-k})w_{kp} \qquad (15)$$

$$BY^{(2)}(P_n\text{-odd}) = \sum_{p=1}^{2}(1+2\sum_{j=2}^{2k}10^{1-j}+10^{-2k})w_{1p}+\sum_{p=1}^{2}\sum_{j=2}^{k}(2+4\sum_{j=2}^{i-1}10^{1-j}+$$

$$+3*10^{1-i}+2\sum_{j=i+1}^{2k+1-i}10^{1-j}+10^{i-2k-1})w_{ip}+(2+4\sum_{j=2}^{k}10^{1-j}+2*10^{-k})w_{k+1} \qquad (16)$$

Despite relative complexity, such recurrences are useful in the case of weighted graphs (see below). It is obvious that they are not suitable for large values of n. Considering sum associativity, $Y^{(1)}$ and $Y^{(2)}$ can be written, respectively:

$$Y^{(1)} = k'\left[\sum_i\sum_j y_{ij}*j^{-3}\right]^{-1} = k'\left[\sum_j\sum_i y_{ij}*j^{-3}\right]^{-1} \qquad (17)$$

$$Y^{(2)} = \sum_i\sum_j y_{ij}*10^{1-j} = \sum_j\sum_i y_{ij}*10^{1-j} \qquad (18)$$

Thus, the matrices B, E, S can be written as sums of columns:

$$\sum_i B(P_n) = [\,2(n-1)\,;\,4(n-j)+2\,]\,;\; j\in\{2,n\} \qquad (19)$$

$$\sum_i E(P_n) = \{2(n-j);\ j \in \{1, n-1\}\} \quad (20)$$

$$\sum_i S(P_n) = \{2(n-1);\ 3(n-j)+1;\ 1 \mid j \in \{2, n-1\}\} \quad (21)$$

Hence, the Y-indices can be easier computed if n is either odd or even :

$$BY^{(1)} = 2n(n-1)\left[2(n-1) + \sum_{j=2}^{n} [4(n-j)+2]*j^{-3}\right]^{-1} \quad (22)$$

$$BY^{(2)} = 2(n-1) + \sum_{j=2}^{n}\left[4(n-j)+2\right]*10^{1-j} \quad (23)$$

$$EY^{(1)} = n(n-1)\left[2\sum_{j=2}^{n}(n-j)*j^{-3}\right]^{-1} \quad (24)$$

$$EY^{(2)} = 2\sum_{j=1}^{n-1}(n-j)*10^{1-j} \quad (25)$$

$$SY^{(1)} = 3n(n-1)\left[2(n-1) + \sum_{j=2}^{n-1} 3(n-j)+1\right]*j^{-3} + n^{-3}\Big]^{-1} \quad (26)$$

$$SY^{(2)} = 2(n-1) + \sum_{j=2}^{n-1}\left[3(n-j)+1\right]*10^{1-j} + 10^{1-n} \quad (27)$$

All these indices tend towards infinity when n increases.

In the previous paper [1] we also introduced recurrences based on the previous term :

$$BY^{(2)}(P_n) = BY^{(2)}(P_{n-1}) + \Delta B \quad (28)$$

$$\text{where } \Delta B = 2 + 4\sum_{j=2}^{n-1} 10^{1-j} + 2*10^{1-n} \quad (29)$$

Similarly, for $EY^{(2)}$, one can write :

$$EY^{(2)}(P_n) = EY^{(2)}(P_{n-1}) + \Delta E \quad (30)$$

$$\text{where } \Delta E = 2\sum_{j=1}^{n-2} 10^{1-j} + 2*10^{2-n} \quad (31)$$

No recurrence is needed for $SY^{(2)}$, as

$$SY^{(2)}(P_n) = 1/2\,[BY^{(2)}(P_n) + EY^{(2)}(P_n)] \quad (32)$$

Recurrences for cycloalkanes. The recursive relations for cycloalkanes depend on the parity of elementary cycles. Table 1 shows the recurrences for cycloalkanes.

In a future paper [7], general recursions for $MY^{(2)}$ (that do not depend on cycle parity) will be presented.

Table 1

Recurrences for cycloalkanes

C_{2k}	C_{2k+1}
$B = \|\|2k(2, 4 \ldots 4, 2)\|\|$ with $k - 1$ digits 4	$B = \|\|(2k + 1)(2, 4 \ldots 4)\|\|$ with k digits 4
$E = \|\|2k(2, \ldots 2)\|\|$ with k digits 2	$E = \|\|(2k + 1)(2, \ldots 2, 1)\|\|$ with k digits 2
$BY^{(1)} = 2k\left[1 + 2\sum_{j=2}^{k} j^{-3} + (k+1)^{-3}\right]^{-1}$	$BY^{(1)} = (2k+1)(1 + 2\sum_{j=2}^{k+1} j^{-3})^{-1}$
$BY^{(2)} = 4k(1 + 2\sum_{j=2}^{k} 10^{1-j} + 10^{-k})$	$BY^{(2)} = (2k+1)(1 + 2\sum_{j=2}^{k+1} 10^{1-j}$
$EY^{(1)} = 2k(2\sum_{j=1}^{k} j^{-3})^{-1}$	$EY^{(1)} = (2k+1)\left[2\sum_{j=1}^{k} j^{-3} + (k+1)^{-3}\right]^{-1}$
$EY^{(2)} = 4k(\sum_{j=1}^{k} 10^{1-j})$	$EY^{(2)} = (2k+1)(2\sum_{j=1}^{k} 10^{1-j} + 10^{-k})$

All indices given in Table 1 increase indefinitely when n (i.e.k) tends towards infinity.

Recurrences for stars, $K_{1,n'}$ ($n' = n-1$). For stars, the matrices B and E can be written either in linear form, or columnwise (eq. 33 to 36):

$$B(K_{1,n'}) = \|\, n'(1, n', n'-1)\,;\ (n', n', 0)\,\| \tag{33}$$

$$\sum_i B(K_{1,n'}) = \|\, 2n'\,;\ n'(n'+1)\,;\ n'(n'-1)\,\| \tag{34}$$

$$E(K_{1,n'}) = \|\, n'(1, n'-1)\,;\ (n', 0)\,\| \tag{35}$$

$$\sum_i E(K_{1,n'}) = \|\, 2n', n'(n'-1)\,\| \tag{36}$$

Hence, the relations for $MY^{(t')}$ can be easily derived (eq. 37 to 40):

$$BY^{(1)} = 2(n'+1)[2 + 2^{-3}(n'+1) + 3^{-3}(n'-1)]^{-1} \tag{37}$$

$$BY^{(2)} = n'[2 + 0.1(n'+1) + 0.01(n'-1)] \tag{38}$$

$$EY^{(1)} = (n'+1)[2 + 2^{-3}(n'-1)]^{-1} \tag{39}$$

$$EY^{(2)} = n'[2 + 0.1(n'-1)] \tag{40}$$

When n tends towards infinity, $BY^{(2)}$ increases towards infinity and $BY^{(1)}$ tends towards 12.343

Recurrences for complete graphs, K_n. The complete graphs can be characterized by the following recurrences (eq. 41 to 46):

$$B(K_n) = \|\, n(n-1)\,;\ n-1)^2\,\| \tag{41}$$

$$E(K_n) = \left\| n(n-1) ; \binom{n-1}{2} \right\| \quad (4$$

$$BY^{(1)} = 2^3 * n(n+7)^{-1} \quad (4$$

$$BY^{(2)} = 2 * \binom{n}{2} * (0.9 + 0.1n) \quad (4$$

$$EY^{(1)} = 2^4 * n(n+14)^{-1} \quad (4$$

$$EY^{(2)} = \binom{n}{2} * (1.8 + 0.1n) \quad (4$$

When n tends towards infinity, $BY^{(1)}$ and $EY^{(1)}$ tends towards 8 and 16, respe tively whereas the other TI's tend towards infinity.

Applications. We have tested the correlating ability of the $BY^{(2)}$ index wit the octanol-water partition coefficient (log p) in a heterogeneous series of straigh chain compounds including alcohols, ethers, primary and secundary amines (s Table 2, and ref. [41]). The single variable QSPR's are presented in eq. 47, 4 49:

$$\log p = -1.15977 + 0.14554 BY^{(2)}(S)$$

$$N = 27 ; \ S = 0.14519 ; \ r = 0.99077 ; \ F = 1335.66 ; \ T = 36.55 \quad (4$$

$$\log p = -1.23580 + 0.20015 BY^{(2)}(HG)$$

$$N = 27 ; \ S = 0.14711 ; \ r = 0.99052 ; \ F = 1300.34 ; \ T = 36.06 \quad (4$$

$$\log p = -1.01311 + 0.68007 DSI$$

$$N = 27 ; \ S = 0.16013 ; \ r = 0.98876 ; \ F = 1093.57 ; \ T = 33.07 \quad (4$$

In the homogeneous sets of alcohols and primary amines, the correlation improved:

$$\log p_{alcohols} = -1.28604 + 0.20198 BY^{(2)}(HG)$$

$$N = 9 ; \ S = 0.09113 ; \ r = 0.99803 ; \ F = 1768.06 ; \ T = 42.05 \quad (5$$

$$\log p_{amines} = -1.26297 + 0.21348 BY^{(2)}(HG)$$

$$N = 7 ; \ S = 0.10003 ; \ r = 0.99675 ; \ F = 765.85 ; \ T = 27.67 \quad (5$$

One can observe that a very good correlation coefficient ($r > 0.99$) w found both if valence (DS) electronegativities [8] were used to weight the over straight-chain ($BY^{(2)}(S)$ — eq. 47) or only the hetero-group ($BY^{(2)}(HG)$ — e 48, 50 and 51). Thus, it is obvious that recurrences of type (13 to 16) are usef in computing Y-indices on partial weighted graphs. Table 2 includes for compa son DSI (a Randic type connectivity index based on DS — electronegativiti [8], which shows a lower correlation ($r = 0.98876$; eq. 49). Table 2 also includ the estimated log p (o/w) according to eq. 47, 48, 50 and 51 respectively.

Correlation of $BY^{(2)}$ and DSI with log p (o/w)

No	Substance	$BY^{(2)}$ (S)*	$BY^{(2)}$ (HG)*	DSI	Obs.** log p	Calculated log p with $BY^{(2)}$(S)	Calculated log p with $BY^{(2)}$(HG)	Calculated log p with $BY^{(2)}$(HG)
1	CH_3-OH	3.7136	3.0294	0.593	−0.66	−0.6193	−0.6295	−0.6742
2	CH_3-CH_2-OH	7.1254	5.5323	1.310	−0.32	−0.1227	−0.1285	−0.1686
3	$CH_3-(CH_2)_2-OH$	10.5069	7.9826	2.034	0.34	0.3694	0.3619	0.3263
4	$CH_3-(CH_2)_3-OH$	13.8855	10.4276	2.757	0.88	0.8612	0.8513	0.8201
5	$CH_3-(CH_2)_4-OH$	17.2637	12.8721	3.481	1.40	1.3529	1.3406	1.3138
6	$CH_3-(CH_2)_5-OH$	20.6420	15.3166	4.205	1.84	1.8445	1.8299	1.8076
7	$CH_3-(CH_2)_6-OH$	24.0202	17.7610	4.928	2.34	2.3362	2.3191	2.3031
8	$CH_3-(CH_2)_7-OH$	27.3984	20.2055	5.652	2.84	2.8279	2.8084	2.7950
9	$CH_3-(CH_2)_8-OH$	30.7766	22.6499	6.376	3.15	3.3196	3.2976	3.2887
10	$CH_3-O-(CH_2)_2-CH_3$	14.0909	10.7595	2.710	1.03	0.8911	0.9177	—
11	$CH_3-CH_2-O-CH_2-CH_3$	14.1065	10.8130	2.707	1.03	0.8933	0.9284	—
12	$CH_3-O-(CH_2)_3-CH_3$	17.4693	13.2046	3.434	1.53	1.3828	1.4071	—
13	$CH_3-CH_2-O-(CH_2)_2-CH_3$	17.4865	13.2634	3.431	1.53	1.3853	1.4189	—
14	$CH_3-(CH_2)_2-O-(CH_2)_2-CH_3$	20.8665	15.7137	4.154	2.03	1.8772	1.9093	—
15	CH_3-NH_2	3.6179	2.9337	0.608	−0.57	−0.6332	−0.6486	−0.6367
16	$CH_3-CH_2-NH_2$	7.0201	5.4271	1.327	−0.93	−0.1380	−0.1496	−0.1044
17	$CH_3-(CH_2)_2-NH_2$	10.4007	7.8764	2.050	0.48	0.3540	0.3407	0.4185
18	$CH_3-(CH_2)_3-NH_2$	13.7792	10.3213	2.774	0.75	0.8457	0.8300	0.9404
19	$CH_3-(CH_2)_4-NH_2$	17.1574	12.7658	3.498	1.49	1.3374	1.3193	1.4622
20	$CH_3-(CH_2)_5-NH_2$	20.5356	15.2102	4.221	1.98	1.8291	1.8086	1.9841
21	$CH_3-(CH_2)_6-NH_2$	23.9139	17.6547	4.954	2.57	2.3207	2.2978	2.5059
22	$CH_3-NH-CH_2-CH_3$	10.4382	8.0368	2.041	0.15	0.3594	0.3728	—
23	$CH_3-CH_2-NH-CH_2-CH_3$	13.8210	10.5274	2.764	0.57	0.8518	0.8713	—
24	$CH_3-NH-(CH_2)_3-CH_3$	17.1953	12.9305	3.488	1.33	1.3429	1.3523	—
25	$CH_3-(CH_2)_2-NH-(CH_2)_2-CH_3$	20.5783	15.4256	4.210	1.67	1.8353	1.8571	—
26	$CH_3-(CH_2)_2-NH-(CH_2)_3-CH_3$	23.9566	17.8705	4.934	2.12	2.3270	2.3410	—
27	$CH_3-(CH_2)_3-NH-(CH_2)_3-CH_3$	27.3348	20.3154	5.658	2.68	2.8186	2.8304	—

* see text; ** from ref [4]

Acknowledgements. Thanks are addresed to professor A. T. Balaban (Polytechnic Institute, Bucharest) for heplful discussions.

REFERENCES

1. M. V. Diudea, O. M. Minailiuc, A. T. Balaban, *J. Comput. Chem.*, **12** (1991) 527.
2. V. A. Skorobogatov, A. A. Dobrynin, *Math. Chem.*, **23**, 105–151 (1988).
3. S. B. Elk, *Math. Chem.*, **23**, 19–33 (1988).
4. L. B. Kier, L. M. Hall, „Molecular Connectivity in Chemistry and Drug Research", Aca Press, New York, 1976.
5. B. Mohar, Preprint Ser. Dept. Math. Univ. E. K. Ljubljana 26, 385–392 (1988).
6. M. V. Diudea, T. Cipăianu, L. Bal, B. Pârv, *Studia Univ. Babeș-Bolyai, Chem.*, **35** (1) 2 (1990).
7. M. V. Diudea, L. Bal, B. Pârv, „Branching index Y in regular graphs" (manuscript i preparation).
8. **M. V. Diudea**, I. Silaghi-Dumitrescu, *Rev. Roum. Chim.*, **34**, 1175–1182 (1989

STUDIA UNIV. BABEŞ-BOLYAI, CHEMIA, XXXV, 1, 1990

MOLECULAR TOPOLOGY. 6. [1.] NEW Y-TYPE INDICES OF MOLECULAR BRANCHING

MIRCEA V. DIUDEA*, TEODORA CIPĂIANU*, LUCINIA BAL** and BAZIL PÂRV***

Received: February 10, 1990

New y-type 1 indices for characterizing the molecular branching were proposed and their correlation with some physico-chemical properties was tested in the set of heptane isomers.
From Y^2 — index some information indices were derived.

1. **Introduction.** In the previous papers of this series 1,2 we presented some aspects of the intuitive concept of branching as well as the reasons why this remains an unsolved graph-theoretical problem. We also showed how molecular branching is reflected in some physico-chemical properties such as boiling points, molecular van der Waals volumes, formation enthalpies, partition coeficients etc. of isomeric alkanes (4-trees). In this respect, the reader can consult 3, 4 on the ground of new layer matrices B, E and S, we proposed 1 a distance regressive branching index, Y, as in Eq. (1):

$$MY^{(t')} = k'[\sum_i [(YRi^{(t)})^p + (YLi^{(t)})^p] Wi]^{p'} \qquad (1)$$

where:

M — stands for the type of matrix (B, E, S);
t'), (t) — are the labels for global (operational stage) and local (assignment) stage) operators, respectively;
k' — is a normalizing multiplicator, differing for different (t') global operators;
YRi(t) — represents the regressive degree of vertex i, by the (t)-operator;
YLi(t) — is the local contribution for multigraph (if the case), by the (t)-operator;
p, p' — are exponents, varying with (t');
Wi — is a weighting factor, characterizing the vertices by group electronegativities or fragmental van der Waals volumes (see [1]; for nonweighted graphs, Wi = 1.).

Table 1 details eq. (1) about the above mentioned [1] and the new operators (devised in the present paper).

* *University of Cluj, Faculty of Chemical Technology, 3400 Cluj-Napoca, Romania*
** *Territorial Computing Center, 3400 Cluj-Napoca, Romania*
*** *Computing Center, University of Cluj, 3400 Cluj-Napoca, Romania*

Table 1

Details of eq(1*)

t′	t	k′	M	p′	p	$YR_i^{(t)}$	$YL_i^{(t)}$	Ref.
1	1	2v · e	B	−1	1	$\sum_{j=1}^{j_{max}} m_{ij} \cdot j^{-3}$	$f_i \cdot \sum_{j=1}^{2} m_{ij} (j+1)^{-3}$	1
1	1	v · e	E	−1	1	〃	〃	1
1	1	3v · e	S	−1	1	〃	〃	1
2	2	1	BES	1	1	$\sum_{j=1}^{j_{max}} m_{ij} \cdot 10^{1-j}$	$f_i \cdot \sum_{j=1}^{2} m_{ij} \cdot 10^{-j}$	1
3	2	1	BES	1/2	2	〃	〃	1
4	3	1	B	1	1	$\sum_{j=1}^{j_{max}} \binom{b_{ij}}{2} \cdot 10^{1-j}$	$f_i \cdot \sum_{j=1}^{2} \binom{b_{ij}}{2} \cdot 10^{-j}$	this work
5	4	1	B	1	1	$\sum_{j=1}^{j_{max}} (\log_2 b_{ij}) \cdot 10^{1-j}$	$f_i \cdot \sum_{j=1}^{2} (\log_2 b_{ij}) \cdot 10^{-j}$	this work
6	5	v	B	1	−1	$\sum_{j=2}^{j_{max}} (b_{ij})^{j/2d_{max}}$	$f_i \cdot \sum_{j=2}^{3} (b_{ij})^{(j-1)/2d_{max}}$	this work

(*)$f_i = \sum_j (C_{ij} - 1)$; C_{ij} = conventional bond order (1, 2, 3 or 1.5)

2. New operators, (t) and (t') on B-matrices

2.1. *Local operators, (t).*

With the aim to broaden the use of B-matrices (newly introduced by [1]) we propose now other three local operators: (t) = 3, 4 and 5 (see Table 1)

Operator (t) = 3

— regards the degrees of each layer, in a row of the B matrix as points of complete graphs, then counting their edges.

Operator (t) = 4

— uses the binary information logarithm.

The distance regressive character of the two above operators is given by the factor $10^{[1-j]}$. They eliminate the external vertices (with degree 1).

Operator (t) = 5

— is, conversely, a distance progressive operator.

It enhances the contribution of more distant vertices.

The summation starts from j = 2, because the forst column in B refers to the zero distant sphere (of degree), vs. the vertex i.

Graph invariants induced by the operators (t) = 2 to 5 and the derived $Y^{(t)}$-indices (B is omitted, in the following, from the label $BY^{(t)}$) for the identity 4-trees, $G_1 - G_5$ (see [1]), are given in Table 2.

2.2. *Global operators, (t').*

In the effort to find good topological indices (TI 's) which adequately express the topology of molecules the information indices played an important role [5]. Works of Shannon [6], Onicescu [7] or Bonchev [8] in the field are well known (see also [9—11]).

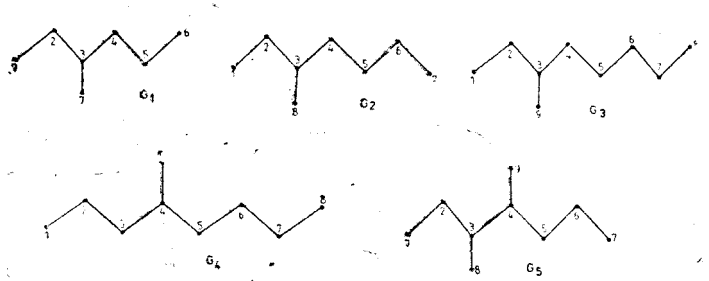

Fig. 1.

Table 2.

Graph invariants for identity 4-trees, $G_1 - G_5$*

G	Vertex t′ t	1	2	3	4	5	6	7	8	9	Y(t′)
	2 2	1.2332	2.4321	3.5310	2.5410	2.3331	1.2233	1.3431	—	—	14,6368
	4 3	0.1331	1.6310	4.0300	2.0600	1.3330	0.1133	0.3630	—	—	9.6634
1	5 4	0.1175	1.2168	1.8330	1.2522	1.1759	0.1117	0.1801	—	—	5.8872
	6 5	0.1537	0.1988	0.2652	0.2567	0.192	0.1501	0.1882	—	—	9.8385
	2 2	1.2332	2.4322	3.5321	2.5520	2.4431	2.3233	1.2223	1.3432	—	17.0814
2	4 3	0.1331	1.6311	4.0310	2.1010	1.6630	1.3133	0.1113	0.3631	—	11.3469
	5 4	0.1175	1.2169	1.8340	1.2564	1.2216	1.1702	0.1112	0.1802	—	7.1080
	6 5	0.1311	0.1621	0.2048	0.2461	0.1954	0.1559	0.1268	0.1564	—	11.0296
	2 2	1.2332	2.4322	3.5322	2.5531	2.4541	2.4333	2.4233	1.2222	1.3432	19.5259
3	4 3	0.1331	1.6311	4.0311	2.1030	1.7060	1.6333	1.3113	0.1111	0.3631	13.0231
	5 4	0.1175	1.2170	1.8341	1.2570	1.2252	1.2176	1.1697	0.1111	0.1802	8.3294
	6 5	0.1139	0.1364	0.1660	0.1985	0.1954	0.1579	0.1310	0.1099	0.1331	12.0798
	2 2	1.2233	2.3332	2.5422	3.5431	2.5531	2.4432	2.3233	1.2223	1.3443	19.5280
4	4 3	0.1133	1.3331	2.0611	4.0630	2.1030	1.6631	1.3133	0.1113	0.3663	13.1275
	5 4	0.1118	1.1760	1.2533	1.8387	1.2570	1.2217	1.1702	0.1112	0.1807	8.3206
	6 5	0.1127	0.1346	0.1638	0.2011	0.1984	0.1609	0.1329	0.1114	0.1543	12.3309
	2 2	1.2343	2.4432	3.6421	3.6520	2.5531	2.3343	1.2234	1.3542	1.3552	19.7918
5	4 3	0.1363	1.6631	4.5610	4.6010	2.1030	1.3363	0.1136	0.4061	0.4101	15.3305
	5 4	0.1180	1.2217	1.8645	1.8677	1.2570	1.1765	0.1118	0.1838	0.1841	7.9851
	6 5	0.1247	0.1550	0.1991	0.2437	0.1906	0.1496	0.1210	0.1511	0.1742	13.5810

Mean information content [6] can be expressed, in terms of $Y^{(2)}$-operator, by a Shannon formula, Eq. (2):

$$Y^{(7)} = -\sum_i p_i \log_2 p_i \quad (2)$$

where the probability p_i is given by:

$$p_i = YRi/Y^{(2)} \quad (3)$$

Complementary information content [11] is given by a Basak formula, Eq. (4):

$$Y^{(8)} = \log_2 Y^{(2)} - Y^{(7)} \quad (4)$$

Total information content [6, 8] based on $Y^{(2)}$ — operator/index, is similar to Bonchev's index I_D^W

$$Y^{(9)} = Y^{(2)} \log_2 Y^{(2)} - \sum_i YR_i \cdot \log_2 YR_i \quad (5)$$

Table 3 lists values of global operators/indices $Y^{(4)} - Y^{(9)}$ for alkanes up to octanes.

3. **Discussions.** From Table 3 one can observe that $Y^{(7)}$ — values decreas with increasing graph branching, whereas $Y^{(8)}$ —values increase with branching The graph ordering induced by these new $Y^{(t)}$—indices is different from that induced by $Y^{(2)}$: $Y^{(7)}$ and $Y^{(8)}$ presents two inversions vs $Y^{(2)}$, $Y^{(4)}$ and $Y^{(5)}$ show three inversions, whereas $Y^{(6)}$ and $Y^{(9)}$ are the most different indices. The differences in the graph ordering increase with increasing the number of vertices.

In the next paper of this series [12] we shall use this last operator to introduce the notion of graph centricity (values in the range [0, 1] with maximal value for the complete graphs).

The dispersion of $Y^{(t)}$ —values, computed for octane isomers according to Eq. (6), [9]:

$$\text{Disp. } Y^{(t)} = \frac{Y^{(t)}_{max} - Y^{(t)}_{min}}{Y^{(t)}_{av}} \quad (6)$$

where *max*, *min* and *av* stand for maximal, minimal and average, respectively. Dispersion shows high values for $Y^{(4)}$ and $Y^{(6)}$ (79.80 and 61.67 percents, respectively), these indices providing a good disciminating ability.

We tested, on the set of heptane isomers, the ability of all Y—indices to correlate with some physico-chemical properties: ΔHF = formation enthalpy, MR = = molar refraction, BP = boiling points, ΔHV = vaporisation enthalpy and AW = = van der Waals areas [10]. Table 4 presents the corresponding values in heptane set, the $Y^{(2)}$—values being included. The correlation coeficients are tabulated in table 5.

It can be observed that molecular branching expressed by $Y^{(t)}$—indices except $Y^{(6)}$ and $Y^{(9)}$ correlates with ΔHF, BP, ΔHV and AW in heptanes set (in the range: 0,8001—0,9296) but no causal correlation exists with the molecular refraction. This is consistent with the observation of Rouvray [3], namely that different physicochemical properties require different orderings of isomers.

Table 3.

$^{(t)}$ — Indices for alkanes

No.	Alkane	$^{(2}$	$^{(4)}$	$^{(5)}$	$^{(6)}$	$^{(7)}$	$^{(8)}$	$^{(9)}$
1.	C_2	2.200	0.0000	0.0000	4.0000	1.0000	0.1365	2.2000
2.	C_3	4.6200	1.3000	1.3000	5.6952	1.5222	0.6857	7.0326
3.	C_4	7.0620	2.8200	2.5370	6.2952	1.9303	0.8898	13.6318
4.	$2-Me-C_3$	7.2600	4.2300	2.2489	8.9754	1.8586	1.0014	13.4927
5.	C_5	9.5062	4.4520	3.7600	7.6236	2.2567	0.9926	21.4526
6.	$2-Me-C_4$	9.7240	6.0010	3.4695	9.0465	2.1926	1.0890	21.3208
7.	$2,2-Me_2-C_3$	10.1200	9.1200	3.0634	12.9444	2.1181	1.2210	21.4351
8.	C_6	11.9506	6.1042	4.9929	8.5234	2.5261	1.0529	30.1884
9.	$2-Me-C_5$	12.1704	7.7461	4.6807	10.1328	2.4743	1.1310	30.1132
10.	$3-Me-C$	12.1902	7.8970	4.6807	10.6176	2.4644	1.1433	30.0415
11.	$2,3-Me_2-C_4$	12.4080	9.4640	4.3723	12.1186	2.4195	1.2137	30.0212
12.	$2,2-Me_2-C_4$	12.6060	11.1730	4.2618	12.3247	2.3981	1.2579	30.2305
13.	C_7	14.3951	7.7674	6.2161	9.7015	2.7544	1.0931	39.6499
14.	$2-Me-C_6$	14.6159	9.4186	5.9014	10.8058	2.7117	1.1577	39.6315
15.	$3-Me-C_6$	14.6368	9.5634	5.8873	11.2218	2.7000	1.1737	39.5194
16.	$3-Et-C_5$	14.6586	9.9213	5.8762	13.3105	2.6927	1.1810	39.4712
17.	$2,4-Me_2-C_5$	14.8368	11.1544	5.5862	12.8302	2.6698	1.2212	39.6113
18.	$2,3-Me_2-C_5$	14.8764	11.4861	5.5747	13.4625	2.6560	1.2389	39.5118
19.	$2,2-Me_2-C_5$	15.0543	13.0323	5.4759	13.0539	2.6469	1.2644	39.8480
20.	$3,3-Me_2-C_5$	15.0942	13.6349	5.4653	14.0963	2.6317	1.2842	39.7234
21.	$2,2,3-Me_3-C_4$	15.3120	14.9429	5.1671	15.7159	2.5993	1.3373	39.8005
22.	C_8	16.8395	9.4326	7.4385	10.6316	2.9476	1.1305	49.6361
23.	$2-Me-C_7$	17.0595	11.0929	7.1233	11.8425	2.9293	1.1632	49.9724
24.	$3-Me-C_7$	17.0815	11.3469	7.1080	12.2024	2.9075	1.1868	49.6647
25.	$4-Me-C_7$	17.0835	11.4419	7.1007	12.4975	2.9065	1.1880	49.6532
26.	$3-Et-C_6$	17.1054	11.7093	7.0873	13.7184	2.8984	1.1980	49.5783
27.	$2,5-Me_2-C_6$	17.2797	12.7534	6.8082	13.1993	2.8807	1.2303	49.7776
28.	$2,4-Me_2-C_6$	17.3034	13.0931	6.7902	13.6884	2.8719	1.2411	49.6936
29.	$2,3-Me_2-C_6$	17.3232	13.2739	6.7862	13.7842	2.8670	1.2477	49.6656
30.	$3,4-Me_2-C_6$	17.3450	13.5306	6.7735	14.2434	2.8592	1.2573	49.5928
31.	$3-Et-2-Me-C_5$	17.3470	13.6398	6.7713	16.4134	2.8460	1.2770	49.3696
32.	$2,2-Me_2-C_6$	17.4995	14.7252	6.6900	13.4392	2.8597	1.2696	50.0434
33.	$3,3-Me_2-C_6$	17.5430	15.2457	6.6737	14.3938	2.8452	1.2876	49.9133
34.	$2,3,4-Me_3-C_5$	17.5648	15.2024	6.4707	16.4987	2.8281	1.3066	49.6750
35.	$3-Et-3-Me-C_5$	17.5846	15.6983	6.6605	17.1019	2.8319	1.3043	49.7978
36.	$2,2,4-Me_3-C_5$	17.7232	18.5559	6.9626	15.9358	2.8251	1.3224	50.0698
37.	$2,2,3-Me_3-C_5$	17.7826	17.0933	6.3639	16.7181	2.8100	1.3424	49.9691
38.	$2,3,3-Me_3-C_5$	17.8024	17.2791	6.3612	17.2615	2.7901	1.3639	49.6704
39.	$2,2,3,3,-Me_4-C_4$	18.2380	20.7780	5.9578	19.6567	2.4699	1.7190	45.0460

Table 4.

Y — indices and physico-chemical values in heptane-isomers

No	Molecule	$Y^{(4)}$	$Y^{(5)}$	$Y^{(6)}$	$Y^{(7)}$	$Y^{(8)}$	$Y^{(9)}$	ΔHF a)	MR a)	BP b)	ΔHV a)	AW c)
1.	C_7	7.7674	6.2161	9.7015	2.7544	1.0931	39.6499	44.89	34.555	98.4	8.739	334.36
2.	$2-Me-C_6$	9.4186	5.9014	10.8058	2.7117	1.1577	39.6315	46.60	34.595	90.0	8.325	322.91
3.	$3-Me-C_6$	9.6634	5.8873	11.2218	2.7000	1.1737	39.5194	45.96	34.464	92.0	8.391	216.67
4.	$3-Et-C_5$	9.9213	5.8762	13.3105	2.6927	1.1810	39.4712	45.34	34.287	93.5	8.425	303.15
5.	$2,2-Me_2-C_5$	13.0323	5.4759	13.0539	2.6469	1.2645	39.2715	49.29	34.621	79.2	7.764	306.53
6.	$2,3-Me_2-C_5$	11.4861	5.5747	13.4625	2.6560	1.2389	39.5117	46.65	34.328	89.8	8.191	303.11
7.	$2,4-Me_2-C_5$	11.1544	5.5862	12.8302	2.6698	1.2212	40.1927	48.30	34.623	80.5	7.872	309.97
8.	$3,3-Me_2-C_5$	13.6340	5.4653	14.0963	2.6317	1.2842	39.7234	48.17	34.336	86.0	7.901	297.20
9.	$2,2,3-Me_2-C_4$	14.9490	5.1671	15.7159	2.5913	1.3373	39.6779	48.96	34.378	80.9	7.669	292.89

a) [13]; b) [14]; c) [10]

Table 5

Correlation coefficients of Y-indices with physicochemical properties in heptanes

T.I.	ΔHF	MR	BP	ΔHV	AW
Y_4	0.87670	0.28346	0.81490	0.92946	0.87966
Y_5	0.88747	0.23920	0.86230	0.93268	0.88129
Y_6	0.67504	0.54670	0.66491	0.80210	0.97810
Y_7	0.83602	0.36018	0.80010	0.91670	0.92960
Y_8	0.85480	0.32780	0.81230	0.92640	0.91290
Y_9	0.15280	0.23030	0.21860	0.17620	0.17470
Y_2	0.88380	0.26420	0.82910	0.93730	0.87480

Table 5 also illustrates the different character of $Y^{(6)}$ which shows converse correlations vs. the other $Y^{(t)}$ indices. Notice that in comparison with the other Y—indices, this index correlates fairly well with the van der Walls areas of molecules (values given in [10]).

Computer program

The program GRAF Ø9 performs the followings:

1) reads the graph in a dictionary form from a file which is created by a text editor;

2) computes and lists the matrices: A, B, C, D, E, F, and S (adjacency branch, connectivity, distance, edges, frequency and sigma, respectively)

3) computes and lists F—based TI's;

4) computes and lists B(E,S)-based TI's,

The interface program-user operates by means of appropriate menues. The program is written in FORTRAN — 77 on a PDP — 11 compatible system.

Concluding, we stress that B—matrix represents a real ground for describing of molecular topology. Different operators may extract different useful information in the field.

Acknowledgements. Thanks areadd ressed to Dr. I. Motoc (Bristol—Myers Co., Wallingford) for preprints and encouragements.

REFERENCES

1. M. V. Diudea, O. M. Minailiuc, A. T. Balaban, *J. Comput. Chem.*, 12 (1991) 527.
2. M. V. Diudea, L. Bal, *Studia Univ. Babeş-Bolyai*, **35** (1), 17 (1990).
3. D. H. Rouvray, *Discr. Appl. Math.*, **19**, 317 (1988).
4. S. H. Bertz, *Discr. Appl. Math.*, **19**, 65 (1988).
5. A. T. Balaban, I. Motoc, D. Bonchev, O. Mekenyan, *Top. Curr. Chem.*, **114**, 21 (1983).
6. C. Shannon, W. Weaver, „Mathematical Theory of Communication", Univ. Illinois, Urbana 1949.
7. O. Onicescu, *C. R. Acad. Sci., Paris, A*, **263**, 841 (1966).
8. D. Bonchev, N. Trinajstic, *J. Chem. Phys.*, **67**, 4517 (1977).
9. O. Ivanciuc, *Rev. Roumaine Chim.*, **34**, 1361 (1989).
10. J. Labanowski, I. Motoc, R. A. Dammkoehler, *Comput. Chem.*, **15**, 47 (1991)
11. S. C. Basak, V. R. Magnuson, *Discr., Appl. Math.*, **19**, 17 (1988).
12. M. V. Diudea, T. Cipăianu, I. Kacso, *Studia Univ. Babeş-Bolyai*, **35** (1), 37 (1990).
13. L. B. Kier, L. H. Hall, „Molecular Connectivity in Chemistry and Drug Design", Acad. Press, New York, 1976.
14. H. P. Schultz, J. Chem. Inf. Comput, Sci., **29**, 227 (1989).

STUDIA UNIV. BABEŞ BOLYAI, CHEMIA, XXXV, 1, 1990

MOLECULAR TOPOLOGY. 7 [1]. NEW METRIC CHARACTERISTICS IN ALKANES (4 — TREES)

MIRCEA V. DIUDEA*, TEODORA CIPĂIANU* and IRINA KACSO*

Received: March 2, 1990

New metric characteristics, devised by the mean of a distance progressive operator, are discussed in comparison with analogous parameters in literature. These characteristics well correlate with the van der Waals areas of alkane isomers. Recursive relationships are given in the case of linear graphs (n-alkanes).

1. **Introduction.** In graph theory, the metric analysis deals with metric characteristics [2] which mainly depend on the topological distance between the vertices of a graph. Within these characteristics, two major classes can be distinguished: i) eccentric — and ii) distance characteristics. Skorobogatov and Dobrynin [2] tabulated these characteristics in a recent extensive paper. One can separate in G some vertex sets the function of values of the graph characteristics, called graph constructions (nonnumerical characteristics) suchas: center of graph, graph periphery or graph center of gravity [2].

The center of graph is a set of vertices, $i \in V(G)$, for which their eccentricity is minimal (and equals the radius of graph). Vertex eccentricity, e(i), is defined as the maximal distance between vertices i and j, belonging to the vertex set V(G) of a graph G:

$$e(i) = \max_{i,j \in V(G)} l(i,j) \qquad (1)$$

Summation over the whole set V(G) gives the eccentricity of graph.

Several approaches were proposed for finding the center of graph 3—7 and estimating the graph centricity. Due to the complexity of problem, especially in cyclic systems, an extension of the graph center concept was needed. In the following, we present three of them:

i) *1D—3D criteria* form an interative approach based on distance frequency matrix, F [6], or on *vertex distance code* (VDC) as was originally defined by Bonchev et al [7]. 1D — 3D criteria are as follows:

(1D) — Minimum vertex eccentricity, e(i) = min. This is just the radius of the graph, eq. (2), implied in the classical definition of graph center [8].

(2D) — Minimum vertex, distance sum, d(i) = min;

(3D) — Minimum number f_{ij} in F matrix (or K in VDC) of occurence of the largest distance, $f_{ij_{max}} = \min$.

If $f_{ij_{max}} = f_{kj_{max}}$, $i \neq k$, the next largest distance ($j_{max} - 1$) is considered, and so on. By deleting all but the central vertices cf. 1D — 3D, one obtains a Kernel of G. Criteria 1D — 3D are iterated over the Kernel until two subsequent iterations fail to reduce further the number of central vertices. The result is the

*University of Cluj, Faculty of Chemical Technology, 3400 Cluj-Napoca, Romania

graph center (or a polycenter). Criteria 1D—3D are applied hierarchically ([7]);

ii) *1P — 3P Criteria* are constructed by analogy to the 1D — 3D criteria by replacing the distance notion with that of path [9]. The application of 1P — — 3P criteria results in an oligocenter;

iii) *IVEC algorithm* (Iterative Vertex and Edge Centricity [5] takes into account both metric properties and vertex — edge incidence. Its ground assumption is: „central are those vertices that are incident to the most central vertices". IVEC is built on VDC and EDC (edge distance code) and is particulary useful in polycyclic graph analysis. The application of IVEC results in a different centric ordering of vertices/edges vs. the other approaches. It finds correctly vertex and edge orbits of the graph's automorphism group [5].

In this paper we present some new approaches expressing the graph (molecular) eccentricity/centricity in comparison with other similar characteristics.

2. **Centric criterion and graph eccentricity.** In order to simplify the procedure to determine the center/polycenter of graph, according to 1D — 3D criteria, we proposed [6] a power operator ME (matrix eccentricity)

$$ME_{(i)} = \sum (m_{ij})^{j/2d_{max}} \tag{2}$$

where: m_{ij} — are the elements of a topological layer matrix, M; d_{max} — is a selected maximal distance for unitary description of a set molecules by ME (a distance progressive) operator.

In [6] we took $2\,d_{max} = d(G)$ and ME operated on the distance frequency matrix F, with its elements f_{ij}. Next, we normalized the FE (i) — values by min FE(i), thus deriving a $CC_{v,1}$ („centric criterion") — vector:

$$CC(i) = FE(i)/\min FE(i) \tag{3}$$

The central vertices will show CC(i) = 1, whereas for the others, the CC(i) — values will exceed unity. This means that for any graph CC(G) = 1 (the radius derived by the CC-operator) in agreement with the definition given in [8].

Thus, the meaning of FE(i)—parameters closes the vertex eccentrity. The summation over all vertices in G leads to a global FE(G) invariant:

$$FE(G) = \sum_i FE(i) \tag{4}$$

By analogy, the ME operating on the B matrix leads to corresponding BE (branch eccentricity) — parameters:

$$BE(G) = \sum_i BE(i) \tag{5}$$

Eccentric characteristics FE(i) and FE(G) in the C_{12}/McC_{11} set are given in Table 1. It can be seen that the v_{12} — vertex eccentricity decreases when it tends to the center of graph.

Table 2 collects FE and BE — values in heptane isomers. Since these values are large, they can be scaled (e.g. by a factor of 10^{-1}). Another possibility is to use the average values (see Tables 1 and 2).

$$ME_{av}(G) = 1/v \cdot ME(G) \tag{6}$$

Table 1

Metric characteristics in C_{12} MeC_{11}*

graph	Vertex no.; FE(i)/FC(i)												FE(G)	FE (G)
	1	2	3	4	5	6	7	8	9	10	11	12	FC(G)	
C_{12}	11.0000	10.0353	9.1070	8.2166	7.3653	6.5545	6.5545	7.3653	8.2166	9.1070	10.0353	11.0000	104.5574	8.7131
	0.0909	0.0996	0.1098	0.1217	0.1358	0.1526	0.1526	0.1358	0.1217	0.1098	0.0996	0.0909	1.4208	
$2MeC_{11}$	10.0718	9.0565	8.1514	7.2862	6.4623	5.5814	6.5965	7.4912	8.4265	9.4013	10.4142	10.0718	99.1111	8.2593
	0.0993	0.1104	0.1227	0.1372	0.1547	0.1760	0.1516	0.1335	0.1187	0.1064	0.0960	0.0993	1.5058	
$3MeC_{11}$	10.1096	9.1070	8.1282	7.2610	6.4349	5.6515	6.5545	7.4478	8.3816	9.3548	10.3660	9.1813	97.9782	8.1649
	0.0989	0.1098	0.1230	0.1377	0.1554	0.1769	0.1526	0.1343	0.1193	0.1069	0.0965	0.1089	1.5202	
$4MeC_{11}$	10.1487	9.1448	8.1514	7.2378	6.4097	5.6241	6.4623	7.4058	8.3382	9.3098	10.3195	8.3300	96.8821	8.0735
	0.0985	0.1094	0.1227	0.1382	0.1560	0.1778	0.1547	0.1350	0.1199	0.1074	0.0968	0.1200	1.5366	
$5MeC_{11}$	10.1892	9.1840	8.2166	7.2610	6.3865	5.5989	6.4349	7.3653	8.2962	9.2664	10.2746	7.5192	95.9928	7.9994
	0.0981	0.1089	0.1217	0.1377	0.1566	0.1786	0.1554	0.1358	0.1205	0.1079	0.0973	0.1330	1.5516	
$6MeC_{11}$	10.2311	9.2245	8.2562	7.2862	6.4097	5.5757	6.4097	7.2862	8.2557	9.2245	10.2311	6.7504	95.1405	7.9284
	0.0977	0.1084	0.1211	0.1372	0.1560	0.1793	0.1560	0.1372	0.1211	0.1084	0.0977	0.1481	1.5686	

* $d_{max} = 10$

Table 2

Metric characteristics in heptane isomers

Graph	FE(G)	$FE_{av}(G)$	FC(G)	FCC(G)	BE(G)	$BE_{av}(G)$	BC(G)	BCC(G)	Aw
C_7	33.5012	4.7859	1.5284	0.1903	37.1095	5.3014	1.3859	0.2833	334.36
$2MeC_6$	29.9413	4.2773	1.7008	0.2643	33.1456	4.7351	1.5437	0.3156	322.91
$3MeC_6$	28.9710	4.1387	1.7508	0.2735	31.7991	4.5427	1.6031	0.3277	316.67
$2,4Me_2C_5$	25.3980	3.6283	2.0373	0.3182	28.3012	4.0430	1.8329	0.3747	309.97
$2,2Me_2C_5$	25.0642	3.5806	2.0589	0.3216	27.7070	3.9581	1.8648	0.3812	306.53
$3EtC_5$	24.5973	3.5139	2.0974	0.3276	27.2397	3.8914	1.9015	0.3887	303.15
$2,3Me_2C_5$	24.3893	3.4842	2.1116	0.3298	26.8374	3.8339	1.9233	0.3932	303.11
$2,3Me_2C_5$	23.2559	3.3223	2.1997	0.3437	25.5030	3.6439	2.0138	0.4117	297.20
$2,2,3Me_3C_4$	20.4950	2.9279	2.4720	0.3861	22.6622	3.2375	2.2451	0.4590	292.89

3. **Graph centricity.** A characteristic which is inverse to eccentricity should express the centricity of vertex/graph. The simple inversion of FE(i)/BE(i) provides a measure of vertex centricity:

$$MC(i) = (ME(i))^{-1} \quad (7)$$

and hence the graph centricity:

$$MC(G) = \sum_i (MC(i)) = \sum_i (ME(i))^{-1} \quad (8)$$

MC(G) — values for dodecanes and heptanes are given in Tables 1 and 2, respectively. These values can also be scaled (e.g. by a factor of ten).

We assume now that in a complete graph, Kv, all vertices are more central than in any other graph. This assumption is based on the vertex transitivity in Kv and also on the minimal distance (unity) between its vertices. Next, the centricity of a vertex/graph can be expressed vs. the vertex/graph centricity in the complete graph with the same number of vertices:

$$MCC(G) = MC(G)/MC(Kv) \quad (9)$$

The expansion of eq. (9) leads to:

$$MCC(G) = k^{(M)} \cdot \sum_i \left[\sum_j (m_{ij})^{j/2d_{max}} \right]^{-1} \quad (10)$$

where: $k^{(M)}$ is the inverse centricity of the complete graph, Kv and MCC(G) stands for „matrix' complete centricity,". The expansion of $k^{(M)}$ requires the general expression of matrix M for the complete graph:

$$F(Kv) = || v.(v-1) || \quad (11)$$

$$B(Kv) = || v.(v-1)(v-1)^2 || \quad (12)$$

When M = B, the summation starts from j = 2, so that $k^{(M)}$ will be:

$$k^{(F)} = 1/(v(v-1)^{-1/2d_{max}}) \quad (13)$$

$$k^{(B)} = 1/(v(v-1)^{-2/d_{max}}) \quad (14)$$

Since the centricity of Kv is maximal, MCC(G) takes values in the range [0, 1]. It is obvious that when MCC(G) equals unity, then G = Kv. Table 2 includes eccentric/centric characteristics in heptanes, computed on the ground of both F and B matrices. For comparison, in Table 3 we present some eccentric characteristics according to literature [2], in the same set of alkanes:

4. **Recurrences for eccentric/centric characteristics in n-alkanes.** It is useful to derive recursive relationships for eccentric/centric characteristics in n-alkanes which are path graphs. Taken into account both parity and symmetry in path graphs (and implicitly in the F and B matrices) we are able to give the following relationships:

$$FE(i_{P_{2k}}) = 2k - i + \sum_{i=1}^{i} (2^{(i-1)/2d_{max}} - 1); \; i \in [1, k]; \quad (15)$$

Table 3

Metric characteristics [2] in heptane isomers: $e_{av}(G)$ = average vertex eccentricity in graph; ΔG = = eccentric of graph; ΔG^* = centralization; $m^*(G)$ = graph dispersion

Graph	$e^{av}G)$	ΔG	ΔG^*	$m_2^*(G)$
C_7	4.7143	0.8980	28	4.0000
$2MeC_6$	4.1429	0.7347	27	3.2857
$3MeC_6$	4.0000	0.5714	30	2.8571
$2,4Me_2C_5$	3.4286	0.6531	26	2.5714
$2,2Me_2C_5$	3.8751	0.5102	29	2.4286
$2EtC_5$	3.2857	0.6122	33	2.1429
$2,3Me_2C_5$	3.2857	0.6122	29	2.1429
$3,3Me_2C_5$	3.1429	0.4898	32	1.7143
$2,2,3Me_3C_4$	2.7143	0.4082	28	1.7143

$$FE(i_{P_{2k+1}}) = 2k + 1 - i + \sum_{j=1}^{i} (2^{(j-1)/2d_{max}} - 1)\,;\ i \in [1, k+1)\,]\,; \tag{16}$$

$$FE(P_{2k}) = 2\sum_{i=1}^{k}\left[2k - i + \sum_{j=1}^{i} (2^{(j-1)/2d_{max}} - 1)\right] \tag{17}$$

$$FE(P_{2k+1}) = 2\sum_{i=1}^{k}\left[2k + 1 - i + \sum_{j=1}^{i} (2^{(j-1)/2d_{max}} - 1)\right] + \\ + [i - 1 + \sum_{j=1}^{i} (2^{(j-1)/2d_{max}} - 1)\,];\ i = k + 1 \tag{18}$$

Let's denote the last bracket as $\Delta(i=k+1)$. The corresponding centric characteristics will be:

$$FC(i_{P_{2k}}) = [2k - i + \sum_{j=1}^{i} (2^{(j-1)/2d_{max}} - 1)\,]^{-1};\ i \in [1, k] \tag{19}$$

$$FC(i_{P_{2k+1}}) = \left[2k + 1 - i + \sum_{j=1}^{i} (2^{(j-1)/2d_{max}} - 1)\right]^{-1};\ i \in [1, k+1] \tag{20}$$

$$FC(P_{2k}) = 2\sum_{i=1}^{k}\left[2k - i + \sum_{j=1}^{i} (2^{(j-1)/2d_{max}} - 1)\right]^{-1} \tag{21}$$

$$FC(P_{2k+1}) = 2\sum_{i=1}^{k}\left[2k + 1 - i + \sum_{j=1}^{i} (2^{(j-1)/2d_{max}} - 1)\right]^{-1} + (\Delta_{(i=k+1)})^{-1} \tag{22}$$

For FE(G) we are able to give recurrences based on the precedent term:

$$FE(P_{2k+1}) = FE(P_{2k}) + 2k + \Delta(i = k+1) \tag{23}$$

$$FE(P_{2k+2}) = FE(P_{2k1+}) + 2k + \Delta(i = k) \tag{24}$$

Since B matrix is more complicated, in path graphs than F matrix, the corresponding recursive relationships for eccentric/centric characteristics will have more terms: one for terminal, second for intermediary and third for central vertex/vertices:

$$BE(P_{2k}) = 2\left[\sum_{j=2}^{2k-1} 2^{j/2d_{max}} + 1\right] + 2\sum_{i=2}^{k-1}\left[\sum_{j=2}^{i-1} 4^{j/2d_{max}} + 3^{i/2d_{max}} + \sum_{j=i+1}^{2k-i} 2^{j/2d_{max}} + 1\right] + 2\left[\sum_{j=2}^{k-1} 4^{j/2d_{max}} + 3^{k/2d_{max}} + 1\right] \quad (25)$$

$$BE(P_{2k-1}) = 2\left[\sum_{j=2}^{2k} 2^{j/2d_{max}} + 1\right] + 2\sum_{i=2}^{k}\left[\sum_{j=2}^{i-1} 4^{j/2d_{max}} + 3^{i/2d_{max}} + \sum_{j=i+1}^{2k-1-i} 2^{j/2d_{max}} + 1\right] + \left[\sum_{j=2}^{k} 4^{j/2d_{max}} + 2^{(k+1)/2d_{max}}\right] \quad (26)$$

$$BC(P_{2k}) = 2\left[\sum_{j=2}^{2k-1} 2^{j/2d_{max}} + 1\right]^{-1} + 2\sum_{i=2}^{k-1}\left[\sum_{j=2}^{i-1} 4^{j/2d_{max}} + 3^{i/2d_{max}} + \sum_{j=i+1}^{2k-i} 2^{j/2d_{max}} + 1\right]^{-1} + 2\left[\sum_{j=2}^{k-1} 4^{j/2d_{max}} + 3^{k/2d_{max}} + 1\right]^{-1} \quad (27)$$

$$BC(P_{2k-1}) = 2\left[\sum_{j=2}^{2k} 2^{j/2d_{max}} + 1\right]^{-1} + 2\sum_{i=2}^{k}\left[\sum_{j=2}^{i-1} 4^{j/2d_{max}} + 3^{i/2d_{max}} + \sum_{j=i+1}^{2k+1-i} 2^{j/2d_{max}} + 1\right]^{-1} + \left[\sum_{j=2}^{k} 4^{j/2d_{max}} + 2^{(k+1)/2d_{max}}\right]^{-1} \quad (28)$$

5. **Discussion.** Metric characteristics such as eccentric and distance characteristics of graphs have been focussed on many papers as reviewed in [2, 10]. Within the distance characteristics a major attention is paid to the graph center of gravity, graph compactness and graph centralization [2]. The problem of graph center is of particular interest in coding of chemical structures [11] and in universal chemical nomenclature [12]. The center selection may be of interest in pattern recognition [13].

The goal of this paper was to find an expeditive way in coding of vertices and molecular graphs in the light of their eccentric and centric characteristics. This way was done by the power operator, ME (a distance progressive operator) of which application on the F and B matrices provided good eccentric/centric ordering of vertices/graphs (Tables 1 and 2).

The ordering of molecular graphs induced by our operator in the set of heptanes is identical with that given by the van der Waals areas, as calculated by Moţoc et al. [14] (Table 2). Linear regression analysis showed good correlation of eccentric/centric parameters with van der Waals areas (Aw): FE = 0.9896; FC = = 0,9714; FCC = 0.9751; BE = 0,9859; BC = 0,9781; and BCC = 0,9781 For comparasion, among the indices tested in [14], only I corelates better than FE: r = 0,99. An inspection of tables 2 and 3 reveals the discriminatory power

of our metric characteristics in comparison with the analogous parameters of literature.

Centric parameters FCC/BCC were proposed with the aim to give a general (normalized) measure of graph centricity. This was made with the wiew to offer a reliable scale of graph ordering according to generaized graph center criteria [5]. In the next paper [15] the centric parameters will be tested in cyclic graphs, in comparison with the IVEC criteria given by Bonchev et al. [5].

Concluding, the metric characteristics newly introduced in this paper offer a good tool for the topological description of molecules. They are properly useful in structure-property/activity correlations.

Acknowledgements. We express our thanks to dr. B. Pârv (Computing Center, University of Cluj) for his technical assistance.

REFERENCES

1. a) *Part.* 4. M. V. Diudea, O. M. Minailiuc, A. T. Balaban, „Regresive vertex degrees (new graph invariants) and derived topogical indices", *J. Comput. Cham.*, **12** (1991) 527.
b) *Part.* 5. M. V. Diudea, L. Bal, „Recursive relationships for computing Y-indices in some particular graphs", *Studia Univ. Babeş-Bolyai*, **35** (1), **17** (1990).
c) *Part.* 6. M. V. Diudea, T. Cipăianu, L. Bal, „New Y-tipe indices of molecular branching", *Studia Univ. Babeş-Bolyai*, **35** (1), 29 (1990).
2. V. A. Skorobogatov, A. A. Dobrynin, *Math. Chem.*, **23**, 105 (1988).
3. A. T. Balaban, *Theoret. Chim. Acta*, **53**, 355 (1979).
4. A. T. Balaban, I. Moţoc, D. Banchev, O. Mekenian, *Top. Curr. Chem.*, **114**, 21 (1983).
5. D. Bonchev, O. Mekenyan, A. T. Balaban, *J. Chem. Inf. Comput. Sci.*, **29**, 91 (1989).
6. M. V. Diudea, B. Pârv, *Math. Chem.*, **23**, 85 (1988).
7. D. Bonchev, A. T. Balaban, O. Mekenyan, *J. Chem. Inf. Comput. Sci.*, **20**, 106 (1980).
8. F. Harary, „Graph Theory", Addison Wesley, Reading (Mass), 1971.
9. D. Bonchev, A. T. Balaban, M. Randic, *Int. J. Quantum Chem.*, **19**, 61 (1981).
10. J. Plesnik, *J. Graph Theory*, **8**, 1 (1984).
11. D. Bonchev, O. Mekenyan, A. T. Balaban, in „Mathematics and Computational Comcepts in Chemistry", N. Trinajstic, Ed. Ellis Horwood: Chichester U. K. 1986; Chapter 5.
12. D. Bonchev, *Pure Appl. Chem.* **55**, 221 (1983).
13. G. L. Ritter, T. L. Isenhour, *Comput. Chem.*, **1**, 145 (1977).
14. J. Labanowski, I. Moţoc, R. A. Dammkoehler, Comput. and Chem. **15**,47 (1991).
15. M. V. Diudea, D. Horváth, I. E. Kacsó, O. M. Minailiuc, „Centricities in molecular graphs. The MOLCEN algorithm," *J. Math. Chem.* **12** (1992)0000.

THIOCYANATO-CHROM (III)—KOMPLEXE IN DER CHEMISCHEN ANALYSE

50. Mit indirekte volumetrische und spektrophotometrische Methode zur Bestimmung von Hidroxizin

ION GĂVESCU*, und ION POPA*

Eingegangen am 17. Januar 1990

Thiocyanato-Chromium (III) Complexes in the Chemical Analysis. Part 50. An Indirect Volumetric and Spectrophotometric Method for the Determination of Hydroxizin. Hidroxizin forms with an excess of $NH_4[Cr(NCS)_4$ (aniline)$_2]$ and NH_4 [Cr(NCS)$_4$ (morpholine)$_2$] solution hidro-alcoolic sparingly soluble precipitate. After filtration the precipitate was decomposed by NaOH solution 5% and formed $Cr(OH)_3$ was titrated by $KMnO_4$, $KBrO_3$ or KIO_3 solutions by using ICl and extractions with CCl_4 as an endpoint indicator of titration.

The precipitation of Hidroxizin by NH_4 [Cr(NCS)$_4$ (aniline)$_2$] and dissolving of precipitate in acetone enables for spectrophotometric determination of Hidroxizine, measuring the absorbance of acetone solution of the complex at λ = = 540 nm. Molar absorbtivity equals 687 $cm^{-1} \cdot mol^{-1}$.

Wie wir beobachteten, bildet Hidroxizin in sauren Lösungen mit einigen Komplexsalzen, wie $K[BiI_4]$, $K_2[HgI_4]$, $K_3[Cr(NCS_6)]$, $NH_4[Cr(NCS)_4(NH_3)_2]$ und mit Reineckesalzanalogen Verbindungen.

Amin. H $[Cr(NCS)_4(Amin)_2]$ schwer lösliche Salze.

Von diesen können die Thiocyanato-chrom (III)-Komplexe auch für analytische Zwecke verwendet werden. Die Zusammensetzung der sehr schwer löslichen, in Form rotvioletter, mikrokristalliner Massen ausfallenden Tetrathiocyanato-diamin-chromiate entspricht der allgemeinen Formel: Hidroxizin. $H_2[Cr(NCS)_4(Amin)_2]_2$ (vgl. Tab. 1).

Tabelle 1

Neue Thiocyanatochrom (III) — Komplexe des Hidroxizine

No.	Verbindung	Mol. masse	Ausb. (%)	d.Th	Analyse ber.	Analyse gef.
1	HZ. $H_2[Cr(NCS)_4(NH_3)_2]_2$	1035,91	92	Cr	10,04	9,92
				S	24,76	24,57
2	HZ. $H_2[Cr(NCS)_4$ (Anilin)$_2]_2$	13,40,19	98	Cr	7,76	7,64
				S	19,14	19,06*
3	HZ. $H_2[Cr(NCS)_4$(Morpholin)$_2]_2$	1243,43	97	Cr	8,36	8,25
				S	20,63	20,49
4	HZ. $H_2[Cr(NCS)_4$ Py$_2]_2$	1284,10	92	Cr	8,10	8,02
				S	19,97	19,85
5	HZ. $H_2[Cr(NCS)_4$(Benzilamin)$_2]_2$	1396,19	95	Cr	7,45	7,38
				S	18,37	18,26
6	HZ. $H_2[Cr(NCS)_4$(Imidazol)$_2]_2$	1240,19	89	Cr	8,39	8,30
				S	20,68	20,53

%Cr als Cr_2O_3; %S als $BaSO_4$; HZ = Hidroxizins.

* *Lehrstuhl für anorganische und analytische Chemie der Universität, 1100 Craiova, Rumänien*

Zur Bestimmung wurden $NH_4[Cr(NCS)_4(Anilin)_2]$ und $NH_4[Cr(NCS)_4(Morpholin)_2]$ (Darstellung vgl. [2, 4]) herangezogen. Die Erfassung des Komplex gebundenen Thiocyanats erfolgt durch oxydimetrische Titration (vgl. Tab. 2). Wir beschrieben hier auch eine indirekte volumetrische Methode, welche auf der komplexometrischen Bestimmung des Chromgehaltes der Proben beruht (vgl. Tab. 3).

Daneben ist die photometrische Bestimmung des Komplexes möglich. Der molare Extinktionskoeffizient der Komplexverbindungen in Aceton ist $\varepsilon = 687$ cm^{-1} Mol^{-1}.

Tabelle 2

Oxydimetrische Bestimmung von Hidroxizin

Methode*	X mg	t_a	t_b	$t_{n-1,\alpha}$
Anilin Komplex				
Permanganometrisch	10,870	0,00193	0,0761	2,56
Bromatometrisch	10,870	0,965	1,564	2,56
Iodatometrisch	10,866	0,075	0,621	2,56
Morpholin-Komplex				
Permanganometrisch	10,868	0,0051	0,092	2,56
Bromatometrisch	10,878	0,00524	0,0925	2,56
Iodatometrisch	10,861	0,590	1,397	2,56

* n = 10 Bestimmungen; „t" Student-Parameter, $\alpha = 95\%$ [3]
1 ml 0,1 N Oxidationsmittel ($KMnO_4$, KJO_3, $KBrO_3$) äquiv. 1,5026 mg Hidroxizin

Tabelle 3

Die Rezultate der Komplexometrischen Bestimmung des Hidroxizin als $HZ.H_2Cr(NCS)_4(Anilin)_2$

HZ genommen mg	Zahl der Bestimmungen	Mittelwert X mg	Mittlere quadratische Abweichung einiger Bestimmung, S	t_a	t_b	$t_{n-1,\alpha}$
16,320	10	16,316	$5,44 \cdot 10^{-2}$	0,0018	0,036	2,26

1 ml 0,01 M E.D.T.A. sind 3,971 mg Hidroxizinäquivalent

Experimenteller Teil. 1. Oxydimetrische Bestimmung als Hidroxizin. $H_2[Cr(NCS)_4(Anilin)_2]_2$ und Hidroxizin. $H_2[Cr(NCS)_2(Morpholin)_2]_2$ 2—27 mg Hidroxizin in 25—50 ml H_2O werden in einem Becherglas mit verd. CH_3COOH angesäuert und mit überschüssiger 3proz. Reagenslösung bis zur Rotfärbung behandelt. Der entstehende Niederschlag wird nach 5—10 min abfiltriert, mit H_2O gewaschen und mit dem Filterpapier in ein Becherglas gebracht. Der Thiocyanat-Komplex wird mit 20 ml 5 proz. NaOH in der Siedehitze zerstört.

Das gebildete Chrom (III)-hydroxid wird in HCl gelöst und die Säurekonzentration auf annähernd 1,7 n eingestellt. Dann werden 5 ml CCl_4 und 10 Tropfen JCl-Lösung [1] hinzufügt. Es wird mit 0,1 n $KMnO_4$ oder $KBrO_3$ oder KJO_3 unter mehrmaligem Umschütteln bis zur Entfärbung der CCl_4-Schicht titriert.

Zur Bestimmung des Hidroxizins aus Dragées wird es aus 5—10 feingepulverten Dragées mit 50—100 ml $CHCl_3$ extrahiert, die Lösung filtriert, auf dem Wasserbade eingedampft und der getrocknete Rückstand in 5—10 ml C_2H_5OH und 20—30 ml 1 n CH_3COOH gelöst. Dann wird wie oben beschrieben gefällt und weiter verarbeitet.

2. Spektrophotometrische Bestimmung als Hidroxizin. $H_2[Cr(NCS)_4\ (Anilin)_2]_2$

1—12 mg Chloridiazepoxid in etwa 20—25 ml Probelösung werden wie oben beschrieben mit überschüssiger 3 proz. $NH_4[Cr(NCS)_4\ (Anilin)_2]$ — Lösung gefällt, der Niederschlag wird auf einer Glasfritte G_4 abgesaugt mit H_2O ausgewaschen, in Aceton gelöst, die Lösung in einem Meßkolben von 15 ml bis zur Marke aufgefüllt und die Extinktion der Lösung bei 540 nm gemessen.

3. Komplexometrische Bestimmung als Hidroxizin. $H_2[Cr(NCS)_4\ (Anilin)_2]_2$

2—27 mg Hidroxizin in 20—25 ml Probelösung werden wie oben ausgefällt, auf einem Glasfilter abgesaugt und dann mit Aceton (etwa 60—80 ml) behandelt und zum Sieden erhitzt. Nach 10—15 min Kochen wird die ganze Chrom (III)-Menge komplexiert. Die überschüssige E.D.T.A.-Menge wird mit 0,01 M Zinkacetat in Anwesenheit von Eriochrom-T — Indicator und 10—20 ml 0,1 M NH_4Cl — 0,1 M NH_3 — Pufferlösung zurücktitriert (vgl. Tab. 3).

LITERATUR

1. G. Desmuch, M. Ioshi, *Z. analyt. Chem.*, **142**, 275 (1969).
2. I. Gănescu, *Stud. Univ. Babeş-Bolyai, Ser. Chem.*, **12**, 103 (1967).
3. W. Jouden, „Statistical Methods for Chemists", 2nd Edit., S. 40, John Wiley, Sons Inc., New York, 1955.
4. I. Gănescu, Cs. Várhelyi, A. Hantz, I. Papa, *Z. anorg. allg. Chem.*, **520**, 196 (1985).

STUDIA UNIV. BABEŞ-BOLYAI, CHEMIA, XXXV, 1, 1990

NEW NONELECTROLYTES OF COBALT (III) WITH GLYOXIME

ION GĂNESCU*

Received: February 6, 1990

The formation of nonelecrolytes of cobalt (III) of the type $[Co(Glyox.H)_2(NCX)(amine)]$ was proved by the substitution reaction of $[Co(Glyox.H)_2(NCX)_2]^-$ with various amines in the presence of ammonium acetate buffer solution. (Glyox.H_2-glyoxime: $C_2H_4N_2O_2$, NCX-NCS and NCSe, respectively).

A number of nine new compounds were characterized by chemical analysis and infrared spectra.

The reaction of glyoxal with hydroxilamine hydrochloride leads to the formation of glyoxime. The neutron diffraction measurements [1] show the antiisomeric modification to be formed in this way. As compared with the other alphatic dioximes, the glioxime was only a little studied from co-ordination chemical point of view. The $M(Glyox.H)_2$ (M = Ni, Pd, Pt.) were obtained and its structure determined by means of x-ray measurements [2, 3]. The $Ni(Glyox.H)_2$ was proposed for detection of nickel [4] and for the spectrophotometric determination of cobalt (II) in basic media [5]. The glyoxime is able to form various mixed chelates of the types: $[M(Glyox.H)_2XY]^n$ (X = Y or X ≠ Y = Cl,, Br, I, NCS, SO_3, amine, etc.) n = −3, −2, −1, 0, +1. M = Co(III), Rh(III) Ir(III) [6, 7].

The Rh and Ir chelates are formed only by substitution reactions. The cobalt(III) complexes can be obtained by means of oxidation of a mixture of cobalt(II) salts, glyoxime and monodentate ligands (e, g. Cl, Br, I, NCS, amine, phosphine, etc.).

Results and discussion. We have observed that the alkaline salts $Na[Co(Glyox.H)_2(NCS)_2]$ and $Na[Co(Glyox.H)_2(NCSe)_2]$ obtained by the oxidation of the mixture of cobalt(II)—acetate, glyoxime and NaCNS or NaCNSe, respectively (molar ratio: 1 : 2 : 3), undergo a substitution reaction with monodentate neutral ligands.

The monodentate pseudohalogeno ligands can be substituted partially with amines or phosphines by the following substitution reaction in ammonium acetate buffer solution:

$$[Co(Glyox.H)_2(NCX)_2]^- + \text{a nine} = [Co(Glyox.H)_2(amine)(NCX)] + NCX^-$$

Some new derivatives with aromatic and heterocyclic amines are characterized in Table 1.

These substitution reactions were carried out in boiling aqueous alcoholic solutions. The nonelectrolytes are sparingly soluble in water and soluble in acetone, dimethylformamide etc.

* University of Craiova, Department of Inorganic and Analytical Chemistry, 1100 Craiova, Romania

Table 1

New nonelectrolytes of the type $[Co(Glyox.H)_2(NCX)(amine)]$

No.	Formula	Mol. wt. calcd.	Aspect	Analysis, (%)		
				Calcd.		Found
1.	[Co(Glyox.H)$_2$(NCS)(p-toluidine)]	398.2	brown, thin needles	C	36.08	36.00
				H	3.66	3.79
				N	21.00	21.02
2.	[Co(Glyox.H)$_2$(NCSe)(p-toluidine)]	445.1	brown crops	C	32.35	32.25
				H	3.39	3.30
				N	18.81	18.77
3.	[Co(Glyox.H)$_2$(NCS)(p-anisidine)]	414.2	short, brown prisms	C	34.79	34.73
				H	3.64	3.60
				N	20.27	20.19
4.	[Co(Glyox.H)$_2$(NCSe)(p-anisidine)]	461.1	thick, irregular brown prisms	C	31.25	31.19
				H	3.27	3.18
				N	18.21	18.17
5.	[Co(Glyox.H)$_2$(NCS)(γ-picoline)]	384.1	long, brown needles	C	34.38	34.83
				H	3.40	3.37
				N	21.86	21.80
6.	[Co(Glyox.H)$_2$(NCSe)(γ-picoline)]	431.1	yellow-brown, thin plates	C	30.67	30.59
				H	3.05	2.93
				N	19.48	19.40
7.	[Co(Gloyx.H)$_2$(NCS)(2-methyl-imidazole)]	373.2	brown hexagonale prisms	C	28.96	28.87
				H	3.24	3.20
				N	26.25	26.09
8.	[Co(Glyox.H)$_2$(NCSe)(2-methyl-imidazole)]	420.1	brown irregular prisms	C	25.73	25.66
				H	2.86	2.80
				N	23.32	23.25
9.	[Co(Glyox.H)$_2$(NCS)(benzthiazole)]	427.3	short, irregular brown cryst.	C	33.80	33.73
				H	2.59	2.46
				N	19.70	19.62
10.	[Co(Glyox.H)$_2$(NCSe)(benzthiazole)]	473.1	brown, irregular cryst.	C	30.45	30.30
				H	2.39	2.21
				N	17.75	17.64

Infrared spectra. IR spectra of some nonelectrolytes have been recorded in kalium bromide pellets in the 400 to 4000 cm^{-1} wave number range.

The position of the ν_{CN}, ν_{CX} and δ_{XCN} bands indicates the co-ordination mode of the pseudohalide groups.

In our cases these frequencies are situated:

NCS— derivatives: 2100—2115 (vs), 870—860 (s) 470—480 (m) cm^{-1}

NCSe— derivatives: 2100—2120 (vs), 510—600 (s), 430—450 (m) cm^{-1}

By the alkaline salts: NaCNS and KCNSe these frequency values appear at lower numbers:

NaCNS: 2060 (vs), 749 (s), 470 (m): KCNSe: 2069 (vs), 558 (s), 416 — 424(m) cm^{-1}.

This phenomenon indicates the mentioned ambidentate ligands to be co-ordinated to the central cobalt atom through the N-atom (izo-thiocyanato - and izo-selenocyanato- complexes with Co-NCX- line bondings)

The presence of weak bands: νO—H: 2300 cm^{-1} and δO—H..O:

at 1700—1730 cm^{-1} is due to an intramolecular hydrogen bridge in the $Co(Glyox.H)_2$—grouping with a planar geometric configuration
This hydrogen bridge stabilizes also the trans geometric configuration of the $[Co(Glyox.H)_2(NCX)(amine)]^0$ type complexes.

Experimental *NaCNSe* was obtained by melting of a mixtura of NaCN and matallic selenium (molar ratio) in a sand bath.
Glyoxime was obtained from 30% glyoxale with a stoechiometric amount of hydroxylamine hydrochloride as described earlier.
$Na[Co(Glyox.H)_2(NCX)_2]$ - solutions were obtained by air oxidation of a mixture of cobalt (II) acetate, glyoxime and NaNCX in dil. alcoholic solution as described earlier.
$[Co(Glyox.H)_2(NCX)(amine)]$ — 5 mmoles of $Na[Co(Glyox.H)_2(NCX)_2]$ in 50 ml water were treated on a water bath with 5—6 — mmoles amine in 5—10 ml alcohol and 2 g ammonium acetate. After a warming of about 3—45 minutes the precipitated crystalline product is filtered off and washed with diluted alcohol (1:3).
Analysis: The C, H, N content was determined on the usual microanalytical way.

REFERENCES

1. M. Calleri, G. Ferraris, D. Vitterbo, *Acta Cryst.*, **20**, 73 (1966).
2. M. Calleri, G. Ferraris, D. Vitterbo, *Acta Cryst.*, **22**, 468 (1967).
3. G. Ferraris, D. Vitterbo, *Inorg. chim. Acta*, **1**, 297 (1967).
4. S. Kuse, S. Motomizu, K. Toei, *J. Chem. Soc. Japan, Chem. and Ind. Chem.*, **8**, 1661 (1973).
5. Masuda Nobosuka, Kajiwara Meisetsu, *Bunseki Kagaku*, **17**, 1352 (1968); *Chem. Abstr.* **70**, 63 856 (1969).
6. G. Marcu, Cs. Várhelyi, M. Somay, D. Itul, E. Péter, *Stud. Univ. Babeș-Bolyai, Chem.*, **31**, (1), 68 (1986).
7. I. Gănescu, Cs. Várhelyi, J. Zsakó, Polyhedron (in press)

STUDIA UNIV. BABEŞ-BOLYAI, CHEMIA, XXXV, 1, 1990

SURFACE MOBILITY OF SURFACTANT SOLUTIONS
XIV. Marangoni Flow through Square Sectioned Horizontal „Surface" Canals

EMIL CHIFU*, EUGENIA GAVRILĂ* and MARIUS SĂLĂJAN*

Received: March 7, 1990

Experimental results, obtained in a study of the Marangoni flow through square-sectioned horizontal canals, are presented. The flow is determined by surface tension gradients which are induced by temperature differences, as well as by surfactant concentration differences. The rates of flow, experimentally evaluated, are compared with the values calculated on the basis of a theoretical model previously reported [10]. A satisfactory agreement is found between the experimental values and the ones foreseen by theory.

Studies on the Marangoni instability and flow of liquids find their use in many fields of science and technology (mass transfer processes, motions at the level of biosurfaces etc.), as well as in operations with liquids in microgravity conditions. The Marangoni flow and its effects have been tackled both from the experimental and from the theoretical aspect, in several variants. We mention studies concerning:

a) the behaviour of liquid drops or of gas bubbles [1—5];

b) the behaviour of thin liquid strata [6, 7].

This transport of the liquid can be generated by surface tension gradients, induced especially by surfactant concentration differences [6] or by temperature differences [7].

The surface (Marangoni) flow through canals (surface slits) of triangular section under the action of surface tension gradients has been experimentally investigated, in the case of gas/liquid interface, using the model of the inclined solid plane [6]. In these circumstances the Marangoni flow competes with a bulk flow determined by gravity forces. The share of the two types of flows can be evaluated by the agency of the rates of flow [6, 7]. The flow through horizontal canals, when only the Marangoni flow persists, completes our previous studies.

The flow through horizontal „surface" canals, acted by gradients brought about by unequal concentrations of surfactants, has been investigated between spherical liquid/liquid interfaces (drops) [8], by making use of the Plateau approximation of equidense liquids.

It is to be expected that the obtained results are also valid, in a first approximation [9], for the surface flow caused by temperature differences. But the study of the flow through spherical liquid/liquid interfaces, having as a motive force temperature differences, is not accessible from the exprimental point of view, due to instability of the system. Consequently, we have turned our attention to the surface flow between two plane liquid/gas interfaces, and in the present work we report the obtained results.

* *University of Cluj-Napoca, Faculty of Chemical Technology, 3400 Cluj-Napoca, Romania*

Theoretically, the flow induced by surface tension gradients can be described, in the case of horizontal canals having a triangular, rectangular or square section, by resorting to the complex functions method. In the case of square sectioned canals, a first approximation leads to the following equation for the rate of flow, Q [10]:

$$Q \simeq 3.90 \frac{(\sigma_2 - \sigma_1)\delta^3}{\pi^4 \mu H} \qquad (1)$$

where σ_1 and σ_2 are the surface tensions of the two liquids ($\sigma_2 > \sigma_1$); δ represents the depth of the canal, H is its length, and μ the bulk liquid viscosity; the surface viscosity has been neglected [6].

Experimental. The surface flow through horizontal canals has been watched by means of a device schematically represented in Fig. 1. It is composed of two vessels (1, 2) made of stainless steel, and thermostated. A steel bar, forming one piece with the vessel (1), is engraved with a square-sectioned canal (3) having $\delta = 0.1$ cm and H = 25 cm. The free end of the bar can be fastened to the vessel (2) by means of a teflon gasket. The level vessel (4) helps adjusting the liquid level in the high-temperature vessel (1).

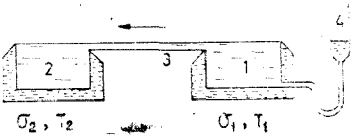

Fig. 1. Outline of the experimental device.

The liquid used in our experiments is water, as it adequately wets the steel surface. Vessel (2) contains water at low temperature T_2 (16 °C), with the surface tension σ_2, and vessel (1) aqueous methylene blue (c = 0.2 g/l), at high temperature T_1, with the surface tension σ_1. In this way, surface tension gradients are created, corresponding to temperature differences from 10 °C to 60 °C. Acted by the surface tension gradient, the liquid in vessel (1) is transported into vessel (2). As methylene blue practically does not influence the surface properties of the solution, it can conveniently be used in the spectrophotometric determination of the rates of flow. In our experiments, samples have been withdrawn from vessel (2) once in ten minutes, for 60–80 min., and their spectrophotometric analyses allowed to calculate the volume of the liquid transported by Marangoni flow. Measurements have been done at the wavelength (λ) of 675 nm where methylene blue has an absorption maximum. A great care has been taken to horizontally level the liquid in the two vessels and in the canal. The watching has been performed by means of a telecobjective throughout the experiment: The losses of liquid due to evaporation in vessel (1) have been corrected by means of the level vessel (4); and those caused by withdrawal of 1 ml aliquots from the entire quantity of 350 ml in vessel (2), by adding back the corresponding liquid quantities. This rigorous maintenance of the arrangement in the horizontal is an imperative condition, because hydrostatic pressure created by an unevenness of 1 mm can give rise to the flow of a volume of liquid (gravitational discharge) comparable with that one determined by the surface forces.

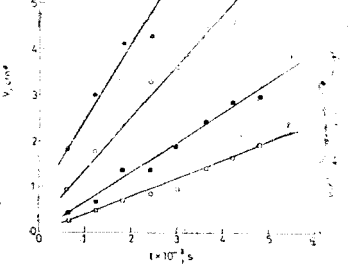

Fig. 2. Variation of the flowed liquid volume as a function of time for different surface tension gradients.
— Curve (1) ($\sigma_2 - \sigma_1$) = 2.8 mN/m;
— Curve (2) ($\sigma_2 - \sigma_1$) = 5.2 mN/m;
— Curve (3) ($\sigma_2 - \sigma_1$) = 7.3 mN/m;
— Curve (4) ($\sigma_2 - \sigma_1$) = 11.5 mN/m

Results and Discussion. The time dependence of the liquid volume of Marangoni flow is represented in Fig. 2. As can be seen, there is a linear variation which points to establishment of a steady flow regime. This conclusion agrees with the fact that the surface tension difference is kept constant during the flow. Some scattering of the experimental points can be attributed to

slight temporary disturbance of the liquid surface horizontal alignment, which cannot be completely avoided, despite the precautious measures taken.

The flow rates have been derived from the slopes of experimental straight lines like those in Fig. 2, by using the least squares method. The such obtained values are given in Table 1, together with those calculated according to Eq. (1).

Table 1

Comparison of the experimental and the calculated rates of flow

No	$(\sigma_2 - \sigma_1)$ mN/m	$Q_{exp} \times 10^4$ cm³/s	$Q_{calc} \times 10^4$ cm³/s	
			$Q = f(\mu_2)$	$Q = f(\bar{\mu})$
1	2.8	3.9	4.0	4.7
2	3.3	3.2	4.8	6.0
3	3.5	3.6	5.1	6.4
4	5.2	6.4	7.5	10.1
5	7.1	10.2	10.3	13.7
6	7.3	10.3	10.6	14.8
7	10.2	12.6	14.7	21.6
8	11.5	15.0	17.0	24.3
9	4.5	7.0	6.8	
10	8.5	9.4	12.6	

No. 1 – 8 — surface tension gradients induced by temperature differences
No. 9 – 10 — surface tension gradients induced by differences in surfactant concentrations.

Taking into account that the variation of the liquid viscosity likewise the canal is not known, the rates of flow have been calculated as functions of the viscosity of the cold liquid μ_2, or of the average viscosity $\bar{\mu}$ (see Table 1). It can be noticed that the experimental values are in a good agreement with the values calculated in the first variant (by means of μ_2). The fact is plausible because when the liquid is about to reach vessel (2) its viscosity is that one corresponding to temperature T_2 ($T_2 < T_1$, $\mu_2 > \mu_1$). One can also suggest that the liquid in the metallic canal has got the viscosity value corresponding to the room temperature — that is a value close to that of the cold liquid (μ_2).

Considering that surface flow can be accompanied by thermal convection, we tried to assess the contribution of the latter to the overall process. That is why we have measured the Marangoni flow, generated by surface tension gradients induced by surfactant concentration differences, at constant room temperature (17°C). The obtained results and the evaluated flow rates are situated within the

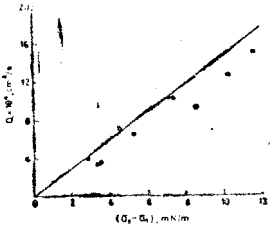

Fig. 3. Dependence of the rate of Marangoni flow upon the tension gradients.
— Theoretical curve Eq. (1): ———
—, Experimental values for gradients induced by temperature differences: ●
— Experimental values for gradients induced by surfactant concentration differences: ○

values determined by temperature differences (Table 1). In Fig. 3 are given the theoretical and the experimental rates of flow, as functions of surface tension gradients generated in the two ways. A satisfactory agreement is found between the two sets of results, what allows us to infer that thermal convection does not play an important rôle in the overall process under consideration. This finding also agrees with some data in the literature [9]. For that reason, we suggest that, in the model of Marangoni flow brought about by temperature differences and experimentally studied by us in the present work, omission of the energy equation is justified.

REFERENCES

1. S. C. Hardy, *J. Colloid Interface Sci.*, **69**, 157 (1979).
2. T. Narasaki, *Adv. Space Res.*, **3**, (5), 137 (1983).
3. E. Chifu, I. Stan, Z. Finta, E. Gavrilă, *Rev. Chim.*, (Bucureşti), **31**, 765 (1980); E. Chifu, I. Stan, *Rev. Roumaine Chim.*, **25**, 1449 (1980); E. Chifu, I. Stan, Z. Finta, E. Gavrilă, *J. Colloid Interface Sci.*, **93**, 140 (1983); I. Stan, E. Chifu, Z. Finta, E. Gavrilă, *Rev. Roumaine Chim.*, **34**, 603 (1989).
4. H. S. Kim, R. S. Subramanian, *J. Colloid Interface Sci.*, **127**, 417 (1989).
5. M. D. LeVan, J. A. Holbrook, *J. Colloid Interface Sci.*, **131**, 242 (1989).
6. E. Chifu, I. Albu, *Stud. Univ. Babeş-Bolyai Chem.*, **13** (1), 99 (1968); E. Chifu, C. I. Gheorghiu, I. Stan, *Rev. Roumaine Chim.*, **29**, 31 (1984); E. Chifu, C. I. Gheorghiu, I. Stan in VI. Internationale Tagung über Grenzflächenaktive Stoffe, Bad Stuer, 1985 pp. 211—217; E. Chifu, C. I. Gheorghiu, *Rev. Roumaine Chim.*, **32**, 945 (1987).
7. E. Chifu, I. Albu, C. I. Gheorghiu, E. Gavrilă, M. Sălăjan, M. Tomoaia-Cotişel, *Rev. Roumaine Chim.*, **31**, 105 (1986).
8. E. Chifu, Z. Finta, M. Sălăjan, E. Gavrilă, *Rev. Roumaine Chim.*, **26**, 1345 (1981).
9. V. G. Levich, „Physicochemical Hydrodynamics", Prenntice-Hall, New Jersey, 1962, pp. 384—390.
10. E. Chifu, R. Deutsch, *Rev. Roumaine Chim.*, **11**, 873 (1966); R. Deutsch, P. Sandru, E. Chifu, *Stud. Univ. Babeş-Bolyai, Chem.*, **10**, (2), 91 (1965).

STUDIA UNIV. BABEŞ-BOLYAI, CHEMIA, XXXV, 1, 1990

THIN LAYER CHROMATOGRAPHY OF SOME DIRECT DYES

SIMION GOCAN*, IOAN PANEA*, ILEANA AXECHITEI*

Received: March 26, 1990

This study deals with the chromatographic behaviour of 12 industrial direct dyes. Precoated Silica Gel 60 Merck plates with concentrating zone were used. As eluent we used the following systems: pyridine/35% ammonia/isobutanol (1 : 1 : 3 v/v), dioxane/35% ammonia/isobutanol (1 : 1 : 3, v/v) and quinoline/35% ammonia/isobutanol (1 : 1 : 3, v/v). These three eluent systems behave very much alike, so they can be considered isopartitives. It has also been found that most of the examined industrial dyes do not have a unitary composition. To conclude, in the described conditions, thin layer chromatography together with photodensitometric quantitative analysis are valuable means to test the quality of industrial direct dyes.

Introduction. Direct dyes used mostly to dye cellulosic materials must have a certain molecular configuration in order to have support affinity. This configuration implies molecular extensive coplanarity, achieved by a system of 8—9 conjugated double bonds which are mostly part of the aromatic systems. The most used modality to obtain direct dyes is the azoic coupling of difunctional diazonium salts or/and coupling components. Under these circumstances many reactions take place, which lead to the formation of many compounds so that, very often, the direct dyes resulted from synthesis are mixtures of isomers or of many other compounds. This is the form in which they are used in dying, taking into consideration on the one hand their compatibility and on the other, the extreme difficulty of their separation into pure components [1—3].

The commercial direct dyes usually contain various other components added in order to bring them to the standard tinctorial strength and also to achieve the desired shade [4]. Consequently, a lot of commercial direct dyes are mixtures [1—5].

This is the reason for which their analysis and separation into components is necessary for a more thorough characterization (inclusive for quality control.) For this purpose we have tried to use thin layer chromatography. This category of dyes contains sulfonic or carboxilic groups which assures the solubility in water in form of sodium salts. This fact led us to the idea of using stationary phases and eluents suitable for a separation mechanism through liquid-liquid distribution.

The stationary phase most often used to separate direct dyes by thin layer chromatography is the silica gel. As a mobile phase phenol/water (4 : 1, v/v) [6]; chloroform/2-propanol/water (1 : 3 : 1, v/v), and n-butanol/ethyl acetate/water (8 : 1 : 3, v/v) [7] has been used. The eluent formed from propanol/isobutanol/ethyl acetate/water (4 : 2 : 1 : 3, v/v) [8] was used to detect the falsification of reactive dyes with worthless direct dyes.

* *University of Cluj-Napoca, Faculty of Chemistry, 3400 Cluj-Napoca, Romania*

Eluent systems with an acid character: n-butanol/acetic acid/water (4 : 1 : 5, v/v) [7], and with a basic character: n-butanol/water/ammonia (2 : 1 : 1, v/v) [9], buthyl acetate/pyridine/water (6 : 9 : 5, v/v) [8, 10], n-butanol/ethanol/ammonia/pyridine/water (8 : 3 : 4 : 4 : 3, v/v) [11], buthyl acetate/pyridine/quinoline/water (3 : 3 : 1 : 3, v/v) [12], ethanol/ammonia with water (1 : 9)/n-butanol (9 : 2 : 5, v/v) [13] and 2-propanol/ammonia/water (7 : 1 : 1, v/v) [7], for different classes of dyes have also been used.

In order to separate direct dyes besides silica gel there were also used cellulose layers and the following eluent systems: propanol/ethyl acetate/water (6 : 1 : 3, v/v) and benzyl alcohol/dimethylformamide/water (4 : 2 : 1, v/v) [7]. Layers with different types of alumina and a system of etanol/water [14] were also used as eluent in different proportions according to the alumina type which was being used.

Experimental. We analysed 12 industrial dyes in their commercial form (Table 1) and other three dyes: a naphtalinic analogue of direct fast yellow EPL (Romania), unconditioned direct fast yellow EPL (Romania) and sirius light yellow GD without inorganics (inorganics were separated by boiling the dye with dimethylformamide, filtration and precipitation of the dye from filtrate with acetone [1]).

Experiments were carried out on precoated Silica Gel 60 Merck plates (the thickness of the thin layer was 0,25 mm) with concentrating zone.

As eluent we used ternary mixtures with the following composition: pyridine/ammonia 35%/isobutanol (1 : 1 : 3, v/v), dioxane/ammonia 35%/isobutanol (1 : 1 : 3, v/v) and quinoline/ammonia 35%/isobutanol (1 : 1 : 3, v/v). These systems were selected according to the Hildebrand solubility parameters and are considered as being isopartitives [15].

The developments were made in N-saturated chambers. We applied 3 µl/spot of 0.1% alcoholic solution from each dye.

The photodensitometry by reflexion was made with ERI 65 Carl Zeiss Jena (DDR) photodensitometer using a 400 nm filter.

Results and Discussion. The results concerning the chromatographic behaviour of the 15 samples of dyes are given in Table 1. From these results we come to the conclusion that most of these dyes do not have a unitary composition, because except for crysofenine and direct yellow 49, all the dyes examined exhibited more chromatographic spots (Table 1). Some of these dyes have a main component, the other components being found in traces (e.g.: direct yellow 1, direct yellow 11, direct yellow 27), while other dyes contained many components of about the same concentrations (e.g. direct yellow 44 and direct fast yellow EPL). These results are confirmed quantitatively in the case of direct fast yellow EPL 250% using the photodensitometric analysis.

The peak area was established with a planimeter. The concentration of each component in the sample is calculated by the so-called normalized peak area: $C = 100\, A_i / \Sigma A_i$ (%). In certain cases we can assume that the normalized peak areas give the concentration directly. This is generally true for most dyes if a relatively small range of closely related components is analyzed. In these cases, the normalized peak area values are usually taken as weight per cent of the individual components in the sample. The results are given in Fig. 1 and Table 2.

Table 1

hR_f values for some industrial direct dyes on precoated SILICA GEL 60 Merck plates with concentrating zone

	Name of the dye	Eluent system		
		Pyridine/35% ammonia/ isobutanol (1 : 1 : 3, v/v)	dioxane/ 35% ammonia/ isobutanol (1 : 1 : 3, v/v)	quinoline/35% ammonia/ isobutanol (1 : 1 : 3m, v/v)
1.	Direct fast yellow EPL unconditioned	0*, 15, 16, 21*, 27*, 31, 34, 45	0*, 3*, 6, 10, 19, 28, 36	0*, 7*, 10, 13, 18, 26, 40
2.	Crysofenine (CI 24895) Direct yellow 12 (Francolor)	46	38	42
3.	Brilliant yellow (CI 24890) Direct yellow 4 (Romania)	0*, 9, 18*	0*, 3, 8*	0*, 4, 10*
4.	Direct yellow 11 (CI 40000) (Bayer)	0, 6*, 10*	0, 8*	0, 3*, 6*
5.	Direct yellow 27 (CI 13950) (Ciba-Geigy)	18*, 32, 63*	—	25, 64*
6.	The analogue with α-naftol of Direct fast yellow EPL (Romania)	0, 18, 28*	0, 14*, 22*, 27, 33*	0, 10*, 11*, 13*, 15, 20*, 24, 33
7.	Direct yellow G Direct yellow 1 (CI 22250) (Romania)	14*, 34	0*, 31	0*, 29, 36*
8.	Direct yellow 44 (CI 29000) (Poland)	26, 29, 33	21, 26, 30	18, 22, 29
9.	Sirius light yellow GD without inorganics	16*, 18*, 25, 33*, 36*	6*, 14, 21*, 33*	6*, 10*, 15, 30*
10.	Sirius light yellow GD Direct yellow 110 (Bayer)	15*, 19*, 25, 33*, 37*	7*, 14, 21*, 33*	5*, 9*, 16, 30*
11.	Direct yellow 134 (CI 29048) (Francolor)	28, 32*, 34*	23, 26*, 29*	17, 27*
12.	Direct yellow 49 (CI 29035) (Geigy)	24	19	15
13.	Direct yellow 50 (CI 29025) (Poland)	8, 25*	0, 12*	0*, 3, 13*
14.	Direct light yellow O—USSR	3, 16*, 44*	0, 10*, 40*	2, 9*, 44*
15.	Direct fast yellow EPL 250% (Romania)	0*, 14, 25, 27, 30, 33, 42, 46*	0, 3*, 5*, 10, 20, 29, 39, 41*	0, 6*, 8*, 13, 18, 26, 40 45*

* Traces of the dye

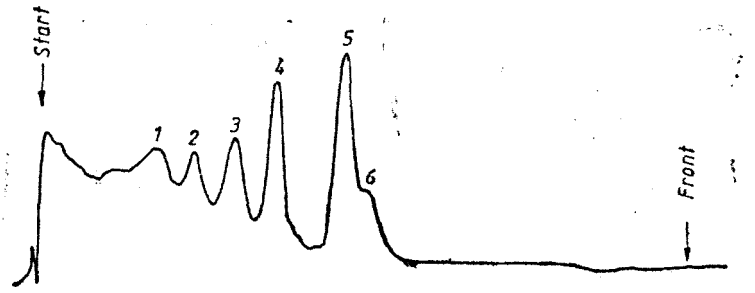

Fig. 1. The photodensitogram of the direct fast yellow EPL 250% dye conditioned with NaCl, obtained at 400 nm. Precoated Silica Gel 60 Merck plates with concentrating zone. Double development with pyridine/35% ammonia/isobutanol (1 : 1 : 3, v/v).

Table 2

The hR_f values and the procentual concentration of the components of the direct fast yellow EPL 250% industrial dye corresponding to the densitogram from Fig. 1. Precoated Silica Gel 60 Merck plates with concentrating zone. Double development with pyridine/35% ammonia/isobutanol (1 :1 :3,v/v.)

Number of peak	hR_f values	Concentration (%)
1	18	9.65
2	24	7.00
3	32	15.20
4	38	24.75
5	48	36.85
6	51	6.58

The quantitative analysis of the densitogram points out that during the synthesis many compounds of different concentrations were formed.

The following structures I—III might appear due to the synthesis of the direct fast yellow EPL 250% dye [15, 16]:

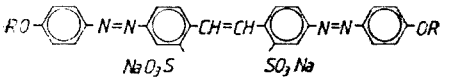

I (R: $-H_2C-\underset{O}{CH}-CH_2$) II (R: $-CH_2-\underset{OH}{CH}-CH_2Cl$)

III (R: $-CH_2-\underset{OH}{CH}-CH_2-OH$) IV (R: $-CH_2-CH_3$)

Once having examined these structures and taking into consideration the adsorption energies for the —O—ether, -Cl and -OH atom groups [17] we could establish the following polarity growing rate for them: IV < I < II < III, and we could also establish the probable peak corespondence in the densitogram (Fig. 1) and (Table 2): peak 5 for structure I; peak 4 for structure II and peak 3 for structure III. The attribution of peak 5 to the dieqoxide is sustained by the fact that it is the most similar to crysofenine (IV). If we examine the chromatographic data from Table 1, we realize that the $hR_f = 46$ value for crysofenine is comparable with the $hR_f = 42$ value of the dieqoxide which is more polar than crysofenine.

The hR_f values in Table 1 point out that the three eluent systems behave in an identical way, so they can be considered isopartitive [18].

To conclude, thin layer chromatography together with photodensitometric quantitative analysis are valuable means to test the quality of the examined industrial direct dyes in the described conditions.

REFERENCES

1. K. Venkataraman, „The Analytical Chemistry of Synthetic Dyes", John Willey and Sons New York, 1977, p. 7, 11, 12, 31.
2. Kirk-Othmer, „Encyclopedia of Chemical Technology", Third edition, Vol. 3, 1978, p.387–433.
3. „Ullmanns Encyclopädie der Technischen Chemie", 4th edition, Vol. **8**, 1974, p. 259–286.
4. G. S. E. Egerton, J. M. Gleadle and N. D. Uffindell, *J. Chromatogr.*, **26**, 62 (1967).
5. G. H. Rettie and C. G. Haynes, *J. Soc. Dyers Colour.*, **80**, 629 (1964).
6. M. N. Mashruvala, H. U. Mehta, *Text. Dyer Printer*, **13** (2), 41 (1979); *Analyt. Abstr.*, **40**, 4C79 (1981).
7. E. Tzicas, *Rev. Tech. Ind. Cuir*, **75** (7), 222 (1983); *Analyt. Abstr.*, **46**, 11C60 (1984).
8. W. B. Achwal, P. N. Abhyankar, *Text. Dyer Printer*, **12** (5), 33 (1979); *Analyt. Abstr.*, **39**, 5C84 (1980).
9. C. D. Sweeny, *Amer. Dyst. Rep.*, **61**, 70 (1972).
10. L. Meckel, H. Milster, U. Krause, *Textil-Praxis*, **16**, 1052 (1961).
11. J. C. Brown, *J. Soc. Dyers Colour*, **80**, 185 (1964).
12. S. Logar, N. Mesicek, *Kem. Ind.* (Zagreb), **17**, 473 (1968); *Chem. Abstr.*, **70**, 79120r (1969).
13. K. Wada, I. Shirai, *Hikaku Kagaku*, **13**, 149 (1968); *Chem. Abstr.*, **68**, 88227s (1968).
14. P. Raban, *Nature*, **199**, 596 (1963).
15. O. Stephenson, *J. Chem. Soc.*, **1954**, 1571.
16. M. Lidarek, J. Kinel, V. Ulbrich, *Chem. Listy*, **50**, 1960 (1956).
17. L. R. Snyder, „Principles of Adsorbtion Chromatography", Wiley-Interscience, New York, 1971.
18. S. Gocan, I. Anechitei, *Studia Univ. Babeş-Bolyai, Chem.*, **34** (1) 75 (1989).

STUDIA UNIV. BABEŞ BOLYAI, CHEMIA, XXXV, 1, 1990

NEW HETEROPOLYOXOMETALATE ANIONS WITH HETEROATOMS IN NON-EQUIVALENT SITES

II. The Study of the Reactions of Formation (1)

ADRIAN PĂTRUŢ* and ALEXANDRU BOTAR*

Received: April 12, 1990

In the studies of the reactions of formation of some heteropolyoxometalate anions containing heteroatoms in non-equivalent sites, of the types $PZMo_2W_9O_{39}(H_2O)^{5-}$ and $P_2ZMoW_{16}O_{61}(H_2O)^{8-}$ (where Z = Mn^{II}, Ni^{II}, Cu^{II}), with modified Keggin and modified Dawson structure respectively, the optimum pH range of formation has been determined by high tension paper electrophoresis.

Introduction. The heteropolyoxometalate anions (HPOM—A) of the types $PZMo_2W_9O_{39}(H_2O)^{5-}$ and $P_2ZMoW_{16}O_{61}(H_2O)^{8-}$, containing heteroatoms in non-equivalent sites, with modified Keggin and modified Dawson structure respectively, are formed according to a general reaction:

$$mZ^{z+} + nL^{q-} \rightleftarrows Z_mL_n^{(nq-mz)-}, \qquad (1)$$

where: $Z^{z+} = Mn^{2+}$, Ni^{2+}, Cu^{2+}; $L^{q-} = HPOM—A^{q-}_{ligand} = PMo_2W_9O_{39}^{7-}$, $P_2MoW_{16}O_{61}^{10-}$.

The study of the reactions of formation in solution aimed to establish the conditions of HPOM—A synthesis, namely:

— the optimum pH range of formation;

— the stoichiometry of the reactions.

This paper is devoted to the determination of the optimum pH range of formation of the studied HPOM—A.

Generally, papers concerned with HPOM—A containing heteroatoms in non-equivalent sites make use of photocolorimetry, spectrophotometry or electrophoresis to establish the pH range of formation. We consider that the electrophoretic methods eliminate some disadavantages of the photocolorimetric and spectrophotometric methods, when the reagents and the reaction products are liable to complex transformations within a restricted pH range, and are especially recommended for the study of the reactions of formation of the coordination compounds in solution.

The high tension paper electrophoresis has been used with good results in the study of the reactions of formation of some HPOM—A [1—8].

* *Institute of Chemistry, 3400 Cluj-Napoca, Romania*

Results and Discussion. Taking into account that the formed HPOM—A are of the type 1 : 1(m=n=1), as it is shown by the study of the stoichiometry of the reactions of formation, and ignoring the electric charges, Eq. (1) becomes:

$$Z + L \rightleftarrows ZL \tag{2}$$

The reactions between the Z transitional cations and the L HPOM—A ligands (where $Z = Mn^{2+}$, Ni^{2+}, Cu^{2+}; $L = PMo_2W_9O_{39}^{7-}$, $P_2MoW_{16}O_{61}^{10-}$) were investigated by paper electrophoresis.

The sum of the electrophoretic mobilities of the ionic species in the system:

$$\mu = \frac{\sum_i \mu_i c_i}{\sum_i c_i} \tag{3}$$

b comes, when the experiments are performed in HPOM—A ligand medium:

$$\mu = \frac{\mu_z [Z] + \mu_{zl} [ZL]}{[Z] + [ZL]}, \tag{4}$$

where: μ = the sum of the electrophoretic mobilities;

μ_i, μ_z, μ_{zl} = the electrophoretic mobilities of the ions i, Z, ZL;

c_i, $[Z]$, $[ZL]$ = the concentrations of the ions, i, Z, ZL.

The optimum pH range of formation of the studied HPOM—A of the type ZL (where $ZL = PZMo_2W_9O_{39}(H_2O)^{5-}$, $P_2ZMoW_{16}O_{61}(H_2O)^{8-}$), can be established by determining the sum of the electrophoretic mobilities for different pH values and by plotting the function $\mu = f(pH)$.

The measurement of the electromigration of the ionic species allows to determine the sum of the electrophoteric mobilities by using the Kunkel — Tiselius relation [9]:

$$\mu_d = d \frac{1}{Vt} \left(\frac{l'}{l}\right)^2 \tag{5}$$

where: μ_d = the sum of the experimentally determined electrophoretic mobilities; d = the migration of the ionic species; V = the applied potential difference; l = the length of the chromatographic paper; l'/l = the porosity factor of the chromatographic paper.

For the determination of the real value of the sum of the electrophoretic mobilities (μ), the adsorption on the chromatographic paper of the formed HPOM-A must be also taken into account, according to the relation:

$$\mu = \mu_d \frac{1}{R_f} \tag{6}$$

The average R_f values for the formed HPOM—A, determined by ascending paper chromatography, are given in Table 1.

Table 1

The average R_f values for HPOM—A (on Karl Schneider Schull chromatographic paper)

HPOM—A	R_f
$PMnMo_2W_9O_{39}(H_2O)^{5-}$	0.90
$PNiMo_2W_9O_{39}(H_2O)^{5-}$	0.94
$PCuMo_2W_9O_{39}(H_2O)^{5-}$	0.97
$P_2MnMoW_{16}O_{61}(H_2O)^{8-}$	0.94
$P_2NiMoW_{16}O_{61}(H_2O)^{8-}$	0.95
$P_2CuMoW_{16}O_{61}(H_2O)^{8-}$	0.98

The migration of the ionic species and the sum of the electrophoretic mobilities as a function of pH, for Z/ZL systems, are given in Tables 2, 3 and 4.

Table 2

The migration of the ionic species and the sum of the electrophoretic mobilities as a function of pH,for the systems $Mn^{2+}/PMnMo_2W_9O_{39}(H_2O)^{5-}$ and $Mn^{2+}/P_2MnMoW_{16}O_{61}(H_2O)^{8}$

pH	$Mn^{2+}/PMnMo_2W_9O_{39}(H_2O)^{5-}$		$Mn^{2+}/P_2MnMoW_{16}O_{61}(H_2O)^{8-}$	
	d (10^{-2}m)	μ ($10^{-8}m^2V^{-1}s^{-1}$)	d (10^{-2}m)	μ ($10^{-8}m^2V^{-1}s^{-1}$)
1.5	−4.2	−1.98	−4.5	−2.03
2.0	−3.4	−1.60	−3.5	−1.58
2.5	+4.2	+1.98	+5.6	+2.52
3.0	+6.7	+3.16	+7.2	+3.24
3.4	+7.2	+3.39	+8.0	+3.60
4.0	+7.3	+3.44	+8.2	+3.69
4.5	+6.8	+3.20	+7.8	+3.51
5.0	+6.0	+2.83	+7.5	+3.38
5.5	+3.4	+1.60	+7.1	+3.20
6.0	+3,0	+1.41	+5.7	+2.57
6.5	—	—	+4.5	+2.03

Table 3

The migration of the ionic species and the sum of the electrophoretic mobilities as a function of pH, for the systems $Ni^{2+}/PNiMo_2W_9O_{39}(H_2O)^{5-}$ and $Ni^{2+}/P_2NiMoW_{16}O_{61}(H_2O)^{8-}$

pH	$Ni^{2+}/PNiMo_2W_9O_{39}(H_2O)^{5-}$		$Ni^{2+}/P_2NiMoW_{16}O_{61}(H_2O)^{8-}$	
	d (10^{-2}m)	μ ($10^{-8}m^2V^{-1}s^{-1}$)	d (10^{-2}m)	μ ($10^{-8}m^2V^{-1}s^{-1}$)
1.5	−3.7	−1.67	−3.8	−1.69
2.0	−2.8	−1.26	−3.1	−1.34
2.5	+3.2	+1.44	+3.5	+1.56
3.0	+4.4	+1.98	+5.1	+2.27
3.5	+4.7	+2.12	+7.0	+3.12
4.0	+4.5	+2.03	+7.8	+3.48
4.5	+4.2	+1.89	+7.9	+3.52
5.0	+3.2	+1.44	+6.7	+3.43
5.5	+2.5	+1.17	+7.5	+3.35
6.0	+2.0	+0.90	+6.1	+2.72
6.5	—	—	+3.5	+1.16

Table 4

The migration of the ionic species and the sum of the electrophoretic mobilities as a function of pH, for the systems $Cu^{2+}/PCuMo_2W_9O_{39}(H_2O)^{5-}$ and $Cu^{2+}/P_2CuMoW_{16}O_{61}(H_2O)^{8-}$

pH	$Cu^{2+}/PCuMo_2W_9O_{39}(H_2O)^{5-}$		$Cu^{2+}/P_2CuMoW_{16}O_{61}(H_2O)^{8-}$	
	d (10^{-2}m)	μ ($10^{-8}m^2V^{-1}s^{-1}$)	d (10^{-2}m)	μ ($10^{-8}m^2V^{-1}s^{-1}$)
1.5	−4.4	−1.92	−4.5	−1.95
2.0	−3.4	−1.52	−3.6	−1.56
2.5	+2.7	+1.18	+5.1	+2.20
3.0	+4.0	+1.74	+6.5	+2.81
3.5	+4.1	+1.80	+7.2	+3.11
4.0	+3.8	+1.68	+7.9	+3.41
4.5	+2.7	+1.21	+7.2	+3.11
5.0	+2.3	+1.00	+6.8	+2.94
5.5	+2.0	+0.87	+4.1	+1.77
6.0	+1.8	+0.78	+3.2	+1.38

The values d and μ are noted with + or — as the ionic species move either towards the anode or the cathode direction.

On the basis of the values shown in Tables 2, 3 and 4, the variation of the sum of the electrophoretic mobilities, as a function of pH, has been plotted (see Fig. 1, 2 and 3).

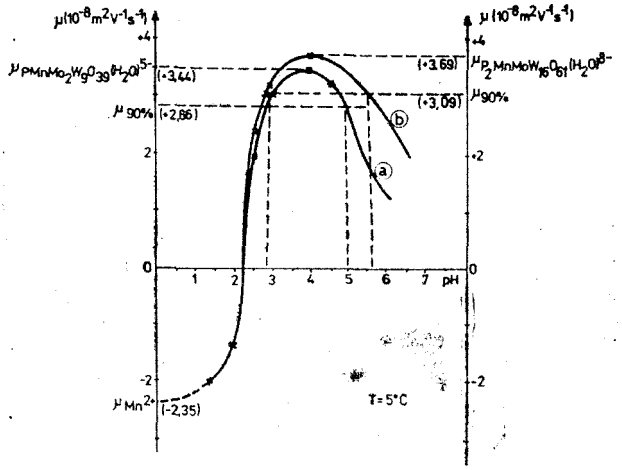

Fig. 1. The variation of the sum of the electrophoretic mobilities, as a function of pH, for the systems:
a) $Mn^{2+}/PMnMo_2W_9O_{39}\ (H_2O)^{5-}$
b) $Mn^{2+}/P_2MnMoW_{16}O_{61}\ (H_2O)^{8-}$

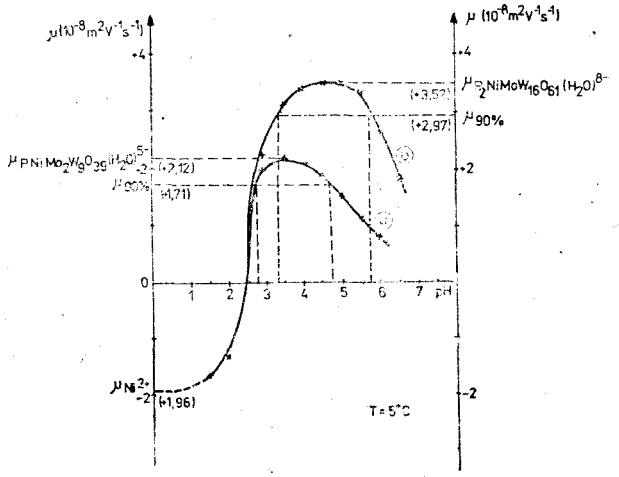

Fig. 2. The variation of the sum of the electrophoretic mobilities, as a function of pH, for the systems:
c) $Ni^{2+}/PNiMo_2W_9O_{39}\ (H_2O)^{5-}$
d) $Ni^{2+}/P_2NiMoW_{16}O_{61}\ (H_2O)^{8-}$

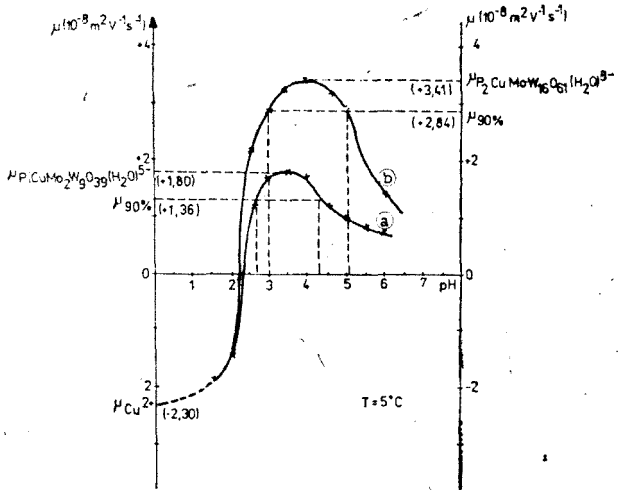

Fig. 3. The variation of the sum of the electrophoretic mobilities, as a function of pH, for the systems:
e) $Cu^{2+}/PCuMo_2W_9O_{39}(H_2O)^{5-}$
f) $Cu^{2+}/P_2CuMoW_{16}O_{61}(H_2O)^{8-}$

The simple S shape of the electrophoretic curves points out the formation of unit coordination compounds, namely HPOM—A containing heteroatoms in non-equivalents sites, and not the formation of mixtures of coordination compounds. The values of the mobilities for the ionic species in the system are obtained by extrapolation at the ordinate the highest and the lowest values of the electrophoretic mobilities (see Table 5).

Table 5

The eletrophoretic mobilities of the ion Z^{2+}, $PZMo_2W_9O_{39}(H_2O)^{5-}$ and $P_2ZMoW_{16}O_{61}(H_2O)^{8-}$

Ion	μ $(10^{-8}m^2V^{-1}s^{-1})$
Mn^{2+}	−2.35
Ni^{2+}	−1.96
Cu^{2+}	−2.30
$PMnMo_2W_9O_{39}(H_2O)^{5-}$	+3.44
$PNiMo_2W_9O_{39}(H_2O)^{5-}$	+2.12
$PCuMo_2W_9O_{39}(H_2O)^{5-}$	+1.80
$P_2MnMoW_{16}O_{61}(H_2O)^{8-}$	+3.69
$P_2NiMoW_{16}O_{61}(H_2O)^{8-}$	+3.52
$P_2CuMoW_{16}O_{61}(H_2O)^{8-}$	+3.41

The range of formation is correlated with the range of stability. We have considered that the optimum range of formation of a ZL HPOM—A is the pH range within which at least 90% out of the Z^{2+} cation is coordinated as a secondary heteroatom into the polyanionic edifice. The sum of the electrophoretic mobilities for the extreme value is:

$$\mu_{90\%} = 0.1\ \mu_Z + 0.9\ \mu_{ZL} \quad (7)$$

The optimum range of formation was determined from the electrophoretic curves, see Fig. 1, 2 and 3, which correspond to a pH range where the condition $\mu \geqslant \mu_{90\%}$ is obeyed.

The values $\mu_{90\%}$ and the optimum pH range of formation for HPOM—A of the types $PZMo_2W_9O_{39}(H_2O)^{5-}$ and $P_2ZMoW_{16}O_{61}(H_2O)^{8-}$ respectively, are presented in Table 6.

Table 6

The optimum pH range of formation for the HPOM-A $PZMo_2W_9O_{39}(H_2O)^{5-}$ and $P_2ZMoW_{16}O_{61}(H_2O)^{8-}$

HPOM—A	$\mu^{90\%}$ ($10^{-8}m^2V^{-1}s^{-1}$)	pH range
$PMnMo_2W_9O_{39}(H_2O)^{5-}$	2.86	2.8—5.0
$PNiMo_2W_9O_{39}(H_2O)^{5-}$	1.71	2.8—4.7
$PCuMo_2W_9O_{39}(H_2O)^{5-}$	1.36	2.7—4,3
$P_2MnMoW_{16}O_{61}(H_2O)^{8-}$	3.09	2.8—5.6
$P_2NiMoW_{16}O_{61}(H_2O)^{8-}$	2.97	3.3—5.7
$P_2CuMoW_{16}O_{61}(H_2O)^{8-}$	2.84	3.0—5.1

If experiments are performed at different concentration of L, HPOM—A ligand, by plotting the dependence of the electrophoretic mobilities on this concentration, the determination of the values of the stability and instability constants of the new formed ZL HPOM—A may be possible, as a rule, on the basis of certain theoretical approximations and graphical extrapolations [1—6, 8].

We consider the theoretical approximations of the electrophoretic method referring to the determination of the respective constants to be too large, particularly for HPOM—A; also the minimum differences of the experimental values, placed within the limits of errors, owing to the precision of the method, exert too great an influence on the final results. That is why, the error of the electrophoretic method for the determination of the stability and instability constants exceeds one order of magnitude.

Owing to the above, we consider the „in extenso" presentation of the results obtained by applying the electrophoretic method for the determination of the respective constants to be inconclusive. Let us just mention that the values of the stability and instability constants of the HPOM—A $PZMo_2W_9O_{39}(H_2O)^{5-}$ and $P_2ZMoW_{16}O_{61}(H_2O)^{8-}$, determined by electrophoresis in aqueous solution

at pH = 4, are included in the range $\beta = 10^3 - 10^5$ and $K = 10^{-3} - 10^{-5}$ respectively.

Experimental. An instalation for high tension paper electrophoresis „Phoretograph-Original Frankfurt Typ 64" (Vetter KG—Wiesloch, GFR) was used. The pH of the solutions was measured using a pH-meter „MV-84" (Clahmann & Grahnert Dresden, GDR).

The experiments were performed in a medium of HPOM—A ligand $L = PMo_2W_9O_{39}^{7-}$ and $P_2MoW_{16}O_{61}^{10-}$ respectively, of concentration 10^{-2} M, in the range of pH = 1,5—6.

The solution containing the transitional cation $Z = Mn^{2+}$, Ni^{2+} or Cu^{2+} was applied on the chromatographic paper using a micropipette.

As reagents were used:

— $K_7[PMo_2W_9O_{39}] \cdot 13H_2O$ and $K_{10}[P_2MoW_{16}O_{61}] \cdot 19H_2O$ for the preparation of the L HPOM—A ligand solutions;

— $MnCl_2 \cdot 4H_2O$, $NiCl_2 \cdot 6H_2O$ and $CuCl_2 \cdot 2H_2O$ for the preparation of the Z transitional cation solutions.

The pH of the solutions was adjusted with 10^{-1} M HCl and 10^{-1} M NaOH. The ionic strength was kept constant by adding 10^{-1} M $KClO_4$.

A „Karl Schneider Schull" (Merck, GFR) chromatographic paper (40 × 4 cm) was used with a porosity paper of I/l = 1,69.

The electrophoresis was performed in the following conditions: potential difference V = 1500 V intensity $I = 2,5 \cdot 10^{-2}$ A, time t = 1800 s and temperature T = 5°C.

The movement of the ionic species by electromigration was observed by watching the specific colour, namely by developing with a diluted solution of $K_4[Fe(CN)_6]$. A glucose solution, electrically neutral, was deposited next to the solution containing the transitional cation. The movement of the ions was related to the glucose position, which may be regarded as a starting point.

The R_f values of the formed HPOM—A were determined by ascending paper chromatography.

Conclusion. In the study of the reactions of formations of HPOM—A containing heteroatoms in non-equivalent sites, of the types $PZMo_2W_9O_{39}(H_2O)^{5-}$ and $P_2ZMoW_{16}O_{61}(H_2O)^{8-}$ (where $Z = Mn^{II}$, Ni^{II}, Cu^{II}), the optimum pH range of formation has been determined by high tension paper electrophoresis.

The results obtained by interpreting the electrophoretic curves can be resumed in the following two points:

1) HPOM—A of the type $P_2ZMoW_{16}O_{61}(H_2O)^{8-}$, with modified Dawson structure, are more easily formed and are more stable than HPOM—A of the type $PZMo_2W_9O_{39}(H_2O)^{5-}$, with modified Keggin structure;

2) The influence of the Z^{2+} transitional cation on the formation and the stability of HPOM—A, within the same series, can be expressed as:

$$Mn^{2+} > Ni^{2+} > Cu^{2+}$$

$$\leftarrow \frac{\text{the stability increase}}{\text{the formation capacity increase}}$$

The above mentioned points have the following consequences:

a) The most easily HPOM—A to prepare, as well as the most stable is $P_2MnMoW_{16}O_{61}(H_2O)^{8-}$;

b) The most difficult HPOM—A to prepare, as well as the less stable is $PCuMo_2W_9O_{39}(H_2O)^{5-}$.

REFERENCES

1. R. Ripan, A. Botar, *Rev. Roumaine Chim.*, **13**, 805 (1968).
2. R. Ripan, V. Cordiş, A. Botar, *Rev. Roumaine Chim.*, **16**, 1717 (1971).
3. Gh. Marcu, I. Todoruţ, A. Botar, *Rev. Roumaine Chim.*, **16**, 829 (1971).
4. M. Rusu, *Thesis*, University „Babeş-Bolyai", Cluj-Napoca (1976).
5. I. Ciogolaş, *Thesis*, Institute of Chemistry, Cluj-Napoca (1980).
6. I. Duca, *Thesis*, University „Babeş-Bolyai", Cluj-Napoca (1981).
7. A. Pătruţ, *Thesis*, Institute of Chemistry, Cluj-Napoca (1986).
8. A. Botar, D. Itul, Gh. Marcu, *Studia Univ. Babeş-Bolyai, Chem.*, **33** (1) 42 (1988).
9. H. G. Kunkel, A. Tiselius, *J. Gen. Phisiol.*, **35**, 89 (1951).

STUDIA UNIV. BABEŞ-BOLYAI, CHEMIA, XXXV, 1, 1990

NEW HETEROPOLYOXOMETALATE ANIONS WITH HETERO ATOMS IN NON-EQUIVALENT SITES
III. The Study of the Reactions of Formation (2)

ADRIAN PĂTRUŢ* and ALEXANDRU BOTAR*

Received: April 12, 1990

Continuing the study of some heteropolyoxometalate anions, containing heteroatoms in non-equivalent sites, of the types $PZMo_2W_9O_{39}(H_2O)^{5-}$ and $P_2ZMoW_{16}O_{61}(H_2O)^{8-}$ (where $Z = Mn^{II}$, Ni^{II}, Cu^{II}), with modified Keggin and modified Dawson structure respectively, the stoichiometry of the reactions of formation in solution was determined by using the molar ratio variation method. The results obtained by spectrophotometry and conductometry show that the reaction products may be considered as 1 : 1 coordination compounds of the transitional cations Mn^{2+}, Ni^{2+} and Cu^{2+} with the unsaturated heteropolyoxometalate anions $PMo_2W_9O_{39}^{7-}$ and $P_2MoW_{16}O_{61}^{10-}$ as ligands.

Introduction. The heteropolyoxometalate anions (HPOM—A) containing heteroatoms in non-equivalent sites, of the types $PZMo_2W_9O_{39}(H_2O)^{5-}$ and $P_2ZMoW_{16}O_{61}(H_2O)^{8-}$, with modified Keggin and modified Dawson structure respectively, are formed according to a general reaction:

$$mZ^{z+} + nL^{q-} \rightleftarrows Z_mL_n^{(mq-nz)-}, \qquad (1)$$

where: $Z^{z+} = Mn^{2+}$, Ni^{2+}, Cu^{2+}; L^{q-} = HPOM—$A^{q-}_{ligand} = PMo_2W_9O_{39}^{7-}$, $P_2MoW_{16}O_{61}^{10-}$.

Continuing the study of the reactions of formation in solution (1), the stoichiometry of the processes was investigated to establish the coefficients m and n of the reagents. With this aim in view, the molar ratio variation method was applied to the spectrophotometric and conductometric study q of the reactions of formation. We note that, although spectrophotometry and photocolorimetry are often used for the determination of the stoichiometry of the reactions of formation of HPOM—A with heteroatoms in non-equivalent sites [1—9], conductometry is less preferred, in spite of its simplicity and several advantages [5].

Results and Discussion. By adding solutions containing hydrated cation Z^{z+}_{aq} to diluted colourless aqueous solutios of L HPOM—A ligand, the occurence of a relatively intense colouration is observed, owing to the rapid formation of Z_mL_n HPOM—A containing heteroatoms in non-equivalent sites. This fact allows the study of the respective reactions of formation by photocolorimetry or, for better accuracy, by spectrophotometry.

Reagent solutions with different molar ratio were mixed and the extinction was measured at determined wavelengths. The chosen wavelengths and the values of the molar extinction coefficients are shown in Table 1.

* *Institute of Chemistry, 3400 Cluj-Napoca, Romania*

Table 1

Experimental wavelengths and molar extinction coefficients in the spectrophotometric study of the reaction of formation of HPOM-A of the types $PZMo_2W_9O_{39}(H_2O)^{5-}$ and $P_2ZMoW_{16}O_{61}(H_2O)^{8-}$ (where Z = Mn^{II}, Ni^{II}, Cu^{II})

Reaction of formation $mZ + nL \rightleftarrows Z_mL_n$	Wavelength λ(nm)	Molar extinction coefficient ε(l. mol^{-1} cm^{-1}) $\varepsilon_{Z_mL_n}$	ε_Z	ε_L
$Mn^{2+}_{aq} + PMo_2W_9O_{39}^{7-} \rightleftarrows PMnMo_2W_9O_{39}(H_2O)^{5-}$	420	165	→0	→0
	460	60	→0	→0
$Mn^{2+}_{aq} + P_2MoW_{16}O_{61}^{10-} \rightleftarrows P_2MnMoW_{16}O_{61}(H_2O)^{8-}$	460	120	→0	→0
	500	75	→0	→0
$Ni^{2+}_{aq} + PMo_2W_9O_{39}^{7-} \rightleftarrows PNiMo_2W_9O_{39}(H_2O)^{5-}$	775	10	1.2	→0
$Ni^{2+}_{aq} + P_2MoW_{16}O_{61}^{10-} \rightleftarrows P_2NiMoW_{16}O_{61}(H_2O)^{8-}$	700	13	2	→0
$Cu^{2+}_{aq} + PMo_2W_9O_{39}^{7-} \rightleftarrows PCuMo_2W_9O_{39}(H_2O)^{5-}$	800	50	9	→0
$Cu^{2+}_{aq} + P_2MoW_{16}O_{61}^{10-} \rightleftarrows P_2CuMoW_{16}O_{61}(H_2O)^{8-}$	870	55	9	→0

For the reactions of formation of the Z_mL_n HPOM—A with Z = Ni^{II} or Cu^{II} as a secondary heteroatom, the determinations were performed at the absorption maximum of the corresponding d-d electronic transition bands, where the absorption of the L HPOM—A ligand tends towards zero, while that of the Ni^{II} or Cu^{II} transitional cation, with absorption maxima at lower wavelenghts, is reduced.

In the particular case of the reactions of formation of the Z_mL_n HPOM—A containing Z = Mn^{II} as a secondary heteroatom, without d-d bands in the spectrum, the determinations were performed on the charge-transfer band, prolonged into the visible range, due to the participation of the secondary heteroatom Mn^{II} in the charge transfer within the anion. In the chosen range, the absorption of the L HPOM—A ligand and that of the Mn^{II} cation is actually zero.

The variation of the extinction of the mixed solutions, as a function of the molar ratio of the reagents, was plotted (see Fig. 1, 2 and 3).

The spectrophotometric curves consist of two segments, with the intersection corresponding to a molar ratio of the reagents m : n = 1 : 1.

In the case of the reaction of formation of the Z_mL_n HPOM—A with Z = = Mn^{II} (see Fig. 1) the extinction increases only to the equivalence point, proportional to the concentration of the reaction product. Experiments were performed at two different wavelenghts, to check out the independence of the results on the wavelength, on the obvious condition that the absorption of the reaction product differ considerably from the reagent absorption one.

In the case of the reaction of formatoin of the Z_mL_n HPOM—A with Z = = Ni^{II} or Cu^{II} (see Fig. 2 and 3) the extinction increases up to the equivalence

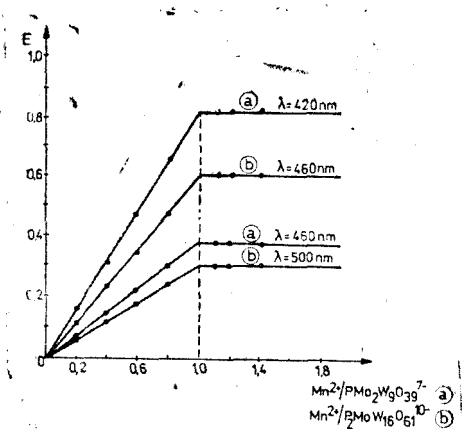

Fig. 1. The variation of the extinction of the solutions obtained by mixing the aqueous solutions of $MnCl_2 \cdot 4H_2O$ and $K_7[PMo_2W_9O_{39}] \cdot 13H_2O$, respectively $MnCl_2 \cdot 4H_2O$ and $K_{10}[P_2MoW_{16}O_{61}] \cdot 19H_2O$, as a function of the molar ratio (the concentration of the reagents $c = 10^{-2}$ M; pH = 4; thickness of the absorbing layer $d = 5 \cdot 10^{-3}$ m).

a) $Mn^{2+}_{aq} + PMo_2W_9O^{7-}_{39}$

b) $Mn^{2+}_{aq} + P_2MoW_{16}O^{10-}_{61}$

point, proportional to the concentration of the reaction product and increase more slowly after the equivalence, owing to the absorption of the Ni^{2+}_{aq} or Cu^{2+}_{aq} cations at the chosen wavelengths.

The high rate and the linear increase of the extinction, proportional with the molar ratio up to the equivalence point, demonstrate that the studied reactions lead to the formation of 1 : 1 coordination compounds, of the type ZL.

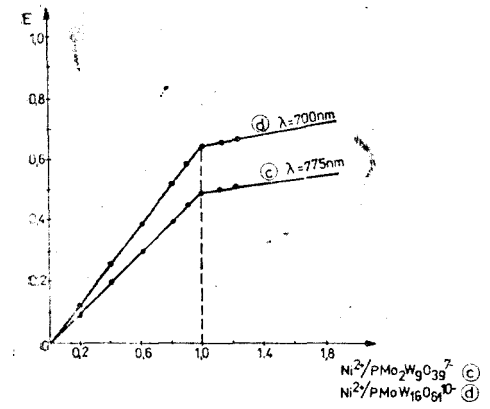

Fig. 2. The variation of the extinction of the solutions obtained by mixing the aqueous solutions of $NiCl_2 \cdot 6H_2O$ and $K_7[PMo_2W_9O_{39}] \cdot 13H_2O$, respectively $NiCl_2 \cdot 6H_2O$ and $K_{10}[P_2MoW_{16}O_{61}] \cdot 19H_2O$, as a function of the molar ratio (the concentration of the reagents $c = 10^{-2}$ M; pH = 4; thickness of the absorbing layer $d = 5 \cdot 10^{-3}$ m).

c) $Ni^{2+}_{aq} + PMo_2W_9O^{7-}_{39}$

d) $Ni^{2+}_{aq} + P_2MoW_{16}O^{10-}_{61}$

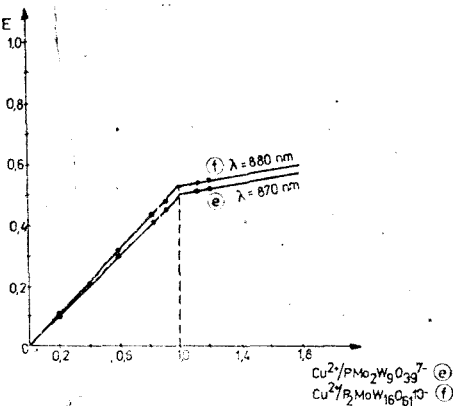

Fig. 3. The variation of the extinction of the solutions obtained by mixing the aqueous solutions of $CuCl_2 \cdot 2H_2O$ and $K_7[PMo_2W_9O_{39}] \cdot 13H_2O$, respectively $CuCl_2 \cdot 2H_2O$ and $K_{10}[P_2MoW_{16}O_{61}] \cdot 19H_2O$, as a function of the molar ratio (the concentration of the reagents $c = 10^{-2}$ M; pH = 4; thickness of the absorbing layer $d = 5 \cdot 10^{-3}$ m).

e) $Cu^{2+}_{aq} + PMo_2W_9O^{7-}_{39}$

f) $Cu^{2+}_{aq} + P_2MoW_{16}O^{10-}_{61}$

representing HPOM—A containing heteroatoms in non-equivalent sites. The good observance of the Lambert-Beer law near the equivalence point suggests relatively high values for the equilibrium constants.

Further on, conductometry was used to establish the stoichiometry of the reactions of formation, following the same molar ratio variation method. Solutions of reagents, with different molar ratios, were mixed and the conductance was measured. The conductance variation, as a function of the molar ratio, was plotted (see Fig. 4, 5 and 6).

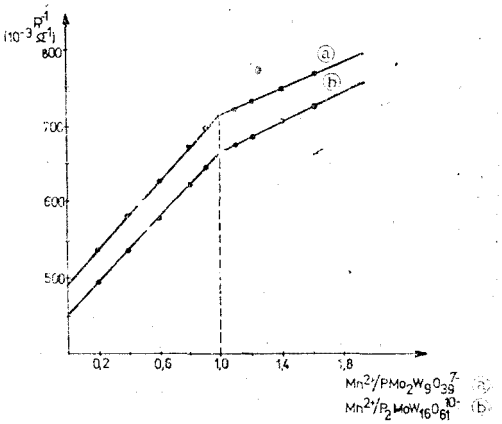

Fig. 4. The variation of the conductance of the solutions obtained by mixing the aqueous solutions of $MnCl_2 \cdot 4H_2O$ and $K_7[PMo_2W_9O_{39}] \cdot 13H_2O$, respectively $MnCl_2 \cdot 4H_2O$ and $K_{10}[P_2MoW_{16}O_{61}] \cdot 19H_2O$, as a function of the molar ratio (the concentration of the reagents $c = 10^{-2}$ M; pH = 4).

a) $Mn^{2+}_{aq} + PMo_2W_9O_{39}^{7-}$

b) $Mn^{2+}_{aq} + P_2MoW_{16}O_{61}^{10-}$

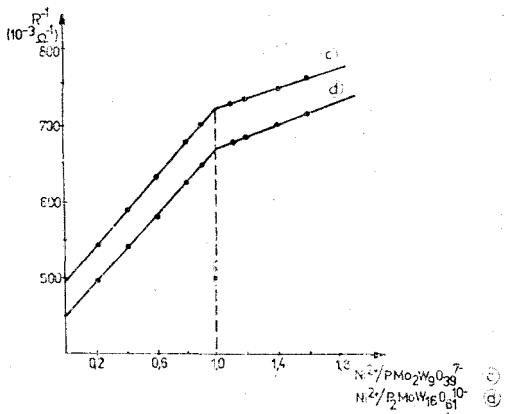

Fig. 5. The variation of the conductance of the solutions obtained by mixing the aqueous solutions of $NiCl_2 \cdot 6H_2O$ and $K_7[PMo_2W_9O_{39}] \cdot 13H_2O$, respectively $NiCl_2 \cdot 6H_2O$ and $K_{10}[P_2MoW_{16}O_{61}] \cdot 19H_2O$, as a function of the molar ratio (the concentration of the reagents $c = 10^{-2}$ M; pH = 4).

c) $Ni^{2+}_{aq} + PMo_2W_9O^{2+}_{aq}$

d) $Ni^{2+}_{aq} + P_2MoW_{16}O_{61}^{10-}$

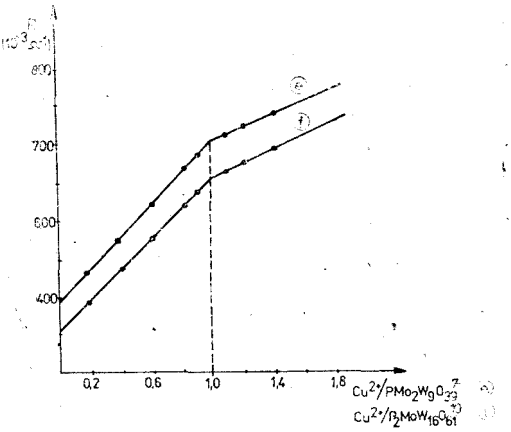

Fig. 6. The variation of the conductance of the solutions obtained by mixing the aqueous solutions of $CuCl_2 \cdot 2H_2O$ and $K_7[PMo_2W_9O_{39}] \cdot 13H_2O$, respectively $CuCl_2 \cdot 2H_2O$ and $K_{10}[P_2MoW_{16}O_{61}] \cdot 19H_2O$, as a function of the molar ratio (the concentration of the reagents $c = 10^{-2}$ M; pH = 4)

e) $Cu^{2+}_{aq} + PMo_2W_9O_{39}^{7-}$

f) $Cu^{2+}_{aq} + P_2MoW_{16}O_{61}^{10-}$

The conductometric curves consist of two segments, with the intersection corresponding to a molar ratio of the reagents $m : n = 1 : 1$.

In order to explain the aspect of the conductometric curves, with a slower increase of the conductance after the equivalence, the reaction between the Mn^{2+}_{aq} cation and the $PMo_2W_9O_{39}^{7-}$ HPOM—A ligand has been chosen as an example:

$$MnCl_2 \cdot 4H_2O + K_7[PMo_2W_9O_{39}] \cdot 13H_2O \rightarrow$$
$$\rightarrow K_5[PMnMo_2W_9O_{39}(H_2O)] \cdot 14H_2O + 2KCl + 2H_2O. \quad (2)$$

Taking into account the ionic species in the aqueous solutions, the process may be written as follows:

$$7K^+ + PMo_2W_9O_{39}^{7-} \xrightarrow[-5H_2O]{+Mn(H_2O)_6^{2+} + 2Cl^-}$$
$$\rightarrow 7K^+ + PMnMo_2W_9O_{39}(H_2O)^{5-} + 2Cl^- \quad (3)$$

The initial solution of HPOM—A ligand contains K^+ and $PMo_2W_9O_{39}^{7-}$ ions. As the solution of $MnCl_2 \cdot 4H_2O$ is added, the $PMnMo_2W_9O_{39}(H_2O)^{5-}$ HPOM—A with heteroatoms in non-equivalent sites appears to be formed, with an equivalent ionic conductibility slightly lower as compared to that of the HPOM—A ligand. The conductance increase up to the equivalence is due to the occurence in the system of the Cl^- ions, with high conductibility.

After the equivalence, the low soluble manganese salt of the resulting HPOM—A is formed, by further adding of $MnCl_2 \cdot 4H_2O$ solution:

$$10K^+ + 2PMnMo_2W_9O_{39}(H_2O)^{5-} \xrightarrow[-6H_2O]{+5Mn(H_2O)_6^{2+} + 10Cl^-}$$
$$\rightarrow Mn_5[PMnMo_2W_9O_{39}(H_2O)]_2 + 10K^+ + 10Cl^- \quad (4)$$

The conductance increase after the equivalence, owing to the same Cl^- ions, is slower due to the formation of the low soluble salt $Mn_5[PMnMo_2W_9O_{39}(H_2O)]_2$.

Experimental. The extinction of the solutions was measured using a „VSU—2P" (Carl Zeiss Jena, GDR) spectrophotometer. The conductance of the solutions was measured using an „O.K—102" (Radelkis, Hungary) conductometer.

Different volumes of solutions containing transitional cations $Z = Mn^{2+}$, Ni^{2+}, Cu^{2+}, were added to solutions of HPOM—A ligand $L = PMo_2W_9O_{39}^{7-}$, $P_2MoW_{16}O_{61}^{10-}$, with the same concentration, to obtain different molar ratios.

As reagents were used:

— $K_7[PMo_2W_9O_{39}] \cdot 13H_2O$ and $K_{10}[P_2MoW_{16}O_{61}] \cdot 19H_2O$, for the preparation of the 10^{-2}M HPOM—A ligand solutions;

— $MnCl_2 \cdot 4H_2O$, $NiCl_2 \cdot 6H_2O$ and $CuCl_2 \cdot 2H_2O$, for the preparation of the 10^{-2}M transitional cation solutions.

The pH of the reagent solutions was adjusted to 4, into the optimum pH range of formation, with 10^{-1}M HCl and 10^{-1}M NaOH solutions.

The ionic strength was kept constant by adding a 10^{-1} M $KClO_4$ solution.

In the case of the spectrophotometric study, the extinction of the solutions resulte dfrom mixing the reagents was measured, for different molar ratios, at determined wavelenghts, as well as the extinction of the reagent solutions. If by mixing the reagent solutions, a precipitate is formed, in excess of transitional cation, the filtrate extinction should be measured.

In the case of the conductometric study, the conductance of the solutions resulted from mixing the reagents was measured, for different molar ratios, as well as the conductance of the HPOM—A ligand solutions.

Conclusion. The stoichiomery of the reactions of formation in solution of HPOM—A containing heteroatoms in non-equivalent sites, of the types $PZMo_2W_9O_{39}(H_2O)^{5-}$ and $P_2ZMoW_{16}O_{61}(H_2O)^{8-}$ respectively (where $Z = Mn^{II}$, Ni^{II},Cu^{II}) was determined.

The results of the spectrophotometric and conductometric studies demonstrate a molar ratio of the reagents equal to 1. As such, the obtained HPOM—A may be considered 1 : 1 coordination compound of the Mn^{2+}, Ni^{2+} and Cu^{2+} transitional cations, with the $PMo_2W_9O_{39}^{7-}$ and $P_2MoW_{16}O_{39}^{10-}$ HPOM — A as ligands.

REFERENCES

1. P. Courtin, F. Chauveau, and P. Souchay, *C. r. hebd. Séanc. Acad. Sci.*, Paris, **C 258**, 1247 (1964).
2. I. F. Škaravski, *Zhur. Neorg. Khim.*, **10**, 1179 (1965).
3. P. Courtin, *Bull. Soc. Chim. France*, **12**, 4799 (1968).
4. M. Petit and R. Massart, *C. r. hebd. Séanc. Acad. Sci. Paris*, **C 268**, 1960 (1969).
5. C. Tourné and G. Tourné, *Bull. Soc. Chim. France*, **4**, 1124 (1969).
6. C. M. Tourné, G. F. Tourné, S. A. Malik and T. J. Weakley, *J. Inorg. Nucl. Chem.*, **32**, 3875 (1970).
7. R. Ripan and A. Botar, *Rev. Roum. Chim.*, **15**, 1577 (1970).
8. R. D. Peacock and T. J. R. Weakley, *J. Chem. Soc. A.*, 1836 (1971).
9. C. Marcu, M. Rusu and A. Botar, *Rev. Roum. Chim.*, **19**, 827 (1974).

STUDIA UNIV. BABEŞ-BOLYAI, CHEMIA, XXXV, 1, 1990

SURFACE EQUATIONS OF STATE FOR OLEIC ACID MONOLAYERS ON ACIDIC AQUEOUS SOLUTIONS

JÁNOS ZSAKÓ*, MARIA TOMOAIA-COTIŞEL*, AURORA MOCANU* and EMIL CHIFU*

Received, April 25, 1990

Compression isotherms (surface pressure (π) vs. molecular area (A) curves) of monolayers of oleic acid are studied. The compressibility factor, $z = \pi A/kT$ shows large deviations from the perfect gas behaviour. Different state equations are tested on oleic acid monolayers at $\pi \leq 7$ mN/m. A new state equation proposed by the authors is found to be better than the formerly used ones predicting also the gas — liquid phase transition in good agreement with literature data. By means of this new equation, interaction parameters are derived from the compression isotherms of the studied substance.

Introduction. Many attempts have been made to give a mathematic description of the compression isotherms, i.e. of the surface pressure (π) vs. mean molecular area (A) curves, recorded with both soluble and insoluble surfactant monolayers at the air/liquid interface. In this respect, we mention for example the following state equations (SE):

Perfect gas SE [1]:

$$\pi A = kT \tag{1}$$

where k is Boltzmann's constant, and T is absolute temperature;

SE-s in which A is corrected for a co-area A_0 [2]:

$$\pi(A - A_0) = kT \tag{2}$$

in which π is corrected for an internal surface pressure π_0:

$$(\pi + \pi_0)A = kT \tag{3}$$

or both corrections are applied simultaneously [3]:

$$(\pi + \pi_i)(A - A_i) = kT. \tag{4}$$

The two dimensional van der Waals equation [4]:

$$(\pi + \alpha/A^2)(A - A_0) = kT \tag{5}$$

SE derived on the basis of scaled particle theory [5]:

$$(\pi + \alpha/A^2)A(1 - A'_i/A)^2 = kT \tag{6}$$

SE for cohering uncharged films [6]:

$$(\pi + \alpha/A^{3/2})(A - A_0) = kT \tag{7}$$

Virial type SE-s are also frequently used [7, 8].

* University of Cluj-Napoca, Faculty of Chemistry, 3400 Cluj-Napoca, Romania

By taking into account the equality of the chemical potential of the solvent molecules in both the bulk sudqhase and in the monolayer phase, for perfect systems, the following SE has been derived [9]:

$$\pi = -\frac{kT}{A_1}\ln x_1 \tag{8}$$

where A_1 and x_1 stand for the cross-section area and for the molar fraction of the solvent molecules in the monolayer, respectively.

Using the duplex film model [3], the following SE has been obtained [10]:

$$\pi + \pi_0 = -\frac{kT}{A_1}\ln(1 - x_2) - \frac{\beta_{12}}{A_1}x_2^2 \tag{9}$$

where β_{12} and x_2 stand for the interaction parameter between the polar head group of the surfactant and water molecules, and for the molar fraction of the head groups in the monolayer, respectively, while π_0 is considered to be the spreading coefficient of the oily layer consisting of hydrocarbon chains of surfactant molecules on the hypothetical surface regular solution of surfactant head groups and interfacial water molecules.

All the above mentioned SE-s were proposed for uncharged films. The present paper aims at testing several of the above equations by using our experimental data [11] concerning the compression isotherms of oleic acid (OA), recorded on aqueous subphases, containing HCl and having pH = 2, since under these conditions the ionization of the carboxyl group was found to be completely hindered, and consequently the monolayer uncharged. Experimental details and surface characteristics derived were presented in [11].

Results and Discussion. *Compressibility factor.* In order to test the deviations from the perfect gas behaviour, the plot of compressibility factor $z = \pi A/kT$ vs. π has been performed. As seen from Fig. 1, at very low π values z is nearly equal to zero, indicating very large deviations from the perfect gas behaviour ($z = 1$) even at the spreading of the film ($A \approx 0.6$ nm^2/molec).

Testing of state equations. As a *first preliminary study*, the Langmuir equation (4) was tested, which, written as:

$$\pi(A - A_0) = -\pi_0(A - A_0) + kT$$

suggests a linearization $\pi(A - A_0)$ vs. $(A - A_0)$, by presuming different A_0 values: π vs. A data obtained for OA have been processed in this way. None of the A_0 values enables us to linearize the whole π vs. A curve, but each of the values used gives a linear portion, allowing us to derive a π_0 value from its slope. Results are summarized in Table 1.

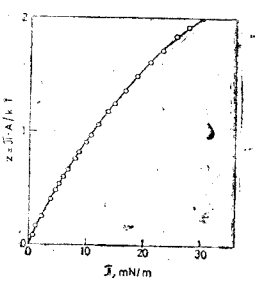

Fig. 1. Compressibility factor of oleic acid monolayers as function of surface pressure.

Our *second preliminary study* concerned Eq. (9). We mention that Eq. (9) can be derived without using the duplex film model. Bearing in mind the equality of the chemical potential of water in the subphase and in the

Table 1

π_0 values derived for OA by means of Eq. (4) · $\Delta\pi$ gives the π range in which the plot is nearly linear

A_0 (nm²/molec.)	π_0 (mN/m)	$\Delta\pi$ (mN/m)
0.10	20.83	3.6 . . . . 16.7
0.18	12.20	1.5 . . . . 21.0
0.20	9.71	0.5 . . . . 18.8
0.27	6.37	0.6 . . . . 7.7
0.41	1.77	0.2 . . . . 2.0

monolayer, considered as being a real solution, instead of Eq. (8), one obtains [12]:

$$\pi = -\frac{kT}{A_1}\ln x_1 - \frac{kT}{A_1}\ln f_1 = \pi_k + \pi_i \tag{10}$$

where f_1 stands for the activity coefficient of water in the monolayer. Eq. (10) shows that π has two components: π_k, which is equal to π in the case of a perfect solution, without intermolecular interactions and it can be considered as a kinetic surface pressure, and π_i, which represents a surface internal pressure due to the intermolecular interactions in the monolayer. It is obvious that $\pi_k > 0$, and one has $\pi_i > 0$, for $f_1 < 1$ and $\pi_i < 0$ for $f_1 > 1$. Considering in a first approximation the monolayer to be a regular solution, f_1 can be expressed as

$$\ln f_1 = \frac{\beta}{kT} x_2^2 \tag{11}$$

where β means

$$\beta = p(\varepsilon_{12} - \frac{\varepsilon_{11} + \varepsilon_{22}}{2}) \tag{12}$$

In Eq. (12), p stands for the number of contacts of a molecule with neighbouring molecules, in the monolayer; ε_{11}, ε_{22} and ε_{12} stand for the potential energy corresponding to a water/water, surfactant/surfactant and water/surfactant contact, respectively. It is worth mentioning that ε_{11}, ε_{22} and ε_{12}, all have negative values. Obviously, one has $\pi_i > 0$ for $\beta < 0$ and $\pi_i < 0$ for $\beta > 0$.

Since the water molecules are inserted between the polar head groups, and there are no water molecules between the air phase hydrocarbon chains, ε_{12} is determined by the interactions between the water molecules and the polar head groups of the surfactant. Further, ε_{22} may be decomposed into two terms: ε_{hh}, corresponding to the head group/head group interactions of dipole/dipole type, and ε_{cc}, coresponding to the chain/chain hydrophobic interactions of dispersive type. Consequently, Eq. (12) can be written as:

$$\beta = p(\varepsilon_{12} - \frac{\varepsilon_{11} + \varepsilon_{hh} + \varepsilon_{cc}}{2}) = \beta_{12} - p\frac{\varepsilon_{cc}}{2} \tag{13}$$

In Eq. (13), β_{12} may be considered to be independent of the mean molecular area, A, but ε_{cc} will depend on the conformation of the hydrocarbon chains, which is a function of A, and it will be referred to as $\varepsilon_{cc}(A)$. Combination of Eqs. (10), (11) and (13) gives:

$$\pi = -\frac{kT}{A_1}\ln x_1 - \frac{\beta_{12}}{A_1}x_2^2 + \frac{p\varepsilon_{cc}(A)}{2A_1}x_2^2 = \pi_k + \pi_h + \pi_{ch} \qquad (14)$$

As it can be seen, by comparing Eqs. (10) and (14), the surface internal pressure π_i can be decomposed into two terms: π_h — expressing the surface pressure due to the intermolecular interactions that occur in the water phase part of the monolayer, and π_{ch} — being a cohesive pressure due to the dispersive type hydrophobic interactions between the air phase hydrocarbon chains of the monolayer forming the surfactant molecules. Obviously, as function of the sign of β_{12}, π_h may have positive or negativ values. Reversely, π_{ch} is always negative and in its expression both $\varepsilon_{cc}(A)$ and x_2 depend on A. Denoting $\pi_{ch} = -\pi_0(A)$, Eq. (14) becomes:

$$\pi + \pi_0(A) = -\frac{kT}{A_1}\ln x_1 - \frac{\beta_{12}}{A_1}x_2^2 \qquad (15)$$

which formally is identical with Eq. (9), but its physical meaning is rather different. In Eq. (9), π_0 has a constant value and it means the hypothetical spreading coefficient of the hypothetical oily layer formed by the hydrocarbon chains of the surfactant upon a hypothetical surface regular solution containing water molecules and the polar head groups of the surfactant. In the case of Eq. (15), $\pi_0(A)$ is considered to be a function of A, and its physical meaning is more realistic, representing the contribution of the hydrocarbon chains to the internal pressure of the monolayer and, according to the above discussions, it will always have positive values.

In order to find a reasonable expression for the dependence of π_0 on A, Eqs. (9) and (15) were tested by using the compression isotherm of OA.

The molar fraction of the surfactant in the monolayer, in Eqs. (9) and (15) can be calculated by using the following expression [10]:

$$x_2 = \frac{A_1}{A - A_2 + A_1} \qquad (16)$$

where A_1 and A_2 stand for the cross-section area of the solvent and surfactant molecules, respectively, in the monolayer. With respect to A_2, there is a certain ambiguity. Even the authors of the SE (9) use for OA its collapse area [10], but later they prefer the collapse area of stearic acid (SA) characterizing carboxylic head group [13]. Consequently, they report very different β_{12} values for OA in their two papers. Since A_2 is used for the calculation of x_2 in the monolayer, it seems to be more reasonable to take for A_2 the cross-section area of the carboxyl group and not the collapse area of OA.

Eq. (9) can be written in the following form:

$$\frac{-\pi_0}{\frac{A_1\pi + kT \ln x_1}{A_1}} + \frac{-\beta_{12}}{\frac{A_1\pi + kT \ln x_1}{x_2^2}} = 1 \qquad (17)$$

allowing us to use Irving's procedure [14]. Eq. (17) represents the equation of a straight line in co-ordinates (π_0) and $(-\beta_{12})$, having the co-ordinate intercepts

$$a = (A_1\pi + kT \ln x_1)/A_1 \text{ and } b = (A_1\pi + kT \ln x_1)/x_2^2,$$

respectively. By using our experimental data and Eq. (16), from each $\pi_i - A_i$ pair an a_i and a b_i value can be calculated, allowing us to construct a straight line in co-ordinates $(-\pi_0)$ and $(-\beta_{12})$. If the compression isotherm can be correctly described by means of Eq. (17), all the straight lines must intersect each other practically in a single point, having the co-ordinates equal to $(-\pi_0)$ and $(-\beta_{12})$, respectively, i. e. to the parameters to be derived.

These diagrams were constructed by taking for A_1 the value $A_1 = (V^{2/3})/(N_A \approx 0.1$ nm^2/molecule, where V and N_A stand for the molar volume of liquid water and for Avogadro's constant, respectively, and by presuming different A_2 values. In all cases, one can find a portion of the isotherm for which the intersection point is approximately the same, but for the whole curve the intersection

Table 2

π_0 and β_{12} values derived for OA by means of Eq. (17). $\Delta\pi$ is the π range in which practically the straight lines have a common intersection point

A_2 (nm^2/molec.)	π_0 (mN/m)	$\beta_{12} \times 10^{20}$ (Nm/molec.)	$\Delta\pi$ (mN/m)
0.41	8.1	0.720	0.2... 2.6
0.27	10.9	0.270	0.6....13.5
0.20	12.6	−0.325	2.6....18.8
0.18	13.6	−0.610	5.1....23.2

exhibits a systematic shift with increasing π. Table 2 contains parameters derived by means of this procedure, as well as the π intervales in which the intersection point is nearly constant. The procedure is illustrated in Fig. 2, giving some of the straight lines obtained on the basis of our experimental data, by taking $A_2 = 0.20$ nm^2/molecule. The two thicker straight lines correspond to the π limits indicated in Table 2, viz. to π values equal to 2.6 and 18.8 mN/m, respectively. On these straight lines the circles indicate the a and b values allowing the construction of the straight lines. As seen, between these π limits, practically all the straight lines are concurrent and the co-ordinates of their common intersection are equal to the parameters given in Table 2.

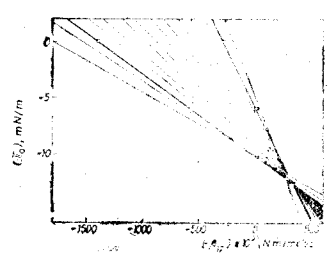

Fig. 2. Testing of Eq. (9) by using Irving's procedure (details in the text).

Eq. (9) allows us to obtain π_0 vs. A urves. For this purpose Eq. (9) is written for two neighbouring

experimental points of the compression isotherm, corresponding to A_i and A_{i+1}. By eliminating β_{12} between these equations, a $(\pi_0)_i$ value is obtained. The $(\pi_0)_i$ values obtained are plotted vs. $A_i' = (A_i + A_{i+1})/2$. As an example, in Fig. 3 this $(\pi_0)_i$ vs. A_i' plot is given for OA [15]. In the corresponding calculations the values used for A_1 and A_2 were 0.1 and 0.2 nm²/molecule, respectively.

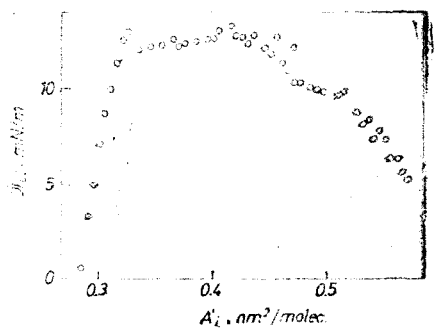

Fig. 3. π_{0i} values derived for OA by means of Eq. (9) from neighbouring points of the compression isotherm [15].

Obviously, there is an interval, comprised between 0.32 and 0.45 nm²/molecule, corresponding to $4 < \pi < 19$ mN/m, in which π_0 is approximately constant, i.e. Eq. (9) seems to be valid. At low surface pressures (high A values), π_0 decreases systematically with increasing A, in agreement with our hypothesis forwarded in discussing Eq. (15) and suggesting the idea to take $\pi_0 = \alpha/A^n$, as in Eqs. (5) – (7). Consequently, we proposed several new semiempirical SE-s [15]. By taking $n = 1$, from Eq. (15) one obtains:

$$\pi = -\left(\frac{\alpha}{A} + \frac{kT}{A_1}\ln x_1 + \frac{\beta_{12}}{A_1}x_2^2\right) \tag{18}$$

For n = 3/2, as in Eq. (7), the following equation results:

$$\pi = -\left(\frac{\alpha}{A^{3/2}} + \frac{kT}{A_1}\ln x_1 + \frac{\beta_{12}}{A_1}x_2^2\right) \tag{19}$$

If n = 2 is taken, as in the van der Waals type SE, one obtains:

$$\pi = -\left(\frac{\alpha}{A^2} + \frac{kT}{A_1}\ln x_1 + \frac{\beta_{12}}{A_1}x_2^2\right) \tag{20}$$

We mention that α/A^n, being equal to $(-\pi_{el})$, one has $\alpha > 0$, for intermolecular attraction, and $\alpha < 0$ for repulsion. Since in expanded monolayers between the hydrocarbon chains of the surfactant molecules practically are acting only attractive forces, in testing Eqs. (18) – (20), one must obtain positive values for α.

Eqs. (18) – (20) have been tested for OA. The same model system has also been used for testing some other state equations, viz. Eq. (1), further Eqs. (2) and (3), containing a single adjusted parameter, as well as Eqs. (4), (7) and (9), with two adjusted parameters [15].

The experimental π vs. A curve of oleic acid is given in Fig. 4 (curve 1).

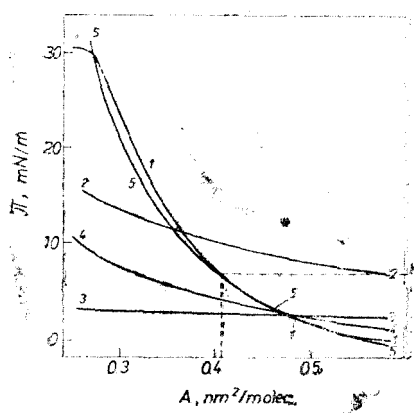

Fig. 4. Experimental (1) and theoretical π vs. A curves for OA monolayer [15]. Theoretical curves calculated by means of: 2 – Eq. (1); 3 – Eq. (2); 4 – Eq. (3); 5 – Eq. (4); by using the parameter values given in Tab. 3.

In the same figure, curve 2 has been calculated by means of Eq. (1). As seen, the behaviour of OA is very far from the perfect one. At low π values, very large negative deviations appear and at high surface pressures important positive ones.

For testing the other state equations containing adjusted parameters a curve fitting method was used. For this purpose, a low surface pressure range has been chosen, viz. $0 < \pi \leqslant 7$ mN m, delimited by dashed lines in Fig. 4. In this range, the surface pressure has been measured at 17 different A values. In the case of the equations with a single adjusted parameter, a certain value was presumed for the latter and theoretical π values were calculated for the 17 experimentally used A values. The standard deviation, Δ, of the experimental π values from the theoretical ones was calculated. The systematic variation of the value of the adjusted parameter allows us to derive the best one, ensuring the minimum of Δ, denoted as Δ_m. If the equation contains two parameters to be derived, a double minimization of Δ is necessary. The adjusted parameter values derived by means of this procedure are given in Tab. 3, and these values have been used for constructing the theoretical curves in Fig. 4. We mention that in the case of Eqs. (9) and (18)–(20), the x_2 values were calculated according to Eq. (16), by taking $A_1 = 0.1$ and $A_2 = 0.2$ nm² molecule [15].

Table 3

Parameters of the state equations and standard deviations derived for OA monolayers ($\pi \leqslant 7$ mN m) [15]

Eq.	π_0 (mN/m)	A_0 (nm²/molec.)	α^*	$\beta_{12} \times 10^{20}$ (Nm)	Δ mN/m
(1)	—	—	—	—	6.09
(2)	—	1.123	—	—	1.95
(3)	6.0	—	—	—	1.19
(4)	10.5	0.169	—	—	0.29
(7)	—	0.268	5.69[1]	—	0.17
(9)	10.46	—	—	−0.08	0.29
(18)	—	—	0.84[2]	−1.07	0.15
(19)	—	—	8.60[1]	−2.28	0.09
(20)	—	—	1.15[3]	−5.73	0.13

* Units: [1] 10^{-20} Nm²; [2] 10^{-18} Nm; [3] 10^{-38} Nm³; in all cases pro molecule

The correctness of the equations in the chosen π range can be judged on the basis of the Δ value, given in Tab. 3 and representing the standard deviation for Eq. (1) and the Δ_m values in the case of state equations with one or two adjusted parameters.

As seen, from Table 3, by using the SE-s given in the literature, the best description is obtained with Eq. (7), which was also found earlier [16, 17] to be a good approximation.

In testing Eqs. (9) and (18)–(20), calculations were performed by presuming $A_2 = 0.2$ nm²/molecule [15]. This is a quite arbitrary hypothesis and it is more reasonable to take also A_2 for an adjusted parameter. In this case, a triple minimization of Δ is to be performed, giving $(\Delta_m)_m$. Results of this triple minimization are given in Table 4.

Table 4

Parameters of Eqs. (9) and (18)—(20) obtained by triple minimization of Δ for OA ($\pi \leq 7$ mN m)

Eq.	A_2 nm²/molec.	π_0 mN/m	α*	$\beta_{12} \times 10^{20}$ (Nm)	$(\Delta_m)_m$ mN/m
(9)	0.349	9.517	—	0.600	0.165
(18)	0.290	—	0.685	0.058	0.096
(19)	0.225	—	7.714	—1.507	0.087
(20)	0.070	—	—4.266	51.880	0.082

* Units: as in Tab. 3.

As seen, on the basis of $(\Delta_m)_m$ Eq. (20) seems to be the best, but this equation does not correspond for several reasons. In order to show this, in Fig. 5 Δ_m obtained by double minimization and the corresponding α and β_{12} values are given as function of A_2. As seen, $(\Delta_m)_m$ corresponds to $A_2 = 0.07$ nm²/molecule, which is less than the cross-section area of a water molecule, consequently, this value is absolutely unrealistic. For $A_2 > A_1$, Δ_m decreases with decreasing A_2 and $\alpha > 0$, $\beta_{12} < 0$. At $A_2 = A_1$ the Δ_m vs. A_2 curve has a singularity since one has $x_2 = A_1/A$ and Eq. (20) becomes

$$\pi = -\frac{kT}{A_1} \ln x_1 - \frac{\alpha + \beta_{12} A_1}{A^2} \qquad (21)$$

Eq. (21) containing a single adjusted parameter $(\alpha + \beta_{12} A_1)$, Δ jumps up to 2.328 mN/m. For $A_2 < A_1$, Δ_m continues to decrease with decreasing A_2 and passes through a minimum but both α and β_{12} change their sign at $A_1 = A_2$. Therefore, we conclude that Eq. (20) is not suitable to describe the compression isotherm and we will consider Eq. (19) to be the best one.

In order to visualize the quality of the approximations discussed, in Fig. 6 the 17 experimental π and A pairs processed are given, as well as 3 theoretical π vs. A curves, viz. those obtained by means of Eqs. (7), (9) and (19), by using the parameter values given in Tabs. 3 and 4, respectively. We have chosen these relations since Eq. (19) is the best approximation and the other two may be considered to be the 'parent' relations in obtaining our SE (19). As seen, the curves calculated by means of Eqs. (7) and (9) show deviations in the opposite direction from the experimental curve, and the curve corresponding to Eq. (19) occupies an intermediate position between the formers.

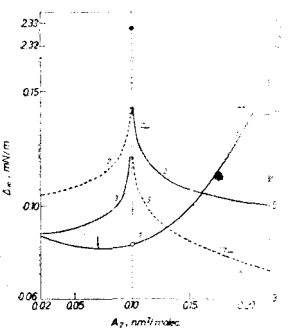

Fig. 5. Testing of Eq. (20) on the compression isotherm of OA for $\pi \leq 7$ mN/m; 1 — Δ_m vs. A curve. The arrow indicates the minimum value given in Tab. 4; 2 — log $|\alpha|$ vs. A_2 curve, $y = \alpha \times 10^{43}$ Nm⁴/molecule, dashed line for $\alpha < 0$. 3 — log $|\beta_{12}|$ vs. A_2 curve, $y = \beta_{12} \times 10^{23}$, Nm/molecule, dashed line for $\beta_{12} < 0$.

Meaning of the parameters derived. The state equations tested contained two kinds of parameters, one of them expressing the own area necessity of the surface-

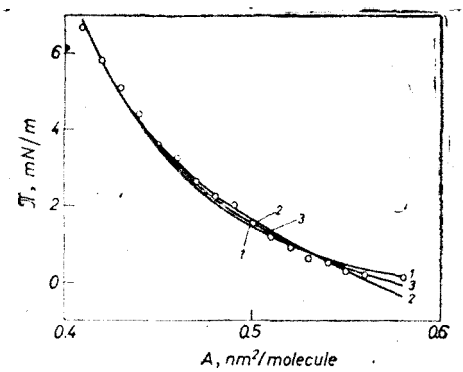

Fig. 6. Experimental $\pi - A$ pairs for OA and theoretical curves calculated by means of: 1 — Eq. (7), parameters given in Tab. 3; 2 — Eq. (9), parameters Tab. 4; 3 — Eq. (19) parameters Tab. 4.

tant molecules, the co-area A_0 of Eqs. (2), (4), (5), (7) and the A_2 value implied in the calculation of x_2 by means of Eq. (16) in the case of the SE-s (9), (18) — (20); the other one takes into account the intermolecular interactions, the cohesive forces, as the internal pressure π_0 of Eqs. (3), (4), (9(and (15). The internal pressure is expressed by means of an interaction parameter α in the case of Eqs. (5), (7) and (18) — (20), reflecting the attractive forces between the surfactant molecules with Eqs. (5), (7) and between the hydrocarbon chains only with Eqs. (18)—(20). Eqs. (9), (15), (18) — (20) contain also the interaction parameter β_{12} corresponding to the attractive forces between the polar head groups and the water molecules.

For A_0 Eq. (2) gives negative values (Tab. 3), which has no physical meaning and it indicates that the intermolecular interactions are mainly responsible for the deviations from the perfect behaviour and not the non-zero molecular area. Eq. (3) gives indeed a better description and π_0 indicates attractive interactions. Nevertheless, both approximations are very rough, as seen from curves 3 and 4 in Fig. 4. A spectacular decrease in Δ is observed if two adjusted parameters are introduced.

In the case of Eq. (4), the choice of A_0 has an important effect, as seen from Tab. 1. The largest linear portion is observed for $A_0 = 0.18$ and 0.20 nm²/molecule, which are very near to the cross-section area of the COOH group, oriented at the air/water interface. The π_0 derived indicates quite strong attractive interactions. Since the attractive forces are short-range ones, the internal pressure depends on A. Consequently, Eq. (7) gives much better results than Eq. (4), as seen from Tab. 3. The A_0 value given by Eq. (4) is near to the cross-section area of the hydrocarbon chain of OA, but the A_0 value derived by means of Eq. (7) is more realistic, being equal to the collapse area of OA.

On the basis of Δ_m Eq. (9) seems to be approximately as good as Eq. (4) As seen from Table 2, π_0 does not depend on the choice of the cross-section area as much as in the case of Eq. (4) (Tab. 1), but β_{12} is very sensitive to the modifications of A_2. For high A_2 values, it expresses strong repulsion ($\beta_{12} > 0$), for low ones, strong attractions ($\beta_{12} < 0$). Since in the oriented structures of the monolayer the H-bond formation between the neighbouring COOH groups has a very small probability, in the expression of β_{12} (see Eq. (13)), $|\varepsilon_{hh}|$ will be less than both $|\varepsilon_{11}|$ and $|\varepsilon_{12}|$. Further, due to the electronattractive effect of the carbonyl O atom, the O atom of the OH groups will have an increased electronegativity, favouring the H-bond formations with water molecules. This might entail $|\varepsilon_{12}| > |\varepsilon_{11}|$. Therefore, negative values may be expected for β_{12} and the use of low A_2 values, corresponding to the cross-section area of the head group of the fatty acids, seems to be correct.

By using $A_2 = 0.20$ nm²/molecule, Eq. (9) gives approximately the same A_0 values as Eq. (4), and in the case of Eqs. (18)—(20), both α and β_{12} correspond to intermolecular attractions (Tab. 3). Δ has the minimum value with Eq. (19), not depassing the experimental errors.

By taking A_2 for adjusted parameter, the standard deviation becomes much less (Tab. 4). The A_2 value obtained with Eq. (9) is comprised between the limiting molecular area A_0 and the collapse area A_c of OA [11] and β_{12} expresses repulsion between the carboxyl groups and water molecules, both results being in disagreement with the basic hypotheses, leading to Eq. (9). Eq. (18) yields also unrealistic positive values for β_{12} and too high A_2 values. Eq. (20) is completely unsuitable, as shown above, since both α and β_{12} values obtained correspond to large repulsive forces, and A_2 is too low.

Eq. (19) gives quite reasonable results. Both α and β_{12} express attraction as expected and A_2 is very near to the molecular area of stearic acid at the π value corresponding to the liquid → solid phase transition, and it might be equal to the real area necessity of the COOH group in an expanded state. We mention that A_c of SA is less, since it is determined by the cross-section area of the hydrocarbon chain and near to the collapse the COOH groups seem to be forced to readily accomodate beneath the hydrocarbon chains.

The parameter values dderive allow us to predict the characteristics of the gas liquid phase transition at the compression of the monolayers. For this purpose, the theoretical π vs. A curve have been constructed for OA by means of Eqs. (7) and (19) respectively, by using the parameter values given in Tabs. 3 and 4. These theoretical isotherms are presented in a semilogarithmic scale in Fig. 7.

As seen, both equations indicate a phase transition. The position of the horizontal dashed line has been established in such a way as the hatched areas above and under this line to be equal to each other. (In Fig. 7 this equality is not obvious because of the logarithmic A scale). The position of the horizontal line indicates the expected equilibrium pressure between the gaseous and liquid phases, i.e. the vapour pressure π_v of the liquid film. The latter value, as well as the corresponding molecular areas in the gaseous (A_v) and in the liquid (A_l) states are given in Table 5.

For the sake of comparison, in the same Table 5 also the experimentally found π_v, A_v and A_l values are given for n-pentadecanoic acid (PDA) monolayers at 20°C and pH = 2 [18].

Since at the spreading area of about 0.6 nm²/molecule, used in our experiments a surface pressure of about 0.1 mN/m was found, the π_v value obtained by means of Eq. (19) seems to be more realistic.

By taking into account that in bulk the boiling points of OA and PDA at p = 100 mm Hg are of 286 and 257°C, respectively [19], one might

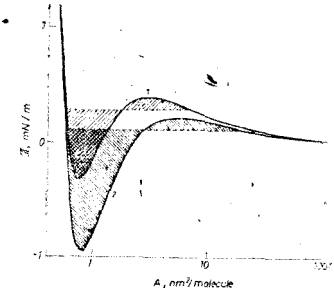

Fig. 7. Theoretical π vs. log A curves constructed for OA monolayers by using Eqs. (7) (curve 1) and (19) (curve 2) and parameter values given in Tabs. 3 and 4, predicting the gas-liquid phase transition.

Table 5

Characteristics of the gas-liquid phase transition of OA as predicted by the state equations

Acid	SE	π_v mN/m	A_v nm²/molec.	A_l nm²/molec.	ref.
OA	(7)	0.290	7.30	0.568	—
OA	(19)	0.118	21.5	0.565	—
OA	—	0.107	—	—	[20]
PDA	—	0.132	15.0	0.415	[18]

expect the vapour pressure of OA to be also in two dimensions, less than that of PDA.

This expectation is in very good agreement with the values predicted by Eq. (19).

The $\pi_v = 0.107$ mN/m value reported for OA monolayers at 27.5°C [20] is also much more consistent with the prediction of Eq. (19), as compared to that of Eq. (7).

Eq. (19), proposed by us, describes much better the behaviour of OA monolayers than the earlier proposed SE-s.

Eq. (19) yields reasonable values for the parameters A_2, α and β_{12} and predicts the characteristic magnitudes of the gas-liquid phase transition of OA in a good agreement with theoretical expectations.

REFERENCES

1. Gaines, G. L. Jr., „Insoluble Monolayers at Liquid-Gas Interface", Interscience, New York 1966, p. 159.
2. Volmer, M., *Z. physik. Chem.*, **115**, 253 (1925).
3. Langmuir, I., *J. Chem. Phys.*, **1**, 756 (1933).
4. Hedge, D. G., *J. Colloid Sci.*, **12**, 417 (1957).
5. Reiss, H., Frisch, H. L. and Lebowitz, J. L., *J. Chem. Phys.*, **31**, 369 (1959).
6. Guastalla, J., *Cahiers phys.*, **10**, 30 (1942); *J. Chim. Phys.*, **43**, 184 (1946).
7. Birdi, K. S., Gabrielli, G. and Pugelli, M., *Kolloid-Z. Z. Polymers*, **250**, 581 (1972).
8. Chattoraj, D. K. and Chatterjee, R., *J. Colloid Interface Sci.*, **54**, 364 (1976).
9. Fowkes, F. M., *J. Phys. Chem.*, **66**, 385 (1962).
10. Lim, Y. C. and Berg, J. C., *J. Colloid Interface Sci.*, **51**, 162 (1975).
11. Tomoaia-Cotişel, M., Zsakó, J., Mocanu, A., Lupea, M. and Chifu, E., *J. Colloid Interface Sci.*, **117**, 464 (1987).
12. Defay, R., Prigogine, J., Bellemans, A. and Everett, D. H., „Surface Tension and Adsorption" Longmans, 1966, p. 211.
13. McArthur, B. W. and Berg, J. C., *J. Colloid Interface Sci.*, **68**, 201 (1979).
14. Irving, H. M. N. H., *Analyst*, **93**, 273 (1968).
15. Tomoaia-Cotişel, M., Zsakó, J. and Chifu, E., *Studia Univ. B. B. Chem.*, **33**, (2), 54 (1988).
16. Ter Minassian-Saraga, L., *J. Chim. Phys.*, **52**, 80 (1955).
17. Chifu, E., Zsakó, J., and Tomoaia-Cotişel, M., *J. Colloid Interface Sci.*, **95**, 346 (1983).
18. Pallas, N. R. and Pethica, B. A., *J. Chem. Soc. Faraday Trans., I*, **83**, 585 (1987)
19. „Chemical Tables" (russ) T. II. Izd. Khimia, Moscow Leningrad, 1964, p. 851, 861.
20. Pagano, R. E. and Gershfeld, N. L., *J. Phys. Chem.*, **76**, 1238 (1972).

PREPARATION OF AIR—PHOSGENE STANDARDS BY DIFFUSION THROUGH A TUBE

V. SIMIANU*

Received: March 21, 1989

The paper presents a method and the related apparatus for the preparation of air-phosgene standard mixtures in ppm range. The method consists of diffusing phosgene vapours through the open head of a glass tube wich leads to the conduit of the carrier gas stream (zero air or nitrogen). Phosgene concentration in the gas stream depends on: the diffusion tube's geometry, temperature, pressure and rate of the carrier gas stream. The concentration of samples has been analysed by a spectrophotometric method.

Introduction. Two main procedures are generally used in preparing gas standards. The static method consists of successively diluting a mixture of a known concentration in separate vessels down to the desired dilution. By this method concentrations of tens of ppm can be obtained; lower concentrations are modified by the absorbtion on the vessels surface. The dynamic method consists of injecting the analysed gas of a known concentration into an inert carrier gas stream. The apparatus based on the latter method allows better precision in the lower concentration range.

For the introduction of vapours in the carrier gas stream several methods are known: gravimetrical methods [1—3], diffusion through a porous layer [4, 5], diffusion through the open head of a tube [6—10], permeation through polymers [11—19], pulverisation [20], chemical generation [21, 22], exponential dilution [23, 24], vapours condensation [25—27], etc.

The method of diffusion through a tube is simple, it does not necessitate prior experiments for the geometrical and technological dimensioning of the installation, and the materials for the installation are available.

This is the first utilisation of the diffusion through a tube method for the preparation of air-phosgene in ppm range. The paper also presents the installation used.

Phosgene (carbonic acid dicloride) has been synthetized first in 1912 (J. Davy) [28] and it was used as a poison gas [29]. Owing to its reactivity, in spite of its high toxicity, phosgene is used in several chemical syntheses (polimers, drugs and dyes). For the calibration of various methods for the detection of the phosgene in air [30] it is necessary to prepare an air-phosgene standard mixture. The threshold-limit value (TLV) of phosgene in air is only 0,12 ppm (0,5 mg/m³).

Experimental. Our installation is shown in Fig. 1. The diffusion through a tube method has been suggested by McKelvey and Hoelscher [8, 9]. The vapours in equilibrium with the liquid phase diffuse through the open end of a glass tube in the carrier gas stream. Fig. 2. shows the dia-

* *University of Cluj-Napoca, Faculty of Chemistry, 3400 Cluj-Napoca, Romania*

gram of the diffusing system. The amount of phosgene vapours that diffuse through the glass tube in the carrier gas stream can be adjusted by selecting the geometrical dimensions of the tube and the temperature and pressure of the liquid phase. The pressure, temperature and the flow rate of the carrier gas are kept constant by (2), (3) and (4), respectively (Fig. 1). After the mixing of the phosgene vapours with the carrier gas in the mixing cell (5), the gas mixture is kept in the storage vessel (7). Standard samples for chemical analysis and for calibration of the detecting methods are taken from the storage vessel. Excess of the mixture is neutralised in the scrubber (8) with 1% NaOH. The working conditions and the tube's geometry are indicated in Table 1. All vessels, tubes and pipes in contact with phosgene are made of glass or PTFE. Previously the vessels, pipes and carrier gas have been carefully dried to avoid the hydrolysis of the phosgene

$$COCl_2 + H_2O = 2HCl + CO_2 \qquad (1)$$

The theoretical basis of the technological dimensioning of the diffusion tubes for phosgene vapours has been dealt in a previous paper [31]. The concentration of the air-phosgene mixture is given by Eq(2'), the basic equation in the dimensioning of the diffusion system:

$$C = 1{,}66 \cdot 10^4 \frac{D \cdot P \cdot M \cdot A}{R \cdot T \cdot L \cdot d} \cdot \ln \frac{P}{P - p} \qquad (2')$$

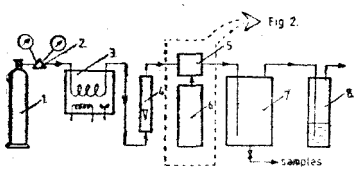

Fig. 1. Schematic diagram of the apparatus
1. carrier gas cylinder, 2. pressure reduction system, 3. thermostat, 4. rotameter, 5. mixing cell, 6. diffusion system, 7. storage vessel, 8. scrubber.

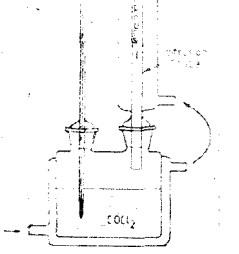

Fig. 2. Diffusion system for phosgene vapours

The diffusion coefficient of the phosgene vapours in air was calculated using Maxwell's formula modified by Gilliland [32, 33]. The value this of coefficient in our working conditions (T = 253 K, P = 1 atm) was D = 0,0619 m²/m. The pressure of the phosgene vapours at the working temperature was calculated using Paterno and Masecchelli's relationship. Beyond the limits of this relationship the following equation is valid [34, 35]:

$$\log p = 7{,}552 - \frac{1314}{T} \qquad (3')$$

The temperature of the liquid phosgene ranged between −25 °C and 0 °C (± 0,1 °C). Thermostated dry air or nitrogen were the carrier gas. The carrier gas flow was measured with a rotameter (60—600 l/h).

The phosgene was brought in from a flask (C. Ch. Rm. Vilcea) containing phosgene 99,86%, chlorine 0,04% and hidrochloric acid 0,1%. A thiosulphate filter (retained) traces of Cl_2 and HCl.

The air-phosgene mixtures were analysed by absorbtion in a 0,1 N NaOH followed by the spectrophotometric determination of Cl^- resulted [36, 37] using calibration plot taken with known Cl^- concentrations in the 2,5—25 μg Cl^-/ml (3,48—34,85 μg $COCl_2$/ml) range (Fig. 3).

$$COCl_2 + 2OH^- = 2Cl^- + CO_2 + H_2O$$

Results and Discussion. For the calculation of the concentration of air phosgene mixture we used the following relationship:

$$C = \frac{(E - b) \cdot V \cdot f}{a \cdot d_a \cdot t \cdot v} \qquad (5')$$

For a quick evaluation of the concentrations, the following plot, based on relationship (5') has been drawn (Fig. 4.). According to the relationship (2'), the working conditions should be chosen for the 0,1—1p mg phosgene/m³ air range (Table 1.).

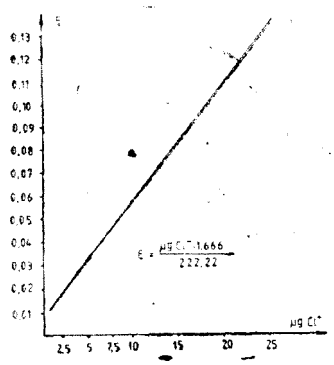

Fig. 3. Cl concentration-absorbance plot

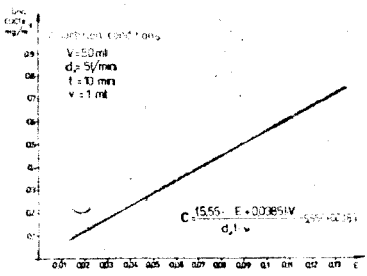

Fig. 4. Concentration of air-phosgene mixture dependence of absorbance, absorbtion conditions

Table 1

Working conditions data

Concentration Range mg · /m³	Tube Length mm	Geometry Diameter mm	Flow Range l/h
0.1 – 1.0	330	0.65	60 – 600
1.0 – 10.0	330	2.00	60 – 600

Errors in experiments are indicated in Table 2. and they are due to the deviations from the calculated working conditions as stated in the relationship (2'). The concentration deviation did not exceed ± 15% of the theoretical values calculated.

The concentration of the phosgene in the carrier gas stream has reached a constant value only in 30 minutes owing to the following facts: the diffusion of the phosgene vapours through the tube, the phosgene vapours are partially absorbed by the inner walls of the installation, the concentration gradients are levelled. The results are displayed in Table 3.

Table 2

Experimental results for two concentration values

Concentration Theoretical mg/m³	Concentration Practical mg/m³	Flow Rate l/h	Concentration Deviation %
0.102	0.092 – 0.114	300 ± 20	– 9.8 + 11.7
3.130	2.761 – 3.550	300 ± 20	– 11.8 + 13.4

Table 3

The homogenisation of the concentration in the storage vessel (stabilisation in time)

Time min.	0	15	30	45	60
Measured Concentration mg/m³	0	0.042	0.107	0.110	0.101
	0	1.79	3.12	3.12	3.

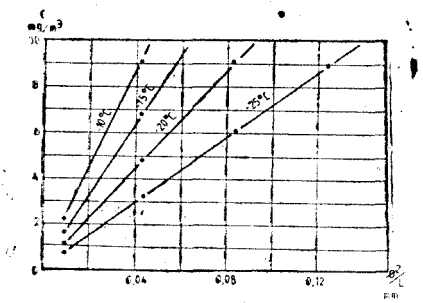

Fig. 5. Evaluation diagram for the geometrical dimensions of the diffusion tube

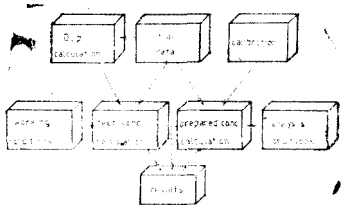

Fig. 6. Flow-chart of the computer program for the tube dimensioning and evaluation of the experimental data

The size of the tube determinates the concentration range, while the fine adjustement is obtained by modifying the carrier gas flow rate. Several diagrams were drawn for each different set of operating conditions, in order to facilitate the design and the construction of the installation. Fig. 5. shows such a diagram for the following set of conditions: temperature of the liquid phase = $= -10, -15, -20, -25$°C, pressure in system = 1 atm, gas flow rate = $= 300$ l/h.

Within each set of operating conditions the equation describing the mixture concentration as a function of the tube's dimensions is:

$$C = K \cdot \frac{z^2}{L} \tag{6'}$$

This is the simplified form of (2).

Both the dimensioning steps and the evaluation of the experimental data were assisted by a computer program (whose flow-chart is shown in Fig. 6.). In this way we can make the optimal choice of the operating conditions and the quick determination of the mixture composition.

Our method of preparing air-phosgene standards presents the following advantages:

— low concentrations, even below 0,1 mg m³ can be obtained
— the precision is $\pm$ 15%
— a simple installation, made of easily available materials.

The signification of the symbols used

C	=	phosgene concentration in the carrier gas stream	mg/m³
D	=	diffusion coefficient of phosgene vapours in air	m²/h
P	=	total preassure in system	atm
M	=	molecular weight of the phosgene	g/mol
A	=	area of tube section	mm²
R	=	gas constant	m³atm/K mol
T	=	temperature	K
L	=	length of the tube	mm
d	=	carrier gas flow rate	l/min

p = vapour pressure of phosgene — atm
E = absorbance
a, b = line's parameters of E = ax + b
x = (calibrating) concentration of Cl^- — g/ml
V = volume of absorbtion solution — ml
t = absorbtion time — min
d = absorbtion rate — l/min
v = volume analysed from the absorbtion solution (number of ml)
f = 1,394 (transformation factor for Cl^- in phosgene — as it results from the equation (4)
Ø = inner diametre of the tube — mm
K = constant depending on the operating conditions

REFERENCES

1. I. A. Fowlis, R. P. Scott, *J. Chromatogr.*, **1**, vol. II, 712 (1963).
2. L. J. Pristley Jr., F. E. Coitchfield, N. H. Ket Cham, J. D. Covender, *Analyt. Chem.*, **37**, 70 (1971).
3. A. G. Vitenberg, M. I. Kostkina, B. V. Ioffe, *Analyt. Chem.*, **56**, 2489 (1984).
4. C. H. Furtin, *Anal. Chim. Acta.*, **15**, 521 (1956).
5. P. Valentin, G. Guighon, *J. Chromatog. Sci.*, **14**, 132 (1976).
6. A. P. Altshuller, I. Q. Cohlen, *Analyt. Chem.*, **32**, 802 (1960).
7. A. P. Altshaller, C. A. Clemons, *Analyt. Chem.*, **34**, 466 (1962).
8. J. M. McKelvey, R. Hoesleher, *Analyt. Chem.*, **29**, 123 (1957).
9. W. Leithe, „The Analysis of Air Pollutants", Ann Arbor Sci. Publ., 51, 1971.
10. A. G. Savitskey, *Analyt. Chem.*, **44**, 1712 (1972).
11. W. L. Bamsberger, F. D. Adams, *Envir. Sci. Tech.*, **3**, 258 (1969).
12. A. Cedergreen, S. A. Frederickson, *Talanta*, **23**, 217 (1967).
13. L. A. Elfers, C. E. Decker, *Analyt. Chem.*, **40**, 1658 (1968).
14. E. E. Hughes, L. A. Rook, E. R. Deardof, *Anal. Chem.*, **49**, 1823 (1977).
15. D. P. Lucerno, *Analyt. Chem.*, **43**, 1744 (1971).
16. H. Muller, A. Mainecke, C. D. Mainecke, J. Tauch Nitz, *Wiss. Z. Kalr-Marx-Univ. Leipzig Math.-Natur. Wiss. R.*, **130**, 92 (1981).
17. Z. Zelinger, Z. Papuskova, M. Jakubkova, P. Engst, *Coll. Czech. Chem. Comm.*, **53**, 749 (1988).
18. F. P. Scarigelli, A. E. O'Keeffe, *Analyt., Chem.*, **42**, 871 (1970).
19. B. E. Saltzman, F. Arthur, A. F. Wartburg Jr., *Analyt. Chem.*, **37**, 1261 (1965).
20. V. A. Punkov, I. P. Rubapenko, Patent S. U. 1217458A, 1986.
21. F. Opekar, *Chemické Listy*, **77**, 884 (1983).
22. T. Tocksteinova, F. Opekar, *Talanta*, **33**, 688 (1986).
23. W. B. Crummet, *Analyt. Chem.*, **28**, 410 (1956).
24. H. P. Wiliams, J. D. Winefordner, *J. Gas Chromatogr.*, **4**, 721 (1966).
25. H. Weber, H. Stenner, A. Kettrup. *Fres. Z. Anal. Chem.*, **64**, 325 (1986).
26. W. B. Croummet, J. D. McLean, *Analyt. Chem.*, **37**, 424 (1965).
27. H. Weber, H. Stener, U. Giese, A. Ketrtrup, *Chem.-Technik*, **6**, 18 (1986).
28. J. Davy, *Phil. Trans. Roy Soc.*, **102**, 144 (1912).
29. A. H. Wailt, „Gas Warfare", Duell, Sloan and Pearce Publ. New York, 1942.
30. P. N. Nigam, S. Prasad, *Indian J. Environ. HLTH*, **3**, 218 (1986).
31. V. Simianu, Mia Morar, Mihaela Simianu, Irina Ciurchea, A. Pop, Ana-Maria Incze, *Rev. Chim.* (Bucureşti) (1990), in press.
32. E. A. Bratu, „Procese Utilaje şi Operaţii în Industria Chimica", Ed. Tehnică, Bucureşti, 1985, vol. III, p. 14.
33. R. Z. Tudose, „Operaţii Unitare în Ingineria Chimică", Ed. Did. şi Ped., Bucureşti, 1977, p. 188.
34. Landolt-Börnstein, „Physikalisch-chemische Tabellen", 1965, band II, p. 1343.
35. H. Guerin, „Traite de Manipulation et d'Analyse des Gaz", Mason de Cie, 1952, p. 454.
36. „Metode de analiza toxicologică" (Fosgen), Min. Ind. Chim., 1981.
37. M. Cotrau, A. Butuc, „Texicologia vaporilor şi gazelor", Min. Ind. Chim., Bucureşti, 1982, p. 161.

STUDIA UNIV. BABEŞ BOLYAI, CHEMIA, XXXV, 1, 1990

THE KINETICS AND MECHANISM OF THIOMALIC ACID OXIDATION BY HEXACYANOFERRATE (III)

MARIA-MARILENA GIURGIU* and IOAN BÂLDEA*

Received: June 8, 1990

Kinetics and mechanism of thiomalic acid oxidation by hexacyanoferrate (III) in perchloric acid solution has been investigated spectrophotometrically at 420 nm.

The kinetic behaviour of the system is complex. The reaction rate, expressed by means of the $Fe(CN)_6^{3-}$ ion, is first-order with respect to the concentration of hexacyanoferrate (III) ions at hight acidities (from 0.8 to 1.60 M). The large excess of thiomalic acid concentration is responsible for the first-order kinetic law.

A complex dependence on thiomalic acid concentration was observed in our conditions. The dependence of kinetics on hydrogen ion concentration and temperature was also studied and the apparent energy of activation has been evaluated.

A reasonable reaction mechanism was suggested by our results. An inner sphere interaction between the oxidant, $Fe(CN)_6^{3-}$, and RSH molecule, seems to be responsible for the actual electron transfer. A reaction sequence evolving the reactive intermediate, $Fe(CN)_5(CN.SR)^{4-}$ is taken into discussion.

Introduction. The oxidation of thiocompounds with transition metal ions in aqueous solution offers very suggestive examples concerning the kinetics and mechanism of the reaction. Intermediate reactive complexes were detected spectrophotometrically in such systems.

The hexacynoferrate (III) ion, inert to ligand substitution, is a well-known oxidant in aqueous solution ($\varepsilon_0 = 0.356$ V in perchloric acid medium) performing the oxidation of sulphide group to disulphide. The mechanism of thiol oxidation by $Fe(CN)_6^{3-}$ is not well understood. There are many contradictory facts connected with the reactivity of hexacynoferrate (III) towards such reducing organic substrates [1–4].

The present study gives new evidence concerning the complexity of the reaction pathways in the oxidation of thiocarboxilic acids by $Fe(CN)_6^{3-}$. Since the oxidant species is inert to ligand substitution, an outer-sphere reaction mechanism would be expected to be efficient. Our results, however, confirm a reaction order dependent on thiomalic acid concentration. The fact is diagnostic for the inner sphere interactions in the course of the overall redox process. In the inner-sphere redox reactions, there are marked changes in the coordination sphere of the reactants in the formation of the activated complex.

A reaction sequence was suggested [3] for the oxidation of thiols by $Fe(CN)_6^{3-}$, in which ligand displacement on $Fe(CN)_6^{3-}$ takes part. But, of the reaction is carried out in the presence of $^{14}CN^-$, such mechanism should lead to the introduction of $^{14}CN^-$ into $Fe(CN)_6^{4-}$ (the product of the reaction). This is not observed and the mechanism [3] can be ruled out from the results.

* University of Cluj-Napoca, Faculty of Chemistry, 3400 Cluj-Napoca, Romania

The $Fe(CN)_6^{3-}$ ion smoothly oxidizes the organic [5] and protein substrates [6]. Some of reactions of the nitroprusside ion, $Fe(CN_5)NO^{2-}$, and of the $Fe(CN)_5H_2O^{2-}$ ions have been investigated [7—9].

In view of these facts, it is clear that, the iron (III) and (II) cyano complexes offer some very interesting mechanistic aspects in acidic media. It is the scope of the present study to illustrate the reactivity of the $Fe(CN)_6^{3-}$ ions with thiocarboxilic acids (thiomalic acid) on the basis of our kinetic and spectral results.

Experimental. On mixing an acidic solution of potassium ferricyanide with a solution of thiomalic acid, the disappearance of the yellow colour of $Fe(CN)_6^{3-}$ is observed. The reaction products are the hexacyanoferrate (II) and the corresponding disulphide. The overall process is base catalyzed.

Reagents. Solutions. Thiomalic acid solution 0.2 M in concentration was prepared by dissolving a weighed amount of the reagent of biochemical purity in twice distilled water just before the kinetic measurements.

Potassium ferricyanide solution was obtained from the reagent grade chemical. The absorption spectra in the visible and ultra-violet regions were recorded at different perchloric acid concentrations. No changes were observed with the variation of hydrogen ion concentration. (0.5—1.6 M $HClO_4$). A stock solution 2×10^{-2} M in strength was prepared. The extinction coefficient, $\varepsilon = 1 \times 10^3$ mol^{-1} cm^{-1} associated with $Fe(CN)_6^{3-}$, at 420 nm, was determined. The reduction product, $Fe(CN)_6^{4-}$, is almost transparent at 420 nm. This wavelenght was selected for kinetic measurements.

Perchloric acid solution 4.0 M in strength was obtained from a concentrated perchloric acid solution (70%, d = 1,67 g/ml) of high purity. This solution was standardized against sodium hydroxide solution.

Sodium perchlorate solution 4.0 M in concentration was used to maintain the ionic strength at a constant value.

The overall stoichiometry corresponds to the reaction:

$$2\,Fe(CN)_6^{3-} + 2\,RSH = 2\,Fe(CN)_6^{4-} + R-S-S-R + 2\,H^+$$

The optical density values, A_0, of the oxidant solution linearly correlates with the concentration of $Fe(CN)_6^{3-}$ ions at 420 nm in the region investigated in the present paper (*Fig.* 1).

The reaction course was followed at 420 nm, the only absorbing species being the $Fe(CN)_6^{3-}$ ions.

All solutions were thermostated in a water-bath before mixing.

The procedure. The experimental device. The temperature of the reaction mixture in the optical cell was controlled in every case. A Wöbster thermostat was connected to the spectrophotometer.

A small volume (1.5 ml) of potassium ferricyanide solution 1×10^{-3} M was rapidly introduced into 6.0 ml of reducing solution (containing RSH, $HClO_4$ and $NaClO_4$) placed into the optical cell. The reducing solution was used to calibrate the 100% mark of the apparatus (Spekol). d = 4,995cm, 420 nm. The decrease of the optical density of the reaction mixture was followed. The infinite value, A_∞, is *zero* in all cases.

Experimental results. The observed *first-order rate constants*, k_{ob}, were evaluated from the experimental data *optical density — time*. The first-order kinetic law is a result of the large excess of thiomalic acid concentration.

$$r_{ob} = -\frac{d[Fe(CN)_6^{3-}]}{dt} = k_{ob}[Fe(CN)_6^{3-}]$$

No deviation from the first-order kinetics was observed in our experimental conditions.

The influence of hydrogen ion concentration, thiomalic acid concentration and temperature on kinetics was systematically studied.

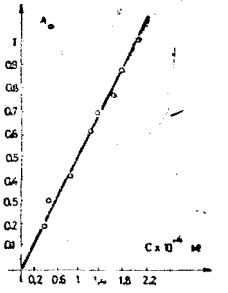

Fig. 1. The dependence of the initial optical density values A_0 on concentration of $Fe(CN)_6^{3-}$ ions. 420 nm, d — 4.995 cm, $[H^+]$ = 1.333 M.

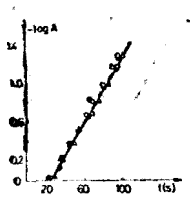

Fig. 2. First-order kinetic plots for three experimental curves recorded in the same conditions 291.5 K
RSH : 4×10^{-2} M
$Fe(CN)_6^{3-}$: 2×10^{-4} M
$HClO_4$: 1.60 M

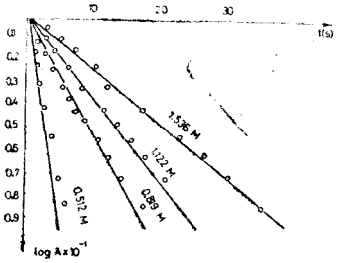

Fig. 3. First-order kinetic plots for the oxidation of thiomalic acid by $Fe(CN)_6^{3-}$ at different perchloric acid concentrations 291.5 K.
RSH : 4×10^{-2} M
$Fe(CN)_6^{3-}$: 2×10^{-4} M

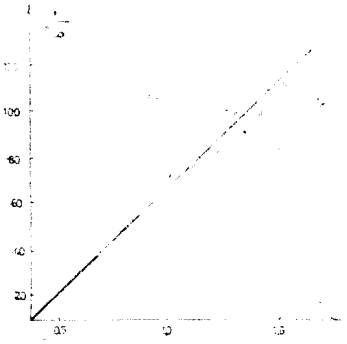

Fig. 4. The dependence of k_{ob}^{-1} values on hydrogen ion concentration at 291.5 K.
RSH : 4×10^{-2} M
$Fe(CN)_6^{3-}$: 2×10^{-4} M

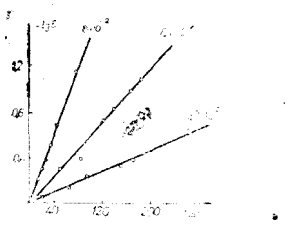

Fig. 5. First-order kinetic plots at different thiomalic acid concentrations, 308.5 K.
$HClO_4$: 1.60M
$Fe(CN)_6^{3-}$: 2×10^{-4}M
a : 8.0×10^{-2}M
b : 6.4×10^{-2}M
c : 3.2×10^{-2}M

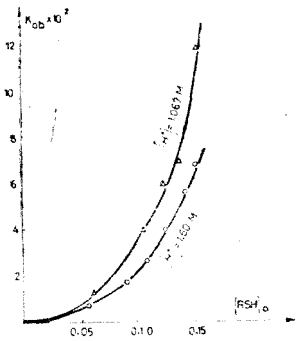

Fig. 6. a. The dependence of the rate constants on thiomalic acid concentration at 302.1 K.

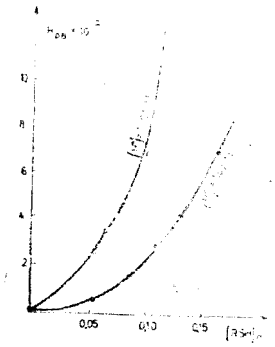

Fig. 6. b. The dependence of the rate constants on thiomalic acid concentration at 312.9 K.

Fig. 2 illustrates the precision of the kinetic method. First-order kinetic plots for three different experiments, under the same conditions, are presented here.

1) The dependence of kinetics on hydrogen ion concentration.

Some first-order kinetic plots for the oxidation of thiomalic acid with $Fe(CN)_6^{3-}$ ion, at different concentrations of perchloric acid are presented in *Fig. 3*. A decrease of the rate constants with the increase of $[H^+]$ from 0.5 to 1.60 M, is observed.

Fig. 4 shows the dependence of the reciprocal values, k_{ob}^{-1}, on $[H^+]$ values.

2) The dependence of kinetics on thiomalic acid concentration.

The influence of temperature on kinetics. Kinetic measurements at different temperatures between 290 and 310 K have been made. The influence of thiomalic acid concentration at a constant temperature and (H^+) has been studied. First-order kinetic plots at different $[RSH]_0$ are presented in *Fig. 5*. The hydrogen ion concentration is 1.60 M.

It can be observed that the rate constants, k_0, increase as the concentration of RSH increases. The dependency of the rate constants on thiomalic acid concentration is illustrated in *Fig. 6 (a, b)* at 302.1 and 312.9 K, respectively.

Three different $[H^+]$ values were investigated kinetically at each temperature.

The same kinetic behaviour was observed over the investigated range (pH values and temperatures). The results are presented in *Tables 1–5*.

Table 1

Kinetic results on thiomalic acid oxidation by $Fe(CN)_6^{3-}$ $[HClO_4]$ = 1.60 M

$[RSH]_0$ M	$[RSH]_0^{-1}$ M^{-1}	$\frac{[H^+]}{[RSH]_0}$	291.5 K		299.7 K		308.5 K	
			k_{ob} s^{-1}	$\frac{[RSH]_0}{k_{ob}}$	k_{ob} s^{-1}	$\frac{[RSH]_0}{k_{ob}}$	k_{ob} s^{-1}	$\frac{[RSH]_0}{k_{ob}}$
8×10^{-2}	12.500	20.00	0.040	2.000	—	—	—	—
6.4×10^{-2}	15.65	25.00	0.018	3.555	—	—	0.0319	2.000
5.82×10^{-2}	17.182	27.491	—	—	0.0219	2.657	—	—
5.60×10^{-2}	17.860	28.576	0.013	4.30	—	—	—	—
5.45×10^{-2}	18.350	20.360	—	—	—	—	0.0166	2.535
5.14×10^{-2}	19.455	31.128	—	—	0.0158	3.252	—	—
4.80×10^{-2}	20.833	33.333	0.0107	4.48	—	—	0.0166	2.900
4.00×10^{-2}	25.000	40.000	0.0085	4.70	0.0120	3.400	—	—
3.42×10^{-2}	29.240	46.784	—	—	0.0074	4.620	—	—
3.20×10^{-2}	31.250	50.000	0.00532	6.15	—	—	0.0082	3.9 0
2.40×10^{-2}	41.660	71.424	0.00318	7.55	0.0040	6.000	—	—
2.24×10^{-2}	44.640	66.665	—	—	—	—	0.0045	4.975
1.71×10^{-2}	58.480	93.560	—	—	0.0024	7.130	—	—

Table 2

The influence of hydrogen ion concentration, temperature and thiomalic acid concentration on kinetics. First-order rate constants in s^{-1}.

$(RSH)_0$, M	291.5 K		302.1 K			312.9 K	
$[H^+]$	1.333 M	1.60 M	1.333 M	1.067 M	1.60 M	1.333 M	1.067 M
0.160	—	0.0645	—	0.117	0.0709	—	0.313
0.147	—	0.0525	—	0.0965	0.0614	—	0.243
0.128	0.037	0.0348	0.0385	0.0567	0.0429	0.454	0.180
0.108	0.021	0.0232	0.0289	0.0362	0.0294	0.0416	0.119
0.089	0.012	0.0142	0.0198	—	—	0.0204	—
0.064	0.0053	—	0.0086	0.0099	—	0.0109	0.0356
0.054	0.0042	0.0045	—	—	0.0055	0.0059	0.0230
0.044	—	—	—	0.004	—	—	—

Obs.: k_{ob} is the average value of 2–3 individual determinations.

Table 3

Kinetic results on thiomalic acid oxidation by $Fe(CN)_6^{3-}$ 291.5 K, k_{ob} in s^{-1}

$[RSH]_0$ M	$[RSH]_0^{-1}$ M^{-1}	1.333 M H^+			1.067 M H^+		
		k_{ob}	$\frac{[RSH]_0}{k_{ob}}$	$\frac{[H^+]}{[RSH]_0}$	k_{ob}	$\frac{[RSH]_0}{k_{ob}}$	$\frac{[H^+]}{[RSH]_0}$
0.128	7.810	0.037	3.459	10.387	0.073	—	8.279
0.108	9.250	0.021	5.140	12.303	0.054	2.000	8.805
0.089	11.230	0.012	7.140	14.936	0.041	2.190	11.904
0.064	15.640	0.0053	10.500	20.801	0.0225	2.840	16.578
0.032	31.250	—	—	44.329	0.0075	4.000	35.330
0.054	18.910	0.0042	12.700	25.150	—	—	—

Table 4

Kinetic results on thiomalic acid oxidation by $Fe(CN)_6^{3-}$ at 302.1 K, k_{ob}, s^{-1}

$[RSH]_0$ M	$[RSH]_0^{-1}$ M^{-1}	1.60 M H^+			1.333 M H^+			1.067 M H^+		
		k_{ob}	$\frac{[RSH]_0}{k_{ob}}$	$\frac{[H^+]}{[RSH]_0}$	k_{ob}	$\frac{[RSH]_0}{k_{ob}}$	$\frac{[H^+]}{[RSH]_0}$	k_{ob}	$\frac{[RSH]_0}{k_{ob}}$	$\frac{[H^+]}{[RSH]_0}$
1.60	6.25	0.0645	2.480	10.00	—	—	—	0.1167	1.370	6.645
0.147	7.14	0.0525	2.800	11.424	—	—	—	0.065	2.174	7.568
0.128	7.81	0.0348	3.678	12.496	0.0385	3.320	10.387	0.0567	2.257	8.279
0.108	9.25	0.0232	4.655	14.800	0.0289	3.730	12.303	0.0362	2.980	9.805
0.089	11.23	0.0142	6.330	17.968	0.0198	4.520	14.936	—	—	11.904
0.064	15.64	—	—	—	0.0086	7.440	20.801	0.00995	6.43	16.578
0.054	18.91	0.0045	12.00	830.256	—	—	—	—	—	—
0.044	22.73	—	—	36.368	—	—	—	0.0044	10.00	24.321

Table 5

Kinetic results on thiomalic acid oxidation by $Fe(CN)_6^{3-}$ at 312.9 K, k_{ob} s^{-1}

$[RSH]_0$ M	$[RSH]_0^{-1}$ M^{-1}	1.60 M H^+			1.333 M H^+			1.067 M H^+		
		k_{ob}	$\frac{[RSH]_0}{[H^+]}$	$\frac{[H^+]}{[RSH]_0}$	k_{ob}	$\frac{[RSH]_0}{k_{ob}}$	$\frac{[H^+]}{[RSH]_0}$	k_{ob}	$\frac{[RSH]_0}{k_{ob}}$	$\frac{[H^+]}{[RSH]_0}$
0.160	6.25	0.0703	2.275	10.000	—	—	—	0.313	0.511	6.625
0.147	7.41	0.0614	2.394	11.424	—	—	—	0.243	0.603	7.568
0.128	7.81	0.0429	2.983	12.496	0.0545	2.348	10.387	0.180	0.708	8.279
0.108	9.25	0.0294	3.673	14.800	0.0416	2.596	12.303	0.110	0.982	9.805
0.089	11.23	—	—	17.968	0.0204	4.362	14.936	—	—	—
0.064	15.64	—	—	25.024	0.0109	5.871	20.801	0.0353	1.813	16.578
0.054	18.91	0.0055	9.818	30.256	0.0059	9.152	25.15	0.0272	2.000	20.045

The dependence of the rate constants, k_{ob}, on thiomalic acid concentration can be represented by the equation:

$$k_{ob} = \frac{k_a[RSH_0]^2}{k_b + k_0[RSH]_0}$$

A linear relationship can be then written:

$$\frac{[RSH]_0}{k_{ob}} = \frac{k_b}{k_a} \cdot \frac{1}{[RSH]_0} + \frac{k_c}{k_a}$$

The data show a plot of the value $[RSH]^{-1}$ *versus* $\frac{[RSH]_0^{-1}}{k_{ob}}$ does fit a linear equation such as in *Fig. 7* at $[H^+] = 1.333$ M at at three temperatures (T_A, T_B, T_C). The slope represents the ratio k_a/k_a

3) The influence of potassium ferrocyanide on kinetics.

The addition of $K_4Fe(CN)_6$ to the initial reaction mixture, at constant ionic strength, results in a decrease of the reaction rate in acidic medium. The kinetic effect is observed in *Fig. 8.*

Discussion. Conclusions on the reaction mechanism. Our kinetic results can be accounted for by assuming the following reaction sequence:

$$RSH \overset{K_a}{\rightleftharpoons} RS^- + H^+ \qquad (1)$$

$$Fe(CN)_6^{3-} + RS^+ \overset{K}{\rightleftharpoons} Fe(CN)_5(CN.SR)^{4-} \qquad (2)$$

$$Fe(CN)_5(CN.SR)^{4-} + RSH \xrightarrow{k} Fe(CN)_6^{5-} + R-S-S-R + H^+ \qquad (3)$$

The step (3) is the rate-determining electron transfer process.

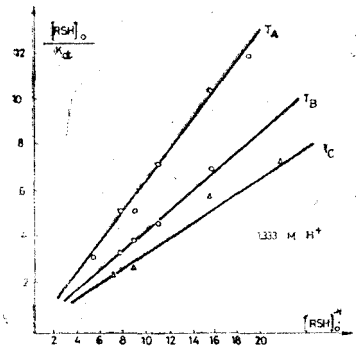

Fig. 7. The variation of $\frac{[RSH]}{k_{ob}}$ values with $[RSH]^{-1}$ at 1.33 MH$^+$ Three different temperatures: 291.5; 302.1 and 312.9 K.

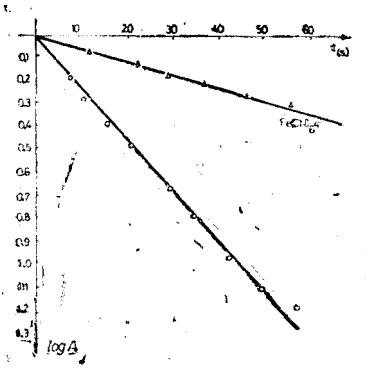

Fig. 8. The influence of $Fe(CN)_6^{4-}$ ions on the reaction rate of thiomalic acid oxidation by $Fe(CN)_6^{4-}$, 291.5 K
$HClO_4$: 1.60 M
RSH : 4×10^{-2} M

Taking into account the value of the acidic dissociation constant, K of the organic substrate, we can write then:

$$Fe(CN)_6^{3-} + RSH \overset{K_f}{\rightleftharpoons} Fe(CN)_5(CN.SR)^{4-} + H^+ \quad (4)$$

with: $K_f = K_a \cdot K$

The reaction scheme probably involves the rapid formation of some iron (III) reactive intermediate, $Fe(CN)_5(CN \cdot SR)^{4-}$.

We conclude that, the immediate product of the electron transfer process is an iron (I) hexacyano complex, $Fe(CN)_6^{5-}$ (?), rapidly stabilized to iron (II) hexacyano species:

$$Fe(CN)_6^{5-} + Fe(CN)_6^{3-} \xrightarrow{fast} 2\,Fe(CN)_6^{4-} \quad (5)$$

the final reduction product.

The retarding effect of $Fe(CN)_6^{4-}$ on the reaction rate can be explained by the formation of a CN^- — bridged complex with the organic substrate:

$$Fe(CN)_6^{4-} + RSH \overset{K'}{\rightleftharpoons} Fe(CN)_5(CN.SR)^{5-} + H^+ \quad (6)$$

The decrease of RSH concentration implies a corresponding decrease of the reaction rate.

There may be other explanations to be taken into account for the influence of $Fe(CN)_6^{4-}$ ions on the reaction kinetics. A binuclear Fe(III)-Fe(II) complex species, inert to electron transfer, may be significant during the reaction course.

A reaction path involving RS. radicals could be responsible for the kinetic behaviour of the reactant system: one-electron transfer assisted by a RSH molecule actually can take place:

$$Fe(CN)_5(CN.SR)^{4-} + RSH \xrightarrow{k} Fe(CN)_6^{4-} + RS. + RSH \quad (7)$$

$$2\,RS. \xrightarrow{fast} R-S-S-R \quad (8)$$

The reaction order with regard to the concentration of $Fe(CN)_6^{3-}$ — the real oxidant species — offers a strong evidence that no iron (III) dimers are involved in the reaction mechanism.

By expressing the reaction rate by means of the rate for the rate-determining step, we obtain finally:

$$r = \frac{k \cdot K_a \cdot K \dfrac{(RSH)^2}{(H^+)}}{1 + K \cdot K_a \dfrac{(RSH)}{(H^+)}} [Fe(CN)_6^{3-}] = k_1 [Fe(CN)_6^{3-}]$$

As it can be observed, there is a complex dependence of the rate constant on thiomalic acid concentration.

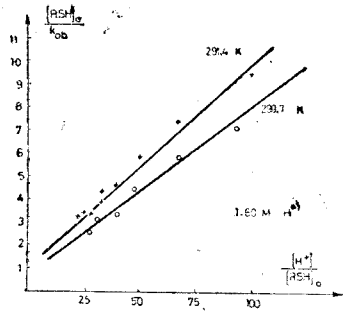

Fig. 9. The variation of $\frac{[RSH]}{k_{ob}}$ values with $\frac{[H^+]}{[RSH]}$ at two temperatures.
a: 291.5 K
b: 299.7 K

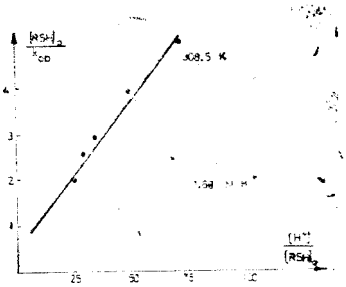

Fig. 10. The variation of $\frac{[RSH]}{k_{ob}}$ values with $\frac{[H^+]}{[RSH]}$ at 308.5 K

The following expression, for the influence of thiomalic acid concentration, can be written:

$$\frac{[RSH]}{k_1} = \frac{1}{k} + \frac{1}{k \cdot K_a \cdot K} \cdot \frac{[H^+]}{[RSH]}$$

where k_1 is the first-order rate constant (identical with the experimental value k_{ob}).

Fig. 9—10 show the linear dependence of the values $\frac{[RSH]}{k_{ob}}$ on $\frac{[RSH]}{[H^+]}$, at three temperatures, in accordance with the postulated reaction mechanism.

The values k and $k \cdot K_a \cdot K$, at $(H^+) = 1.60$, are presented in *Table 6*.

Table 6

The influence of temperature on thiomalic acid oxidation by $Fe(CN)_6^{3-}$ ions.

$HClO_4$: 1.60 M

T, K	k $M^{-1}s^{-1}$	$\frac{kK_aK}{[M^+]}$	kK_aK
291.5	1.66	6.00	9.60
299.7	2.00	6.75	10.80
308.5	2.85	9.42	15.07

The apparent energy of activation has been evaluated from the experimental values of the rate constants *(Table 7)*.

Table 7

The apparent energy of activation for the oxidation of thiomalic acid by $Fe(CN)_6^{3-}$ ions.

$[RSH]_0$, M	E_a, KJ mol^{-1}	E_a, KJ mol^{-1}
2.85×10^{-2}	16.70	
3.07×10^{-2}	15.90	16.20
5.00×10^{-2}	16.25	
6.67×1010^{-2}	16.70	

An average value of 16.20 kJ mol^{-1} has been determined. The low value of the apparent energy of activation can be interpreted in terms of fast preequilibrium steps.

REFERENCES

1.a R. K. Chohan, B. P. Sinha, R. C. Kapoor, *J. Phys. Chem.* **76,** 3641 (1972).
1.b R. C. Kapoor, R. K. Chohan, B. P. Sinha, *J. Phys. Chem.* **75,** 2036 (1971).
1.c O. P. Kachhwala, B. P. Sinha, R. C. Kapoor, *Indian J. Chem.* **8,** 806 (1970).
1.d R. C. Kapoor, O. P. Kavhhwala, B. P. Sinha, *J. Phys Chem.* **73,** 1627 (1969).
1.e I. M. Kolthoff, E. J. Meehan, M. S. Tsao, Q. W. Choi, *J. Phys. Chem.* **66,** 1233 (1962).
1.f E. J. Meehan, I. M. Kolthoff, N. Kakincha, *J. Phys. Chem.* **66,** 1238 (1962).
1.g J. J. Bohning, K. Weiss, *J. Amer. Chem. Soc.* **82,** 4724 (1960).
2. G. Dasgupta, M. K. Mahanti, *React. Kinet. Catal. Lett.* **28,** 153 (1985).
3. K. B. Wiberg, H. Maltz, M. Okano, *Inorg. Chem.* **7,** 830 (1968).
4. J. M. Lancaster, R. S. Murray, *J. Chem. Soc.* A, 2755 (1971).
5. I. R. Wilson, *Pure Appl. Chem.* **16,** 103 (1966).
6. B. H. Havsteen, *Acta Chem. Scand.* **19,** 1227 (1965).
7. J. M. Swinehart, *Coord. Chem. Revs.* **2,** 385 (1967).
8. J. Masek, H. Wendt, *Inor. Chim. Acta.*, **3,** 455 (1969).
9.a J. M. Espenson, S. G. Wolenuk, *Inorg. Chem.* **11,** 2035 (1972).
9.b M. D. Johnson, R. G. Wilkins, *Inorg. Chem.* **23,** 231 (1984).

STUDIA UNIV. BABEŞ BOLYAI, CHEMIA, XXXV, 1, 1990

ÜBER EINIGE KRITERIALEN BEZIEHUNGEN IN NICHTSTATIONAREN KONDUKTIV-KONVEKTIVEM EIGENSCHAFTSTRANSPORT

LIVIU LITERAT*

Eingegangen am 6. Oktober 1990

About some Criterial Relations on the Unsteady-State Transport of Property. From the general matematical model of the conductiv-convective transport, one suggest for momentum, mass, heat and electricity the possibility to grouping any similarity criteria as intrinsic and extrinsic relations. Between this groups they set up criterial and scale-up relations. Through the analysed criteria there are mentioned 3 new criteria implicate in the mass, heat and momentum with electrical charge transport.

Einleitung. Der konduktiv-konvektive Eigenschaftstransport wird mit folgenden Differentialgleichungen beschrieben (vectoriell)

$$\frac{\partial P}{\partial t} + \nabla(P \cdot w) = \mathfrak{D}\Delta^2 P + S_p \qquad (1)$$

wo das erste Glied den nichtstationären Vorgang, das Zweite die konvection, das Dritte die Diffusion (den molekülaren Mechanismus) und das letzte den Beitrag der inneren Eigenschaftsquellen beschreibt (chemische Reaktion, Wärmequellen u.s.w.) [1–3].

Wenn, aus verschiedenen Gründen, die allgemeine Differentialgleichung des Transports nicht gelöst werden kann (am hänfigsten im Falle der technisch, industriellen Vorgänge), dann wird die Erscheinung durch kriterielle Gleichungen der Form

$$f(K_1, K_2, K_3, \ldots, K_n) = 0 \qquad \text{oder} \qquad K_1 = C\, K_2^m \cdot K_3^n \ldots K_n^v \qquad (2)$$

beschrieben, wo $K_1, K_2, \ldots K_n$ Gruppen undimensionaller Grössen, und dimensionelle unveränderliche Grössen (Kriterien), und C, m, n, v experimentell gefundene unveränderliche Grössen sind [2, 4].

Zu diesen kriterialen Formulierungen kann man durch einfache Verhältnisse von Gliedern derselben Differentialgleichung (intrinsecke Glieder), oder deren Homogenen bei der Beschreibung des Eigenschaftstransports (Verhältnisse extrinsker Glieder gelangen [4].

Zum Veranschaulichen wählen wir den eindimensionalen nichtstationären konvektiv-molekularen Eigenschaftstransport im izotropen homogenen Medium

* *Universität Cluj-Napoca, Fakultät für Chemie, 3400 Cluj-Napoca, Rumänien*

($\mathfrak{D}$ = konst.) ohne innere Eigenschaftsquellen wiedergegeben durch die allgemeine Gleichung

$$\frac{dP}{dt} + w_x \frac{dP}{dx} = \mathfrak{D} \frac{d^2P}{dx^2} \tag{3}$$

den wir konkret für den Impulstransport ($P = \rho w$ und $\mathfrak{D} = \nu$), für die Wärme ($P = \rho c_p T$ und $\mathfrak{D} = a$) und die Masse ($P = C$ und $\mathfrak{D} = D$) behandeln und zu dem der für experimentelle Modellierungs- und Simulationsprozesse interesante elektrische Ladungstransport ($P = E$ und $\mathfrak{D} = c$) hinzugefügt wird. [3, 5].

Kriterien der Ähnlichkeit und kriterielle Beziehungen aus Verhältnissen eigentlicher Glieder. Dimensionell geschrieben, führt die Gleichung (3), durch das aufeinander folgende Rapportieren der nichtstationären Glieder (1), Konvektion (2) und Leitfähigkeit (3):

$$\underset{(1)}{\frac{P}{t}} + w \underset{(2)}{\frac{P}{l}} = \mathfrak{D} \underset{(3)}{\frac{P}{l^2}} \tag{4}$$

zu der Bestimmung der drei Kriterien $K_1(Ho)$, K_2, (Fo) und K_3 (Pe) der Form

$K_1(Ho) = (wt)/l$ als Verhältniss (2)/(1); (Konvektion)/(Nichsttationarität)
$K_2(Fo) = (Dt)/l^2$ (3)/(1); (Konduktion)/(Nichtstationarität)
$K_3(Pe) = (wl)/D$ (2)/(3); (Konvektion)/(Konduktivität)

Anders gesagt, ein konduktiv-molekularer nichtstationärer Prozess kann durch kriterielle Funktionen $F(K_1, K_2, K_3) = 0$ oder $f(Ho, Fo, Pe) = 0$, dargestellt werden.

Durch Adaptierung der allgemeinen Gleichung (4) für den entsprechenden Wärmetransport

$$\frac{T}{t} + w \frac{T}{l} = a \frac{T}{l^2} \tag{5}$$

gelangt man zu den bekannten Kriterien Ho(Sr), Fo und Pe die oben als Äquivalente der Kriterien K_1, K_2 und K_3 gebraucht wurden. Im Falle des Massen,- Impuls- und Ladungstransport, findet man immer das Homochroniekriterium (Ho oder Sr Strouhal) und gleichartige Kriterien Fourier (Fo', Fo'' und Fo'''), bzw. Péclet (Pe', Pe'' und Pe'''), die in Tabelle 1 angegeben sind.

Aus der Tabelle 1 ergeben sich einigen Schlussvolgerungen:

1. unabhänging der transportierten Eigenschaft, ist die Entwicklung (im laufe der Zeit) der Konvektiven Prozesse durch das Homocronie-kriterium charakterisiert, Ho (Sr, K_1); (Beziehungen 1, 4, 7 und 10 aus Tabelle 1)

2. die Dynamik der molekularen Prozesse (Konduktion, Diffusion) ist von der Diffusivität (a, ν, D, c) der Eigenschaft in dem Transportmedium bestimmt, und durch die gleichartigen Kriterien Fourier Fo(K_2): Fo', Fo'', Fo''' (Beziehungen 2, 5, 8, 11) beschrieben

3. der Beitrag des konvektiver und molekularen Mechanismus zum Eigenschaftstransport ist von Péclet Kriterien Pe, (K_3), Pe', Pe'', Pe''' (Beziehungen

Tabelle 1

Ähnlichkeits Kriterien als Verhaltnisse intrinsecker Glieder

Transportierte Eigenschaft	Verhältnis von Glieder	Kriterium	Nr.
Wärme	(2)/(1)	(wt)/l = Ho(Sr)	1
	(3)/(1)	(at)/l^2 = Fo	2
	(2)/(3)	(wl)/a = Pe = RePr	3
Masse	(2)/(1)	(wl)/l = Ho	4
	(3)/(1)	(Dt)/l^2 = Fo′	5
	(2)/(3)	(wl)/D = Pe′ = ReSc	6
Impuls (Moment)	(2)/(1)	(wl)/l = Ho	7
	(3)/(1)	(νt)/l^2 = Fo″ = 1/Re	8
	(2)/(3)	(wl)/ν = Pe″ = Re	9
Elektrische Ladung	(2)/(1)	(wt)/l = Ho	10
	(3)/(1)	(et)/l^2 = Fo‴	11
	(2)/(3)	(wl)/e = Pe‴	12

3, 6, 9, 12) wiedergegeben. Diese sind eigentlich abgeleitete Kriterien: Pe = = RePr, Pe′ = ReSc, u.s.w.. (z.B. Pe = (wl)/a = [(wl)/a] · [(ν/ν)] = = [(wl)/ν] [ν/a] = RePr)

4. von den 12 Kriterien, sind in der Literatur Fo″, Fo‴ und Pe″ nicht bekannt (Gl. 8, 11, 12)

5. das Kriterium Pe″ (Gl. 9) ist identisch mit dem Kriterium Reynolds (Re) und Fo″ (Gl. 8) ist mit dessen Kehrwert gleich. Ein spekulativer Standpunkt bezuglich der Kriterien Fourier (Fo, Fo′, Fo″, Fo‴) zeigt einige interesante Schlussfolgerungen. So folgt, aus dem Ausdruck des Kriteriums Fo, derwie folgt wiedergeben wird:

$$Fo = \frac{at}{l^2} = \frac{a}{l(l/t)} = \frac{a}{lw} = \frac{1}{Pe} = \frac{1}{RePr} \qquad (6)$$

dass der Kehrwert des Kriteriums Pe, und desgleichen des Produktes von Kriterien RePr ist. Da Re das Mass des Strömens (Konvecktion) und Pr(Pr = ν/a) der Eigenschaftsdiffusion (molekularer Transport) ist ergibt sich, dass im gesamten Transport (Impuls und Wärme in diesem Fall) der Anteil der zwei Mechanismen komplementär ist (FoPe = 1 oder FoRePr = 1). Zur gleichen Schlussfolgerung gelangt man wenn man das Verhältnis der Kriterien Ho und Fo macht (Ho/Fo = = Pe = RePr und weiter Ho = FoPe = FoRePr = 1), wobei man wieder auf das Kriterium Pe kommt, wobei die Reihe der drei Kriterien (f(Ho, Fo, Pe) = = F(Fo′, Re, Pr), u.s.w.) schliesst.

Für die anderen Eigenschaftsformen folgt durch Analogie dass Fo′ = 1/Pe′ = = 1/ReSc; Fo″ = 1/Re und Fo″ = 1/Pe″ = 1/(ReBr).

In der letzten Beziehung ist das Kriterium Pe'' von der Form

$$Pe'' = \frac{wl}{e} = \frac{wl}{e}\frac{\nu}{\nu} = \frac{wl}{\nu}\frac{\nu}{e} = ReBr \qquad (7)$$

wo das Verhältnis $\nu/e = Br$ ein neues Kriterium ist-Bratukriterium (das wir mit Bescheidenheit als Ehrenbezeigung Proffessors E. u. Bratu vorschlagen). Dieses Kriterium, in der Literatur nicht erwähnt, gibt für die Konduktiven elektrische Ladungs- und Impulsprozesse, analog zum Prandtl Kriterium $Pr(\nu/a)$ für Wärme, Schmidt ($Sc = \nu/D$) für Masse oder Lewis ($Le = a/D$) für Wärme und Masse geben [4].

Man kann bemerken, dass für jeden transportierten Eigenschaftstyp Wechselbeziehungen zwischen Kriterien der Art Ho, Fo, Pe bestehen welche auch durch die Produkte RePr, ReSc, ReBr, u.s.w., wiedergegeben werden können, die die Konkurenz der beiden Mechanismen, konvektiv (Re) und molekular (Pr, Sc, Br) im allgemeinen Eigenschaftstransport betonen. In dieser Hinsicht erläutern wir den Fall des reinen Impulstransports (ohne jede andere Eigenschaft) wo $Fo'' = 1/Pe'' = 1/Re$ oder $Fo''Pe'' = 1$ oder $Fo''Re = 1$, also ist Re das Mass des Transports (q.e.d.).

Die Schlussfolgerung scheint überraschend ($Fo = 1/Re$), weil dieses Kriterium Fo (und seine Analogen Fo', Fo'', Fo''') eigentlich die Dynamik der molekularen Prozesse (K_2) zeigen und nicht die der kovektiven Prozesse, deren Mass das Kriterium Re ist. Dieser Gegensatz lässt sich erklären, wenn in der Formulierung der Kriterien Fo, das Geschwindigkeitsglied sich auf die Bewegung der molekularen Eigenschaftsträger bezieht, und so weist ihr lw Produkt, so wie bei der Beweisführung des Kriteriums Re [6], die Proportionalität (das Verhältnis) zwischen den makroskopischen und molekularen Grössen in der Charakterisierung der Bewegung auf.

Kriterien der Ähnlichkeit als Verhaltnisse von extrinseken Gliedern. Das Verhältnin der analoger Glieder aus den Transportgleichungen mit nominalisierter Eigenschaft (Paarwense konduktiv, konvektiv und nichtstatioär) führt zu einer anderen Gruppe von Kriterien und zu Masstabverhältnissen zwischen diesen Systemen. Dieses wird eigentlich zu Verhältnissen von Kriterien der Art K (Ho'; Ho''/Ho' u s.w.), K_2 (Fo'/Fo ; Fo''/Fo', u.s.w) und K_3(Pe/Pe' ; Pe'/Pe'' Pe''/Pe''' u.s.w.). Wenn die Grössen aus den kriteriellen Gruppen derselben Natur sind, haben die Verhältnisse die Bedeutung von Masstabfaktoren (z. B. Ho/Ho' = 1 wenn die Grössen w, t, l in den zwei Systemen gleich sind oder ihr Verhältnis einheitlich ist und Ho/Ho' ≠ 1 wenn diese verschieden sind), und zeigt deren mengenmässige Korrespondenz in den gegebenen Systeme (Modell-Prototyp)

Im Falle der qualitativ versehiedenen Grössen, sind die Verhältnisse Kriterien (z.B. :Fo''/Fo' = ν/D = Sc ; Pe'/Pe'' = (wl/D:wl/ν) = ν/D = ReSc/Re=Sc)-

Wenn man nur die Bedeutung als Kriterien der neuen Verhältnisse in Betrachtung nimmt, für den Impuls, Wärme, Masse- und elektrische Ladungstransport, so ergeben sich folgende Kriterien :

$$Pr = \frac{\nu}{a} = \frac{Fo''}{Fo} = \frac{Pe}{Pe''} ; \quad Sc = \frac{\nu}{D} = \frac{Fo''}{Fo'} = \frac{Pe'}{Pe''} ; \quad Le = \frac{a}{D} = \frac{Fo}{Fo'} = \frac{Pe'}{Pe} = \frac{Sc}{Pr} \qquad (8)$$

$$Br = \frac{\nu}{e} = \frac{Fo''}{Fo'''} = \frac{Pe'''}{Pe''}; L_1 = \frac{a}{e} = \frac{Fo}{Fo'''} = \frac{Pe'''}{Pe}; L_2 = \frac{e}{D} = \frac{Fo'''}{Fo} = \frac{Pe'}{Pe'''} \quad (9)$$

Alle diese Kriterien sind Verhältnisse der Eigenschaftsdiffusivitäten (Impuls, Masse, Wärme, electrische Ladung). Die ersten (Pr, Sc, Le) sind wohlbekannt in der Literatur (8), die Letzen (Br, L_1, L_2) die den Konduktiven Transport elektrischer Ladung miteinbeziehen (9) sind nicht erwähnt.

Schlussfolgerungen. Die Analyse des mathematischen Modells des nichtstationären Konvektivmolekularen Transports zeigt für Wärme, Masse, Impuls und elektrische Ladung die Möglichkeit der Gruppierung der Grössen und Glieder in Gruppen von Zahlen (Kriteriens) die aus intrinseken bzw. extrinseken Glieder, folgen. Im Rahmen jeder Gruppe, und zwischen den Gruppen bestehen kriterielle Beziehungen und Massstabsverhältnisse.

Zwischen dem analysierten Kriterien sind drei neue Kriterien erwähnt die in dem molekulären Transport von elektrische Ladung, Impuls, Wärme und Masse vorkommen.

LITERATUR

1. E. A. Bratu, „Operații unitare în ingineria chimică", vol. 3, p. 266, Ed. Tehnică, București, 1985.
2. E. R. Eckert, R. M. Drake, „Analysis of Heat and Mass Transfer", Mc Graw-Hill, New York, 1972.
3. F. Chiriac, A. Leca, M. Pop, A. Badea, L. Luca, N. Antonescu, D. Peretz, „Procese de transfer de căldură și masa în instalațiile industriale", Ed. Tehnică, București, 1982.
4. L. Literat, „Fenomene de transfer și utilaje în industria chimică — Procese de transport", Ed. Univ. Cluj-Napoca, 86, 1985.
5. D. Ștefănescu, A. Leca, A. Badea, M. Marinescu, „Transfer de căldură și masă — teorie și aplicații", Ed. Didactică și Pedagogică București, 1983.
6. E. A. Bratu, „Operații și utilaje în industria chimică", Ed. Tehnică, București, p. 260, 1970.

STUDIA UNIV. BABEŞ BOLYAI, CHEMIA, XXXV, 1, 1990

THE REACTION OF SOME DERIVATIVES OF 1-(2-PYRIMIDINYL)-PYRAZOLIN-5-ONE WITH HYDRAZINE HYDRATE

IOAN CRISTEA*

Received: June 20, 1990

The 4-benzylidene-1-(2-pyrimidinyl)-3-methyl-pyrazolin-5-ones Ia...d were reacted with hydrazine hydrate in boiling methanol. As result of a hydrazinolyse and a transhydrazonation, benzalazine (II) of the corresponding aldehyde together with hydrazone of acetoacethydrazide (IV) and pyrimidinylhydrazine derivatives (Va...d) were obtained.

As an extention of our studies on the behaviour of some 1-(2-pyrimidinyl)-3-methyl-pyrazolin-5-ones in reaction with hydrazine hydrate [1], we report now the same reaction of 4-benzylidene-1-(2-pyrimidinyl)-pyrazolin-5-ones (Ia...d). These compunds were prepared by the condensation of the corresponding 5-pyrazolone derivatives with p-dimethylamino-benzaldehyde in basic catalysis [2, 3].

In connection with this question it is worth to note that previous works of A. Mustafa et al. [4] and M. F. Kaschef et al. [5] have shown that by the reaction of 4-benzylidene-1-phenyl-3-methyl-pyrazolin-5-one (II) at room temperature, the benzalazine (III) and 1-phenyl-3-methyl--pyrazolin-5-one (IV) were obtained, while in boiling ethanol the 4,4'-benzylidene-bis (1-phenyl-3-methyl-pyrazolin-5-one) (V) was formed.

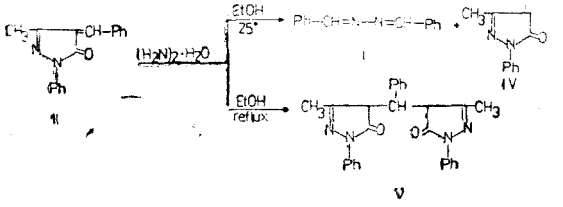

In this way we intended to explore more careful this reaction between some 4-benzylidene-1-(2-pyrimidinyl)-pyrazolin-5-ones and hydrazine hydrate.

* University of Cluj-Napoca, Department of Organic Chemistry, 3400 Cluj-Napoca, Romania

If the solution of the pyrazolones Ia...d and an excess of hydrazine hydrate in methanol was boiled for 1,5 hours, we isolated as reaction products p-dimethylamino-benzalazine (VI), the pyrimidinyl hydrazine (VIIIa...d) and the hydrazone of acetoacethydrazide (VIII).

Ia was reacted with hydrazine hydrate in methanol also at room temperature for 4 hours. In this case in the crude reaction product, the pyrimidinyl-pyrazolone (tautomeric form) IXa was detected by TLC, as show in Fig. 1.

The reaction with hydrazine hydrate is favoured by acid catalysis.

Taking into account the above data, it is suggested as the first step in the reaction of I with hydrazine hydrate the nucleophyle addition of the last one to the α, ß-conjugated carbonyl system, followed by a retro-aldolic splitting up of the C—C bound, to give the benzalazine VI and the pyrazolones IX. Subsequently the pyrazolones IX react with the hydrazine hydrate in the way shown in our previous work [1].

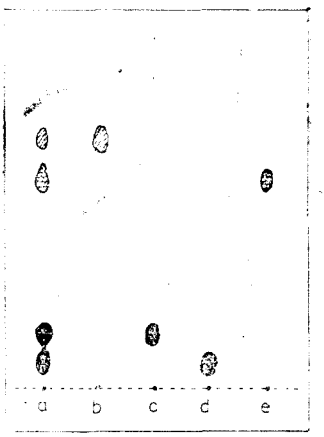

Fig. 1. Thin layer chromatography (TLC) on the reaction of 4-benzylidene-1-(2-pyrimidinyl)-pyrazolin-5-one (Ia) with hydrazine hydrate.
a: reaction products, b: pyrimidinyl-pyrazolone IXa (pure), c: pyrimidinyl-hydrazine VIIa (pure), d: hydrazone of acetoacethydrazide VIII (pure), e: compound IA (pure).

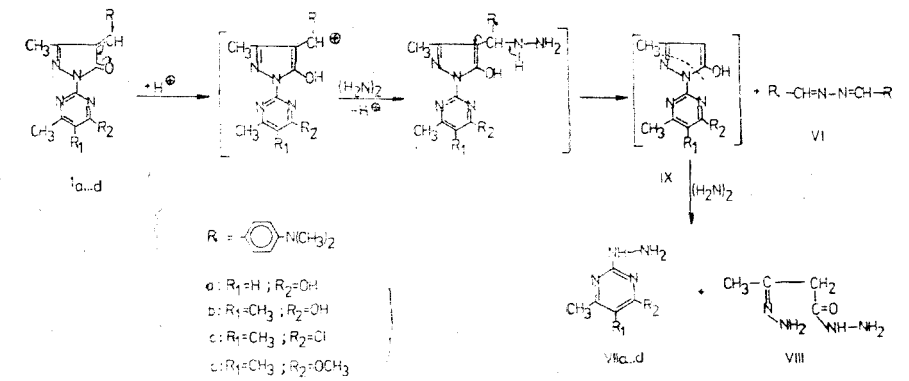

The 1-(4-chloro-5,6-dimethyl-2-pyrimidinyl)-4-formyl-3-methyl pyrazolin-5-one (X) [6] is interesting for a reaction with hydrazine hydrate owing to the presence of three electrophilic centers in the molecule: the formyl group, the position 4 substituted by the chlorine atom and the ring carbonyl. If the reaction was performed in the conditions described in the experimental section, the hydra-

zone of 1-(4-hydrazino-5,6-dimethyl-2-pyrimidinyl)-4-formyl-3-methyl-pyrazolin-5-one (XI) was obtained in good yield. This shows that in this case no ring cleavage takes place, in spit of an excess of the hydrazine hydrate.

This behaviour may be assigned to the electron-with drawing effect of the $CH = N-NH_2$ (or CHO) which stabilize the pyrazolone ring.

Experimental. The purity of the compound was checked by TLC silica gel Merck plates.

The m.p. were determined in capilaries and are uncorrected.

The TLC were performed on silica gel Merck plates using chloroform : methanol 5 : 1 as eluent. The development was performed in saturated N-chromatographic chambers. The detection was made with iodine vapours.

Reactions with hydrazine hydrate.

Reactions of Ia...d. a) To a suspension of 0.01 moles Ia...d in 25 ml methanol, 5 ml (0.1 moles) hydrate hydrazine, were added and the mixtude refluxed for 1,5 hours. After a few minutes the red solution lost colour and VII precipitated. After cooling was filtered and thus the pure VII was obtained. The filtrate was evaporated and residue was treated with 20 ml chloroform and filtered. The insoluble part was recrystallized from DMFA—water 2 : 1 to afford VIII. The chloroformic solution was evaporated and the solid VI recrystallized from ethanol, melts at 251 (lit. 250—253 , /8/). Some data are listed in Table 1.

Table 1

Compounds isolated by the reactions of Ia ...d with hydrazine hydrate

Compound	M.p. °C/lit.1,7	Yield	Compound	M.p. °C	Yield
VIIa	241/238	87			61
VIIb	332/332	79	VIII	320	60
VIIc	206/206	85			58
VIId	115/116	75			65

b) To a solution of 0.001 moles Ia in 5 ml methanol, 0.1 ml (0.002 moles) 100% hydrazine hydrate and a few drops of HCl conc. were added and the mixture stirred for 4 hours at room temperature. After a few minutes the red colour of solution dissapeared. This solution was used for thin layer chromatography, using silica gel Merck plates.

The results are given in Fig. 1.

Preparation of X. To a mixture of 50 ml ice-cooled DMFA and 25 ml $POCl_3$, 10 g X was added The mixture was stirred at 70° for 4 hours, and then poured in ice. The pH was adjusted at 7 with

olution of $NaHCO_3$ 1M, and allowed to stand at room temperature for two hours. The product s filtered and the precipitate washed with water. The crude product was recrystallized from metha--water 2 : 1, m.p. 86°, $C_{11}H_{11}N_4O_2Cl$(266,5). Calcd. N% 21.02, Found. 21.11. ^1H—NMR spectrum DCl_3), δ(ppm): 9.90 (CHO, s); 2.40 (CH_3, s, pyrazol.); 2.50, 2.62 (twoCH_3, s. pyrim.).

Reaction of X. To 0.25 g (0.001 moles) X in 10 ml ethanol 0.2 ml (0.004 moles) hydrazine hydrate re added and the mixture boiled for 1 hour. After cooling the precipitate was filtered. The precipi-e, 0.21 g (80%) was recrystallized from DMFA. Thus pure XI was obtained, m.p. 318°C. $C_{11}H_{16}N_8O$ 6). Calcd. N% 40.57, Found. 40.8. ^1N—NMR spectrum, δ (ppm): 2.30 (CH_3, s, pyrazol.); 2.58, 0 (two CH_3, s, pyrimidin.); 4.15 ($NH-NH_2$, m). ($CDCl_3$).

REFERENCES

I. Cristea, V. Fărcăşan, *Stud. Univ. Babeş-Bolyai, Chemia,* **34,** (1), 60 (1989).
I. Cristea, V. Fărcăşan, *Rev. Chim.* (Bucureşti), **38,** 674 (1987).
I. Cristea, *Stud. Univ. Babeş-Bolyai, Chemia,* **33,** (2), 61 (1988).
A. Mustafa, W. Ascher, *J. Org. Chem.* **27,** 4201 (1962).
M. F. El-Kaschef, S. M. Yassin, *Rev. Roumaine Chim.* **25,** 577 (1980).
Unpublished data.
H. Vanderhaeghe, M. Claisen, *Bull. Soc. Chim. Belg.* **68,** 30 (1959).
N. Knopfer, *Monatsh. Chem.*, **30,** 31 (1934).

STUDIA UNIV. BABEŞ BOLYAI, CHEMIA, XXXV, 1, 1990

IN MEMORIAM

Prof. dr. doc CANDIN LITEANU

With deepest regret we noticed the death of professor Candin Liteanu after a long and he illness on May 30th 1990. Being an outstanding teacher and researcher he initiated generations of you people in persevering to study, to acquire knowledge and to discover new pathways in science.

Born on July 6th 1914 in a modest family of peasants in a small village in Transylvania, af graduation from two higher schools: Agronomy (1937, agronomist) and University of Cluj, Facu of Chemistry (1941), he earned his Ph. D. degree in chemistry in 1945. He held academic positions the same University of Cluj being professor of analytical chemistry from 1951 till his retirement (197 He was head of the Department of Analytical Chemistry 1964—1977. Very active in teaching and search he recognized the importance of fundamental work driving himself much too hard to contrib to the solution of some acute problems in analytical chemistry. Professor Liteanu was very muc leader and innovator with a forceful personality and much shrewdness in the identification of resea topics of future importance. He initiated fundamental studies in the theory of the equivalence poin titrimetry, in chromatography (theory and practice of temperature gradient chromatography), ion-se tive electrodes and statistical theory of trace analysis based on signal interpretation. Being interest in the practical aspects of the analytical chemistry too, he worked out together with his numerous c laborators many new analytical methods for process control, at the same time initiating the product on micro scale of ion-selective electrodes and chromatographic materials requested by our indus

His publications include 341 scientific papers and 9 textbooks and monographs, respective some of them being translated and published abroad. His textbook on titrimetry appeared in 7 e tions is a very useful tool even today for those being interested in the study of analytical chemist His didactical and scientifical activity were recognized by awarding the title of „Honoured Scientis

His death is a heavy loss not only for our Faculty but for the whole chemical community in country as well. He will be remembered by all his pupils, colleagues and friends.

L. KÖKE

RECENZII

nel Haiduc, Cristian Silvestru
ganometallics in Cancer Chemotherapy, Vo-
ne I. Main Group Metal Compounds CRC-
ss Inc., Boca Raton, Florida, 1989.

The book with the above title is the first lume of a monograph dedicated to anticancer ivity of the organometallic compunds, dea- g with the Main Group Metal Derivatives.

The book is written mainly for chemists orking in the synthesis of organometallic npounds) as well as for people who investi- e the biologic properties in general and anti- nor properties in particular. The related as- ts of toxicity, and other than antitumor dical uses were briefly touched, when possi- .

In a short Introduction an overview of field of organometallic chemistry is presen- (the question „what is an Organometallic mpound? is aswered, the ability of Main oup and Transition Metals to form organome- lic derivatives and the chemical bonding in ese compounds are mentioned in this chapter). is is followed by a short discussion of the me- ds of Antitumor Testing Organometallics.

The number of pages and references are licative about the volume of information avai- le about the activity of every metal derivatives, ganoboron, (Chapter 2), p. 21—36, 109 refs: ganosilicon (Chapter 3), p. 41—76, 156 refs; ganogermanium (Chapter 4), p. 83—117, refs; Organotin (Chapter 5), p. 129—165, 8 refs; Organolead (Chapter 6) p. 177—180, refs; Organoarsenic (Chapter 7), p. 185— 7, 156 refs; Organoantimony (Chapter 8) 233—239, 88 refs; Organobismuth (Chapter- p. 243—244, 25 refs; Organotallium (Chapter-), p. 245—246, 16 refs.

Each chapter begins with a general and storical approach of the biologic implication organometallic derivatives, followed by the scussion of biological activity, toxicity and titumor properties in relation to the number metal-carbon bonds.

The results of in vitro and in vivo titumor screening of organometalloid and or- nometallic compounds are presented chrono- gically, and are classified based on their struc- re. When data are available, structure-acti- ty relationships are suggested. The results clinical trials of Spirogermanium and Ge-132are also described. For some type of organometallic compounds considerations on the mechanism of antitumor activity are presented.

The book is presented in remarcable gra- phyc condition.

LUMINIŢA SILAGHI-DUMITRESCU

Modern Thin-Layer Chromatography, Chromatographic Science Series, Volume 52, Nelu Grinberg, Ed. XII + 490 pp., Marcel Dekker, Inc., New York, Basel, 1990.

Since 1956, when Stahl established thin-layer chromatography (TLC) this technique became quickly one of the most popular chromatographic methods, as it is easy to carry out and inexpensive, allowing to saparate wide classes of compounds. TLC has several advantages over the classical column operation. First, the overall throughput can be higher since many samples can be plotted on individual plates and developed simultaneously. A second advantage is the potentially higher resolving power. This book documents the impressive achievements by researchers in TLC.

Preceded by a foreword by B. L. Karger and a preface by Nelu Grinberg, the following items are covered. The „Introduction" (Chapter 1) by Nelu Grinberg outlines some aspects of the history of TLC and the place of TLC among chromatographic techniques. Chapter 2 „Stationary phases in TLC" by S. Gocan offers a deep insight into the properties and characterization of stationary phases used in TLC. The coating materials for TLC are systematically reviewed, starting with the most commonly used silica, cellulose, alumina, or kieselguhr, and followed with polyamides, ion-exchanger resins and other materials like gels, starch, sucrose, mixed adsorbents etc. In general the following aspects are considered: preparation, nature of the surface, activity, effect of structure on the chromatographic properties, applications. This is by far the longest chapter, it contains 10 tables, 31 figures, lists 810 (!) references, and is of 132 pp. in length.

In Chapter 3 „Mobile phases in thin-layer chromatography" by S. Gocan the problems of solvent classification and mobile phase selection are presented. This chapter contains 8 tables 7 figures, lists, 58 references and, 35pp. in lenght.

The theoretical aspects of TLC are presented also by S. Gocan (Chapter 4). This chapter provides valuable information on the kinetics of sample and mobile-phase migration through the layer, on the influence of the vapor phase solute interactions with stationary and mobile phases and separability criteria in TLC. All problems are explained on a sound theoretical basis, the pertinent relationships being presented and thoroughly analyzed. This chapter contains 4 tables, 5 figures, lists 246 references, and is of 72 pp. in leght.

Chapter 5 „Quantation in thin-layer chromatography" by G. Szepesi discusses the problems of quantitative work in detail. Two basic approaches are distinguished: 1) direct methods in which the separated spots are determine in situ on the plate; and 2) indirect methods, in which quantitative measurements are carried out after elution of the spots in the chromatoplate. The separated compounds can be quantified by colorimetric, fluorimetric, spectrophotometric and other methods. The pertinent relationships are also presented, mainly those refering to densitometry. The exact proof and evaluation of the suitability, correctness and precision of each chromatographic process, as well as that of instrumental components are examined in detail (validation). This chapter contains 10 figures, lists 30 references and is of 34 pp. in length. The problems of instrumentation are discussed by G. Szepesi in Chapter 6 considering the sample applications instruments, chamber systems and detection systems. The fundamental aspects of automation and computerization are also dealt with. This chapter contains 16 figures, lists 32 references, and is of 26 pp. in length.

Under the title „Special techniques" (Chapter 7) by N. Grinberg, H. Halasz, S. M. Han and D. W. Armstrong the following topics are presented: continuous TLC, forced-flow TLC, bidimensional TLC, gradients (elution, temperature, stationary-phase) in TLC, chiral separations in TLC and preparative TLC. This chapter contains 10 tables, 68 figures, lists 258 references, and is of 121 pp. in length. Chapter 8 with the title „Mobile phase and time optimizationa" is by R. Blanco. The low cost of chromatographic supports and solvent render their optimization unimportant, so the most important factors to be considered are analysis time and resolution. For this purpose time analysis optimization and mobile-phase optimization are considered in detail. This chapter contains 2 tables, 5 lfigures, lists 26 references, and is of 17 pp. in tength. The topics covered by the last two chapters include a study of „Relationship between thin-layer and column chromatography" (Chapter 9; 12 pp.) by N. Grinberg and „Perspectives in thin-layer chormatography" (Chap 10; 15 pp.) by J. C. Touchstone.

Overall, this is a well written, edited a produced book. The authors have attained tl goals with this text, which is extremly detar and encompass a large amount of knowlec All chapters are well organized being documen with more than 1400 bibliographic citations useful table of contents, that is judiciously vided into a number of subsections, and a ge composite subject index at the end of the bo are helpful in a rapid orientation. There is difficulty in locating a particular topic. All all, „Modern Thin-Layer Chromatography" an outstanding resource for chromatographe analytical, organic and forensic chemists, l chemists, pharmacists, biotechnologists, as w as for graduate students in these disciplii The level and the content of the presentat are such that both newcomers and more exp enced practitioners involved in TLC will f this monograph very useful.

L. KEKEI

Proceedings of the Fourth International Symposium on Instrumental High Performar Thin-Layer Chromatography (Planar Chron tography) Selvino/Bergamo, Italy, Septem 22–25, 1987. Edited by H. Traitler, A. Studi R. E. Kaiser; Published by the Institute Chromatography, Bad Dürkheim, FRG.

The volume comprises a number of papers which extend on 468 pages. By look at the contents of the papers, we can see t most of them deal with quantitative determi tions using adequate instruments: TLC-Scann UV-Vis and Fluorescence; Iatroscan TLC/F system clearly assisted by calculation techni As to the fields of application they cover a v area of compounds from a vast number of cl ses. One of the papers which draws our attent refers to the use of hidrophilic modified sorbe (amino, cyano and diol) by Jost and Hau The development techniques are also pres in the volume by the Camag automated gradie technique. The papers using the OPLC syste are present too. We have to mention a nove in this field, that is the paper: High pressu planar liquid chromatography by Kaiser a Rieder. Then is another group of papers wh deals with the optimization of the mobile pha The rest of the papers cover a great numb of other problems.

The volume is published in a very ne way and due to the quantity of information

contains it should be present on the book-shelvs of all those interested in the practical and theoretical problems of thin-layer chromatography.

S. GOCAN

Proceeding of the International Symposium on Instrumental Thin-Layer Chromatography Planar Chromatography, Brighton, Sussex ,U.K., February 21—24, 1989. Edited by R. E. Kaiser; Published by the Institute for Chromatography, Bad Dürkheim, FRG.

The volume contains 46 papers, but some of them are in abstract form. The papers that deal with the quantitative determination assisted by calculation technique are in great number but we won't discuss them. We are going to review a great number of papers, dealing, with diverse problems which point to the high level of TLC, nowadays. In the field of detection: there is a new detector for radiochromatography (the digital autoradiograph) which measures the position and intensity of the 2-dimensional distributions of ionizing radiation from radioisotope labelled TLC – plates (H. Filthuth). The possibility of direct analysis of HPTLC- plates by laser microprobe mass spectrometry has also been demonstrated. There are also applications of TLC and HPTLC-mass spectrometry (L. D. Wilson). E. Koglin shows the possibility of the acquisition of Raman spectra from HPTLC spots down to 1 μm in size or other forms of microsamples approaching the fentogram level in mass. The surface of the thin layer was activated by using silver colloidal. The on-line coupling between HPLC and automated multiple development (K. Burger), is also present. The problem of eluent optimisation is dealt within the following papers: Fast optimisation of the solvent composition in TLC using a multiple developing chamber (H. Keuker et al.); also: multiple development — a new gradient elution system to realize quiker separations of antraquinone glycosides (A. Koch and Jj. Kraus); trends in analytical forced-flow planar chromatography (Sz. Nyiredy); recent advances in overpressury layer chromatography (Newton R.).

There is another group of papers dealing with separation of enantiomers: TLC enantiomerie resolution (J. Martens et al.); separation of enantiomers in TLC (M. Marek and H. E. Hauck); enantiomeric separation of aminoalcohols by TLC using a chiral counter ion in the mobile phase (Anna-Maria Tivert and Asa Backman) and preparation and application of TLC plates for enantiomer separation (P. E. Wall). Another aspect of reversed-phase TLC is that of using capacity factors for prediction of hydrophobicity of ionogenic aromatic hydrocarbons (P. de Vooggt et al.); Reversed phase ion-pair high performance TLC (G. P. Tomkinson et al.). T. Spurway et al. described preliminary results obtained for a limited number of compounds using C—18 and cyanopropyl bonded TLC plates for chromatography of N—oxide metabolites.

In the end we shall speak of two papers which comment on the future of TLC: Multidimensional and multimodal TLC pathway to the future (C. F. Poole et al.); planar chromatography: state of the art and future trends (R. E. Kaiser).

The papers comprised in this volume have the aim of presenting the stage of development of instrumentalization in TLC. The volume, in all its diversity is a unitary work and of a great interest for all researchers in planar chromatography.

S. GOCAN

Tiparul executat la
Imprimeria „ARDEALUL" Cluj,
Cda: 122/1990

În cel de al XXXV-lea an (1990) *Studia Universitatis Babeş-Bolyai* apare în următoarele serii:

matematică (trimestrial)
fizică (semestrial)
chimie (semestrial)
geologie (semestrial)
geografie (semestrial)
biologie (semestrial)
filosofie (semestrial)
sociologie-politologie (semestrial)
psihologie-pedagogie (semestrial)
ştiinţe economice (semestrial)
ştiinţe juridice (semestrial)
istorie (semestrial)
filologie (trimestrial)

In the XXXV-th year of its publication (1990) *Studia Universitatis Babeş-Bolyai* is issued in the following series:

mathematics (quarterly)
physics (semesterily)
chemistry (semesterily)
geology (semesterily)
geography (semesterily)
biology (semesterily)
philosophy (semesterily)
sociology-politology (semesterily)
psychology-pedagogy (semesterily)
economic sciences (semesterily)
juridical sciences (semesterily)
history (semesterily)
philology (quarterly)

Dans sa XXXV-e année (1990) *Studia Universitatis Babeş-Bolyai* paraît dans les séries suivantes:

mathématiques (trimestriellement)
physique (semestriellement)
chimie (semestriellement)
géologie (semestriellement)
géographie (semestriellement)
biologie (semestriellement)
philosophie (semestriellement)
sociologie-politologie (semestriellement)
psychologie-pédagogie (semestriellement)
sciences économiques (semestriellement)
sciences juridiques (semestriellement)
histoire (semestriellement)
philologie (trimestriellement)

Abonamentele se fac la oficiile poştale, prin factorii poştali şi prin difuzorii de presă, iar pentru străinătate prin „ROMPRESFILATELIA", sectorul export-import presă, P. O. Box 12—201, telex. 10376 prsfir, Bucureşti, Calea Griviţei nr. 64—66.

Lei 55